TECHNICAL UNIVERSITY OF LIBEREC
Faculty of Mechatronics, Informatics
and Interdisciplinary Studies

Synthesis of pyrrole-cyclodextrin conjugates for tissue engineering

Ph.D. thesis

Study program: P3901 – Applied Sciences in Engineering

Field of study: 3901V055 – Applied Sciences in Engineering

Author: **Ing. Jan Lukášek**

Supervisor: prof. Ing. Ivan Stibor, CSc.

Liberec 2019

TECHNICKÁ UNIVERZITA V LIBERCI
Fakulta mechatroniky, informatiky
a mezioborových studií

Syntéza pyrrol-cyklodextrinových konjugátů pro tkáňové inženýrství

Disertační práce

Studijní program: P3901 – Aplikované vědy v inženýrství
Studijní obor: 3901V055 – Aplikované vědy v inženýrství

Autor práce: **Ing. Jan Lukášek**
vedoucí práce: prof. Ing. Ivan Stibor, CSc.

Liberec 2019

Declaration

I hereby certify that I have been informed that Act 121/2000, the Copyright Act of the Czech Republic, namely Section 60, School-work, applies to my dissertation in full scope. I acknowledge that the Technical University of Liberec (TUL) does not infringe my copyrights by using my dissertation for TUL's internal purposes.

I am aware of my obligation to inform TUL on having used or licensed to use my dissertation in which event TUL may require compensation of costs incurred in creating the work at up to their actual amount.

I have written my dissertation myself using literature listed therein and consulting it with my supervisor.

I hereby also declare that the hard copy of my dissertation is identical with its electronics form as saved at the IS STAG portal.

Date:

Signature:

ACKNOWLEDGEMENT

In the first place I would like to thank my wife and family for supporting me throughout writing this thesis and the whole studies.

I am also grateful to prof. Ivan Stibor for his professional leadership and kind attitude. I appreciated his extensive knowledge and experience, which helped me to overcome numerous obstacles I have been facing throughout my research. I could not have imagined having a better advisor and mentor for my Ph.D. study.

I would like to thank all, who assisted me with characterisation of prepared compounds or materials. Namely, to Dr. Markéta Řezanková for measuring NMR spectra, Dr. Pavel Kejzlar for SEM characterisation, Ing. Martin Stuchlík and also to Dr. Jana Müllerová for providing thermogravimetric and IR analysis together with evaluation of the obtained data.

In addition, my sincere thanks go to colleagues from the Department of Nonwovens and Nanofibrous Materials for their cooperation on the project, delivering fibrous samples and the extensive *in-vitro* experiments.

Nevertheless, I would like to express my gratitude to Dr. Michal Řezanka and fellow colleagues from our laboratory for their friendship and creating a pleasant atmosphere during the years spent at Technical University of Liberec.

TARGETS OF THIS WORK

This thesis aims to prepare new composite material for tissue engineering and to understand the effect of surface functionalization on the cell-material interaction. This scaffold will serve as a primary platform for future development towards its ultimate application in the field of nervous tissue regeneration. Despite decades of intensive research, the majority of implants suffers from many drawbacks. One of them is the inertness of material which cannot provide essential cues for cell stimulation and growth. However, contemporary analytical chemistry together with advanced techniques for materials synthesis offers considerable variability in scaffolds design. Therefore, we have decided to combine knowledge from several different research areas and create procedures for the preparation of novel materials with exciting features. Our scaffold is based on the 3D fibrous polymeric network made by electrospinning process. This technique enables the production of materials with tunable mechanical properties, morphology or stability in the physiological environment. Although electrospinning is a random process, there is reasonable control over the diameter and morphology of the fibres. Other indisputable advantages are high productivity and the possibility of incorporating various compounds, nanoparticles or even biomolecules into the fibrous structure. Moreover, aligned fibres can also be prepared using a rotating collector or by drawing technique which is under intensive development in cooperation with our colleagues. The orientation of fibres also imparts another level of control over the cell adhesion and growth.

It is generally known that adhesive proteins mediate cell-material interaction. These biomolecules are absorbed onto the surface and are recognised by specific membrane receptors. Therefore, one option of our research is the synthesis of pyrrole-cyclodextrin monomers which could be copolymerized with pyrrole creating desirable core-shell material with cyclodextrin decorated surface. The alternative route would be based on the preparation of a fibrous matrix with deposited β-substituted polypyrrole layer. In the next step, suitable binding places would be utilised for the final cyclodextrin immobilisation. We believe, that cyclodextrin lipophilic cavity could attract adhesion-mediating proteins by non-bonding interaction and thus create extracellular matrix mimicking structures on the surface. Such interactions allow absorption of proteins in their natural spatial conformation which ultimately leads to significantly better cell adhesion and growth. Moreover, the core-shell 3D matrix with a deposited conductive polypyrrole layer on the surface could be used for cell guidance by external electric stimulation. The study of the scaffold mentioned above should bring us new information about cell-material interaction and make a step forward to the future bioresponsive material for tissue engineering.

Keywords: pyrrole, cyclodextrin, polypyrrole, surface functionalization, tissue engineering

CÍLE PRÁCE

Tato práce si klade za cíl připravit pokročilý materiál pro tkáňové inženýrství a především hlouběji pochopit vliv povrchové úpravy na interakci substrátu s biologickou hmotou. Tento materiál dále poslouží jako platforma pro cílovou aplikaci v oblasti regenerace nervové tkáně. Navzdory intenzivnímu výzkumu v průběhu posledních několika dekád trpí tkáňové nosiče řadou nedostatků. Jedním z nich je netečnost implantátů, které neposkytují nezbytné podněty pro stimulaci buněčného růstu. Současná analytická chemie však disponuje širokou paletou metod, které nám pomáhají pochopit základní děje probíhající při interakci biologické hmoty s povrchem materiálu. Tyto nástroje také hrají důležitou roli při designování nových tkáňových nosičů, které dnes mohou být připraveny řadou pokročilých metod. Nejen proto jsme se rozhodli zkombinovat znalosti z několika různých oblastí a vytvořit postup pro přípravu pokročilého materiálu se zajímavými vlastnostmi pro tkáňové inženýrství. Námi navržený tkáňový nosič je postaven na 3D vlákenné polymerní síti, která byla vyrobena elektrostatickým zvlákňováním. Tato technika umožňuje produkci vlákenného materiálu s variabilními mechanickými vlastnostmi, morfologií nebo stabilitou ve fyziologickém prostředí. Ačkoliv elektrostatické zvlákňování produkuje náhodně uspořádaná vlákna, tak poskytuje dobrou kontrolu nad průměrem vláken či tloušťkou vznikající vrstvy. Orientace vláken dále propůjčuje materiálu schopnost ovlivňovat směr růstu buněk.

Je obecně známo, že interakce většiny typů buněk s materiálem je zprostředkována adhezními proteiny. Tyto biomolekuly jsou adsorbovány na povrchu a následně rozpoznány specifickými membránovými receptory. Záměrem našeho výzkumu je v první řadě syntéza pyrrol-cyklodextrinových derivátů, které mohou být následně deponovány na povrch zvoleného materiálu. Alternativní cestou je pokrytí vlákenného substrátu vhodným β-substituovaným derivátem polypyrrolu, jehož funkční skupiny budou v následném kroku využity pro navázání cyklodextrinových makrocyklů. Věříme, že lipofilní kavita cyklodextrinu umožní díky slabým nevazebným interakcím s proteiny jejich přitažení k povrchu, čímž dojde k vytvoření struktury připomínající extracelulární hmotu. Tato interakce povede k adsorpci proteinů v jejich přirozené prostorové konformaci, což bude mít za následek lepší adhezi a proliferaci buněk. Povrchová vrstva vodivého polypyrrolu může být navíc využita k elektrické stimulaci růstu buněk. Očekáváme, že studium takového tkáňového nosiče přinese zajímavé informace o interakci buněk s materiálem a otevře cestu k pokročilým biologicky aktivním materiálům pro tkáňové inženýrství.

Keywords: pyrrol, cyklodextrin, polypyrrol, funkcionalizace povrchu, tkáňové inženýrství

CONTENT

1. INTRODUCTION

Although thousands of different materials for tissue engineering have been prepared over the last years, human creations are still not precise nor useful as the creations of nature. On the other hand, the understanding of biological processes gone through tremendous development which help us to design tailor-made materials with tunable properties according to a target application. That is why we decided to create new composite material and contribute to a better understanding of cell-material interaction. The work is divided into several follow-up steps, starting with the synthesis of suitable pyrrole derivatives. Then, these compounds will be polymerised onto the 3D matrix, and the structure of resulting core-shell fibrous material will be characterised by analytical methods. There are two possible scenarios for the final cyclodextrin immobilisation. The pyrrole monomer could be directly connected to cyclodextrin and then *in-situ* copolymerized with pyrrole in order to prepare desirable coated material. Alternatively, the fibrous scaffold could be covered with polypyrrole derivative before the cyclodextrin attachment using one of many available conjugation techniques (Figure 1). The effects of surface functionalization and the biocompatibility will be later studied by *in-vitro* experiments.

The theoretical part would provide a reader with brief information about pyrrole derivatisation, conductive polymers and mechanisms of cell-material interaction. Results and discussions represent the core chapter where measured data are critically evaluated. The experimental part describes the exact procedures for the synthesis of pyrrole derivatives with the corresponding spectroscopic analysis. The final section deals with the polypyrrole deposition, cyclodextrin immobilisation, material characterisation and *in-vitro* study.

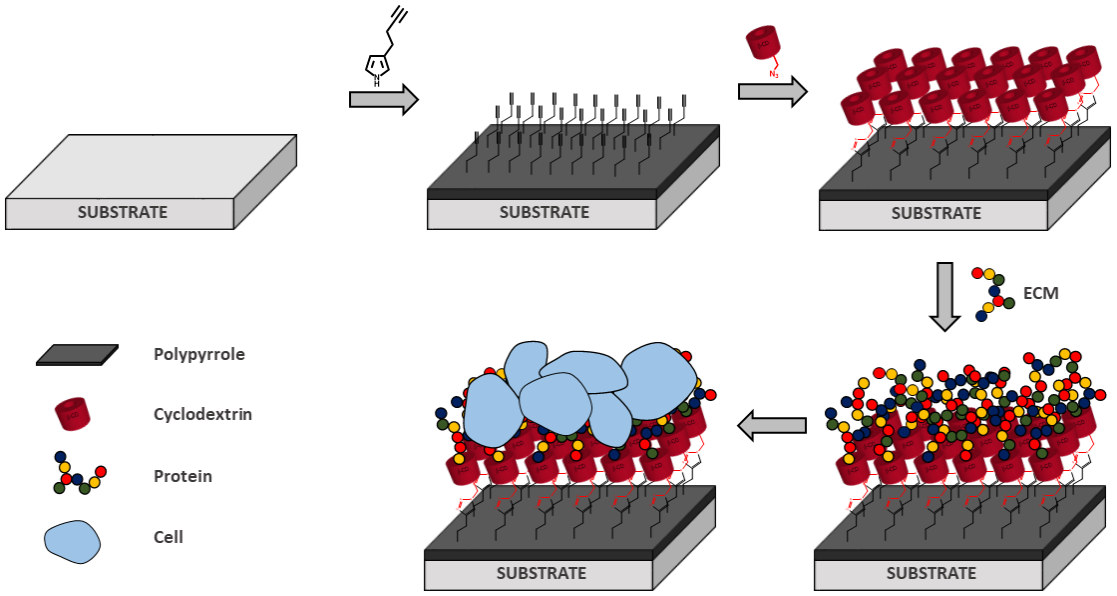

Figure 1. Preparation of PPy-CD material for tissue engineering

2. THEORETICAL PART

2.1. Pyrrole – synthesis and reactivity

Pyrrole is a five-membered heterocycle like furan and thiophene. It is a colourless liquid that darkens upon exposure to air. Unsubstituted pyrrole is produced industrially by treatment of furan with ammonia in the presence of a catalyst. In laboratory scale, it is synthesised by Hantzsch[1], Knorr[2] or Paal-Knorr[3] reaction. Many alkaloids or drugs containing pyrrole heterocycle unit can be directly prepared by multicomponent reactions.[4] Natural products like porphyrins, indoles, bilirubin or vitamin B12 contain pyrrole in their structure as well.[5,6]

Pyrrole is less basic than pyridine due to the conjugation of nitrogen lone electron pair into the aromatic ring. It can be derivatised at the nitrogen or carbon atoms (Scheme 1). Protonation by strong acids occurs mainly (80 %) at C2 and partially (20 %) at the nitrogen atom. Reactions with electrophiles yield 2-substituted pyrroles because of higher electron density at C2 compared to position C3.

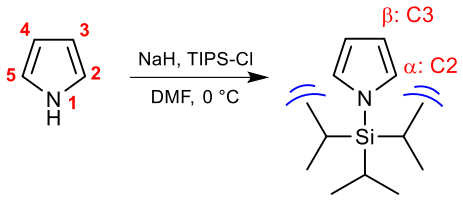

Scheme 1. Structure and numbering of pyrrole

Polysubstituted derivatives can be easily prepared if an excess of the electrophilic agent is used. Halogenation, nitration, sulfonation are well-established methods providing mono-, di-, tri- or tetra- substituted pyrroles with different selectivity.[7–10] Mono-substitution at position C3 is not directly accessible, but various approaches can be used for selective derivatization.[11–13]

1. Introduction of acyl group at C2, which directs substitution to C3 and can be selectively removed after the reaction
2. The acid-catalysed isomerisation of C2 derivatives
3. Blocking of C2 position with bulky *N*-protecting group

The most convenient way for β-substitution is method 3. The nitrogen can be protected with sulfonyl or silyl group which hinder more reactive α–positions, and therefore subsequent electrophilic aromatic substitution affords β–derivatives preferably. Then, protecting group is easily cleaved to yield pyrrole exclusively substituted at position C3.[8,10,14]

2.2. Conductive polymers

2.2.1. Historical milestones

An enormous effort has been made to study and utilise conductive polymers during the last four decades. They are often called “synthetic metals” because of their intrinsic conductivity which is normally associated only with the metals.[15]

The first conductive polymer was probably prepared in 1874 from aniline by treatment with sulphuric acid which resulted in black powder polyaniline. Later, highly explosive sulphur nitride was found to be superconductive at extremely low temperature (T_c = 0.24 K).[16] In 1974 Shirakawa has developed a procedure for the synthesis of *cis* or *trans* polyacetylene by Ziegler Natta catalyst.[17] Despite the crystalline metallic structure, the resulting polyacetylene film was air sensitive insulator. However, just three years later in 1977, an article dealing with the synthesis of the first truly conductive polymer was published.[18] Shirakawa and his co-workers observed a drastic change in infrared absorption of polyacetylene treated with halogen vapours. Joint efforts of two American physicists Alan J. Heeger, Alan G. MacDiarmid and Shirakawa´s team resulted in the discovery of first truly conductive polymer. The series of experiments revealed that conductivity was increased by order 10^9 because of “doping”. Their work opened the way for further study of conductive polymers and was greatly rewarded with the Nobel Prize for Chemistry in 2000.[19] Scientific community quickly realised the potential of this new brand of compounds and several other conductive polymers were synthesised during upcoming years (Figure 2). The most prominent examples were polyaniline, polythiophene, polypyrrole and their derivatives. Such polymers found many applications in electronics, light emitting diodes, flat screen, sensors, supercapacitors or later in tissue engineering.[20–24]

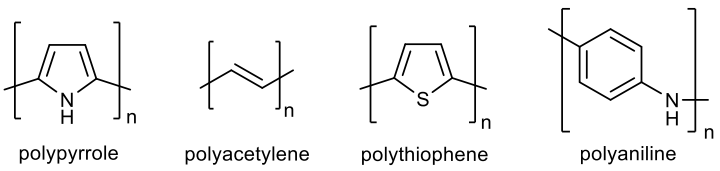

Figure 2. Structures of common conjugated polymers

2.2.2. General facts

In the following chapter, the most critical parameters of traditional conductive materials and intrinsically conductive polymers are compared. The origin of such natural conductivity is hidden in the delocalised system of parallel π-electrons. Heterocycles with lone electron pair at N, O, or S can be transformed into the conjugated polymers. An extensive orbital system only acts as a tunnel through which electrons are transported along the polymer backbone using charge carries. These agents are called dopants, and they play a crucial role in polymer conductivity, mechanical properties, stability and processability.[25] The inorganic semiconductors are also often doped, but the mechanism is different. In general, holes are created in the valence band, or electrons are donated into a conductive band of semiconductors. Even a small difference in the crystal lattice at ppm level has a dramatic impact on the resulting conductivity.

On the other hand, doping in the field of conjugated polymers means, that a high amount of charge caries (inorganic, organic or polymeric dopants) is introduced. The structural defects of delocalised π-electron system are compensated by doping agents to create neutral material which is, in fact, a polymeric salt. Thus, in both cases there is a change of oxidation state, the conductivity is increased, and the dominant mechanism of electron transport is controlled by diffusion of charge carries. In the chemistry of conductive polymers, two other types of doping are possible. A secondary dopant can be introduced to work synergistically with primary doping agent, but it has no impact on the polymer conductivity if used alone. The secondary dopant is inert and does not directly interact with conductive polymer but works only as a supporting molecule. Reversely, co-doping means the introduction of another dopant into the polymer structure to achieve the desired features. Such co-dopants can improve conductivity, environmental stability or solubility of target polymer. For example, small dopants like HCl or $FeCl_3$ show high conductivity but poor mechanical properties which can be altered using dopants like *p*-toluenesulfonic or dodecylbenzensulfonic acid.[26] As we can see, doping represents a potent tool for polymer design. The specific properties can be tailor-made according to the desired application. However, conductive polymers suffer from many drawbacks as well. The most severe issues are poor mechanical properties, the even distribution of charge carriers in the polymer structure and gradual reduction of conductivity due to environmental instability. Recently, an extensive work dealing with the loss of doping agent from the polypyrrole structure has been published by Tabaciarova et al.[27] They found that polypyrrole doped with some derivatives of sulfonic acid loses dopant up to 60 % in just 90 days. The conclusion is that more effective means of doping must be found in the future together with the synthesis of advanced monomers which can further improve overall polymer stability.

2.2.3. Dopants

The properties of conductive polymers are closely related with dopants and the methods of preparation as was described in the introduction above. In this part, the structure of dopants, mechanism of doping and the way how electrons are transported within the conjugate polymer matrix will be discussed in more detail. Dopants can be divided into several classes according to:

1. **Electron transfer**
   a) p-type (introduction of holes)
   b) n-type (donation of electrons)
2. **Chemical structure**
   a) inorganic
   b) organic
   c) polymeric
3. **Doping mechanism**
   a) ion or redox
   b) non-redox or neutral
   c) self-doping
   d) induced doping

Ad 1. Electron transfer

The p-type doped polymers are formed if an electron is removed from the HOMO orbital by the oxidising agent.[28,29] Because the conjugated polymers are electron rich, many electron acceptors like Br_2, I_2, H_2SO_4, $HClO_4$, $FeCl_3$ work very well. This phenomenon was first described on acetylene doped with bromine vapours. In the case of n-doped polymers, a reducing agent (Na/K alloy, LiI) provides an extra electron to the LUMO orbital (Scheme 2). The n-type conductive polymers are not so common because the electron is introduced into the already rich structure. A strong reducing agent is necessary while a mild oxidising agent can be used for the majority of conjugated polymers, e.g. polypyrrole, polythiophene or polyaniline.

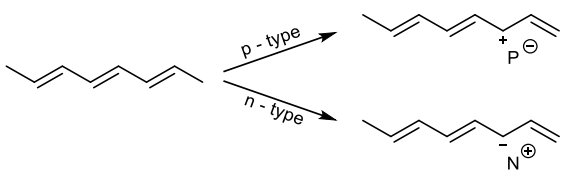

Scheme 2. The schematic structure of n- a p-type polymers

Ad 2. Chemical Structure

The conjugated polymers with inorganic dopant are generally good semiconductors due to the high mobility of small doping molecules in their structure. We can find in the literature that conductivity of polyaniline doped with $HClO_4$ can be as high as 109 S/cm while the same polymer doped with bulky HI has lower conductivity of 0.02 S/cm.[30] The majority of conductive polymers are prepared electrochemically or chemically in the solution. If the electrochemical approach is used the more ionic nature of doping agent significantly improves the overall result.[22,31] The most commonly exploited electrochemical salts have the formula MX where $M^+ = Li^+$ or N^+Bu_4 and $X^- = ClO_4^-$, BF_4^-, PF_6^- or $CF_3SO_3^-$.[32] It was published that the best sulphate for electrochemical synthesis of conductive polymers is K_2SO_4 and KCl as a member of chlorides.[33,34] On the other hand, electrolytically poor inorganic compounds ($FeCl_3$, $SnCl_4$, $NOPF_6$) are preferred when the polymers are prepared by chemical oxidation in the solution.[35] The frequent problem associated with inorganic dopants is their sensibility to moisture and therefore more environmentally stable organic dopants are used alone or together with other supporting molecules.

Although the insolubility of conductive polymers is caused by strong π-π interactions in their structure the proper choice of dopant can alter their solubility. Polypyrrole is often doped with some derivatives of sulfonic acid to improve environmental stability. The resulting polymer is not only more stable but can be dissolved in common organic solvents (DMSO, *m*-cresol, CCl_4). Such feature at first glance does not necessarily look attractive, but higher solubility of final polymer greatly enhances its processability. The introduction of bulky organic dopant with charged sulfonic group interrupts π-π conjugated system and thus increases solubility. Despite the slightly lower conductivity if compared to polymers doped with small and very mobile inorganic anions this approach represents a promising way to future applications.[36]

Polymeric dopants are typically functionalized polymers which improve environmental stability of the conductive polymers. One of the common polymeric dopants is PS-sulfonic acid. It helps with the deposition of conjugated polymer but at the cost of reduced conductivity. The problem probably lies in the weak interaction of huge dopant with considerably rigid polymer structure. If a co-dopant is used, this drawback can be overcome, and the conductivity increased. However, only chemical synthesis can be used for polymer doped conductive polymers because electrochemical preparation is almost impossible.

Ad 3. Doping mechanism

An electron transfers between conjugated polymer and doping agent may not be absolute because the shift of electron density inside the molecular orbitals is sufficient. The ionic redox dopants are firmly bound to the polymer structure in the form of polymeric salts. It is the most common and preferred route for the preparation of conductive polymers *via* electrochemical or direct chemical technique. Non-redox or neutral doping is also used primarily when the acids

work as a doping agent. There is no electron transfer, and the reversible undoping is possible/problematic. Even though examples of environmentally stable material with high conductivity can be found, e.g. dodecyl sulphate doped polypyrrole with conductivity 10^2 S/cm.[37] Next, the self-doped polymers can be prepared to start from suitable monomers. These conductive polymers have covalently bound dopant to their conjugated backbone forming a zwitterion structure (Figure 3). While the conductivity is average and the polymers are often water soluble, which hamper potential application a compelling advantage can be found. The self-doped polymers are pH-independent due to a significant number of available protons.[38] Let us mention another rarely used doping mechanisms which are induced doping, photodoping and charge induction. The induced doping is caused by electron transfer from the appropriate functional group, e.g. O^-Na^+ as already published.[39] The last two doping mechanism are scarcely used because the emerging charge is quickly lost under ambient conditions.

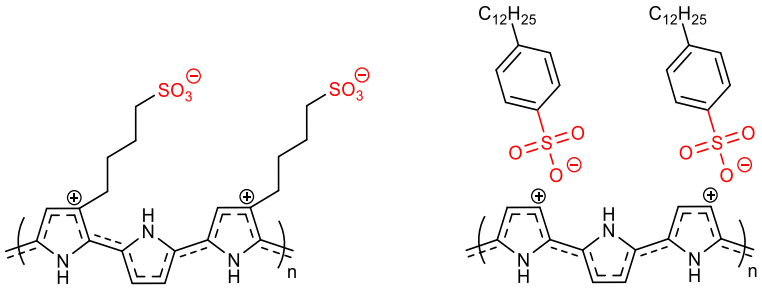

Figure 3. Self-doping of polypyrrole (left) vs common doping with DBSA

2.2.4. Doping techniques

Although dip-coating, layer by layer deposition, self-assembly, vacuum deposition or Langmuir-Blodgett technique are well-established methods, they are beyond the scope of this work. The following text will be thus focused on the electrochemical[40] and chemical[41] techniques used for the preparation of conductive polymers. The electrolysis is not only a great tool for the synthesis of conductive polymers but also an interesting method for the study of their properties.[42] In general, a three-electrode setup is used for both types of polymers (p-type = oxidation, n-type = reduction on the metallic electrode). The voltage can be regulated during the experiment to get control over the distribution of the doping agent in the bulk material. The resulting polymer can be doped *in-situ* during preparation or later in a separate step. However, the one-pot synthesis is preferred because in many cases the resulting polymer has poor mechanical properties with a tendency to peel off the electrode even though some flexibles polymers have been prepared as well.[43] There is a huge variety of available working electrodes, e.g. platinum, stainless steel, gold, indium tin oxide, titan oxide or glass. The same choice exists for the type of electrolyte used and supporting salt like tetraalkylammonium halides. The common non-nucleophilic protic solvents

for electrochemical deposition of conductive polymers are acetonitrile or benzonitrile. However, if the simplicity is taken into account, a direct chemical route brings several advantages over the electrochemistry. First and the most obvious benefit is that no special equipment is needed and the size of the working electrode does not limit the process. Chemical synthesis is also very straightforward and can be easily upscaled. The electrochemical deposition is preferred when some extra control over the polymer formation is needed whereas chemical synthesis in the solution represents a universal approach. A doping process can be done in the gas phase in a closed chamber under reduced pressure as well. An important benefit is that introduction of the same level of doping agent takes a shorter time if compared to the complementary reaction in the solution, e.g. acetylene doped with iodine[44] (vapour 3 h, solution 8 h).

2.2.5. The effect of doping on conductivity

Until now we were talking about the structure of conjugated polymers and how a variety of doping techniques can tune their properties or doping agents. However, about the future application, we should thoroughly discuss the conductivity as the most important parameter associated with conjugated polymers. This phenomenon was precisely described for metals by "The electron sea model". In a metallic bond, electrons are delocalized in the structure and do not orbit the specific nucleus. Therefore, the positive atomic nuclei are surrounded by the sea of delocalized electrons which are free to move and to carry electric current. While the Ohmic materials exactly obey Ohm's law, the electron transfer in semiconductors is described by Fick's law. The conductivity thus depends on the number of electron, charge and the charge diffusion in the lattice.[45] Finally, the mechanism of electron transfer for the inherently conductive polymer is different due to doping, where the overall performance is governed by the mobility of the doping agent and its ability to maintain the electroneutrality. There is a certain threshold for doping of conjugated polymers which depends mainly on charge defects in the polymer structure, charge transfer and dopant migration.

The charge defects and inhomogeneity in the structure of conductive polymers represent a wide topic. It can be simplified to several sentences which help us understand how the undoped and doped state of polypyrrole looks like (Figure 4). The neutral polypyrrole is first oxidised to a cation-radial state called the polaron. Further, bipolaron is created by single electron transfer resulting in a dicationic polymer structure. These structural defects are compensated by dopant which is responsible for electron transfer along the conjugated backbone.

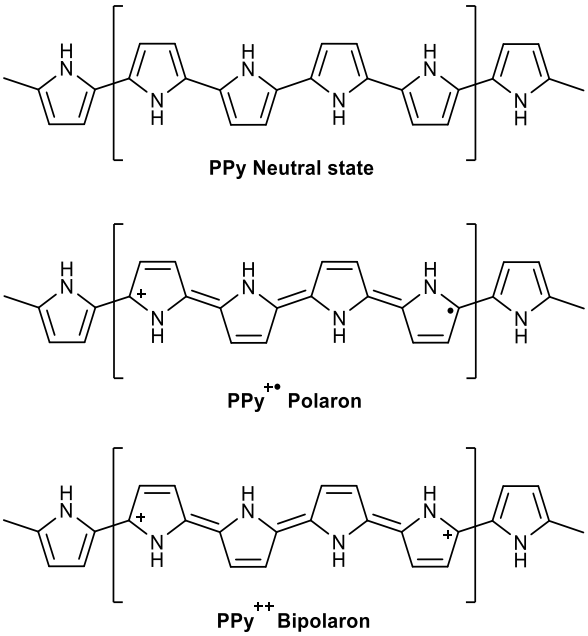

Figure 4. The structure of neutral undoped PPy and corresponding doped states

A dominant mechanism for charge transfer is via polaron or bipolaron structures. Due to dopants strong coulombic interaction, the electrons "hoping" between specific electronic states. The ionising potential is defined as energy need to transfer an electron from the HOMO orbital to the vacuum. On the other hand, electron affinity reflects how easily can be electron transfer from the vacuum to LUMO orbital. Therefore, easily oxidizable polymers have low ionising potential, whereas high electron affinity represents the state when the polymer can be easily reduced. These two parameters are only responsible for the stability of the created charge, but a suitable orbital system is also required to achieve good conductivity. The afford mentioned band gap is expressed as the energy between HOMO and LUMO orbitals. Hence, the lower band gap is, the better electron transfer to the conductive band can be achieved. This energy gap almost does not exist for metals, where electrons can freely move in the sizeable orbital system and thus give the excellent material conductivity. The last parameter connected with electron transfer is the bandwidth which reflects the width of the delocalized system and also increases conductivity due to higher interchain charge mobility.

The ion mobility is not the only limiting factor for charge migration. The crystallinity also plays a vital role in the electron or hole migration across the polymeric skeleton. In the field of conductive polymers, the charge can move in three ways.[45] The first mechanism is mediated *via* intrachain and intramolecular delocalized π-system. The second way is done by charge "hopping" between molecules (interchain or intermolecular). The last possible mechanism is the interparticle transfer called perlocation. Although some aspects of charge transfer are not apparent, several factors that influence the overall conductivity can be postulated. The factors like the crystallinity, the planarity of the conjugated system or crosslinking of the polymer chains can be sum up as a

structural effect. The communication of the macrocycle with the doping agent is closely related to its size, shape and chemical nature. However, the suitable orbital overlap is the ultimate predisposition for the proper charge mobility.

The role of dopant is to keep electroneutrality of conjugated polymer, which can be explained as a migration around some neutral state. The electrons move freely in the polymer structure if an external field is applied and the doping agents compensate such imbalance. The migration is the best in the homogeneous materials, but there is always some structural inhomogeneity. Although bulky organic dopants are less mobile than their small inorganic counterparts, they significantly improve environmental stability. At low applied potential the conductive polymers obey Ohm's law, and the diffusion is the leading mechanism of electron transport. However, the mechanism of charge transport is different when the high potential is applied for an extended period. Another critical parameter connected with conductivity is the level of doping. It was mentioned early in this work, that semiconductors are doped at ppm level to achieve desired electronic properties. On the other hand, the concentration of dopant in the structure of conductive polymers should be ideally in the range 0,1 – 0,5 %. The conductivity does not increase above a certain saturation threshold because the mobility of charge carriers is reduced.[46] The amount of incorporated dopant into the polymer backbone can be measured by elemental analysis, gravimetric methods and spectrometric techniques like EDS or XPS.

2.2.6. The properties and application of conductive polymers

Upon doping the electrical, optical, magnetic and structural properties are altered.[47] The most profound feature of conjugated polymers is in fact that doping can significantly improve conductivity by several orders.[28] However, it is difficult to obtain the polymer with precisely the same level of doping every time. Especially the inorganic dopants are prone to leaking which decreasing the conductivity and limits the final application. However, the conductive polymers represent and interesting compounds which are a great alternative to the traditional materials. The spectroscopic properties are closely related to the delocalized π-conjugated system of mixed energetic states of HOMO and LUMO molecular orbitals. While undoped conjugated polymers are usually colourful, a strong red-shift can be found in doped analogues. The difference between undoped, poorly doped and highly doped conductive polymer is nicely reflected in their UV-VIS spectra. Hence, a doping process brings new absorption bands to the spectrum. A delocalisation is responsible for the significant bathochromic shift in the FTIR spectra due to the weakening of covalent bonds. The Raman spectra are an excellent tool for the study of polaron and bipolar while the solid phase NMR is sensitive to the microscopic changes in the polymer structure.[48,49] The ultimate technique for the study of unpaired electrons in the materials is EPR because the mechanism of doping is closely related to the structure of polarons.

Further, the superior analytical tool for the study of electrochemical properties is cyclic voltammetry or electrical impedance. The electrochemical approach for the synthesis of conductive polymers offers not only to control over the process but is also the analytical method. The influence of temperature on the conductivity is an important topic considering the future application of conductive polymers. The conductivity decreases with rising temperature for the metallic compounds because there is too many moving charge carries and the energy is dissipated in the crystal lattice. However, the current flows better in the semiconductors and the conductive polymers at the elevated temperature due to the higher mobility of charge carries (dopants). A doping process could disturb the structural properties or even crystallinity when the bulky dopant is incorporated into the polymer. Therefore, the dopant-polymer interaction is responsible for the higher ratio of amorphous/crystalline domains.

If we search the Web of Science for the keyword polypyrrole (topic), we can find over 6500 records over the past five years. The most cited articles are focused on supercapacitors, sensing/imaging and also tissue engineering. The reason why conductive polymers attract so much attention is their intrinsic conductivity, variable ways of preparation and tunable properties. On the other hand, there are some issues mainly the inclination to oxidation/reduction changes. Nevertheless, conductive polymers have the potential to become the key players on the field of chemical biosensors[50,51], smart electronic devices, e.g. OLEDs[22] or tissue engineering.[24,52,53] The conductive polymers are studied as sensitive O_3, NO_2, H_2S or other gas sensors which change colour upon the interaction with the analyte. The conductive polymers can be deposited onto various materials (nanoparticles, fibres, flat surfaces, carbon allotropes or even cells[54]) creating a homogeneous nanometre thick layers. Mao et al.[43] recently published synthesis of PPy membrane on the water/chloroform interface. Interestingly, template-assisted oxidation afforded pristine polymer which is flexible even in liquid nitrogen.

The ionic nature and of doped polymers increases their biocompatibility which is utilised in the area of neural implants.[55,56] These conductive materials can be specifically designed to improve cell-surface communication and enhance neuronal growth.[57–59] It was found, that neuron stimulation using electric field leads to an extension of axons length in given direction.[60–62] The combination of conductive polymers with oriented electrospunned fibrous scaffold could further support cell growth in a controlled way.[63,64] Although the neural tissue regeneration still represents a considerable challenge[65], several novel materials and promising biological experiments give hope to people with spinal cord injuries or other similar diagnoses.

2.3. Cell-material interaction

Thousands of promising materials for tissue engineering have been made over the last years. Inorganic, as well as organic materials, found their place in modern medicine, but an ideal material for replacing damaged tissue has not been found yet. Chemical and physical properties of bulk material are well understood and can be tailored according to the desired application. The surface topography and morphology are the next things to consider before designing a new scaffold. Cells can sense different surface roughness even at nanometer level which can cause apoptosis in the worst case. An overall cellular-surface response may be understood as biocompatibility.[66] Such a material improves biological functions, adhesion and growth of cells while it does not cause an inflammatory reaction.

2.3.1. Cell guidance

Materiobiology is a cross-disciplinary field which combines knowledge from biology, chemistry and engineering.[67,68] With an emphasis on understanding interactions between cells and material, we must distinguish between mechanical and chemical properties of the newly designed scaffold. The situation is complicated because we study a dynamic system which can alter its properties based on external stimulus.[69] Further, cells exist in many different shapes, types and functions. So we are striving to outwit the nature that had worked millions of years on the perfection of simple molecules before she finally created a sophisticated living organism.[65]

To design advanced material for tissue engineering we have to track the essential biological signals which drive cell-material interactions.[70] The cell is a fundamental structural and functional unit of all living organisms. While the genetic information is stored in the core protected by the cell membrane surrounded by cytoplasm with several different organelles, the outer phospholipid bilayer physically separates intracellular from the extracellular space.[71]

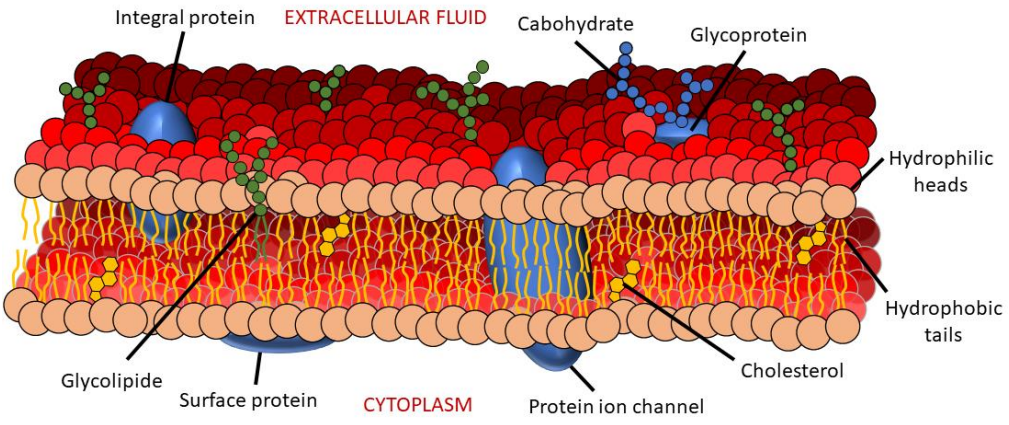

Figure 5. The structure of phospholipid bilayer

It is also responsible for membrane transport and communication with the surrounding environment. Interaction is mediated by different membrane proteins which establish and maintain action potential. The plasma membrane also contains carbohydrates, glycoproteins and glycolipids that enable communication between cells and material. These interactions can be explained in a very simplified manner as follows. First, the surface is covered by ECM proteins to form a dynamic equilibrium. Then, cells bind to adhered proteins *via* specific membrane proteins called integrins. After initial interaction, cells begin to secrete their own proteins and communicate with other cells by one of many signalling pathways. The result is the gene expression followed by cell replication on the protein covered surface (Figure 6).

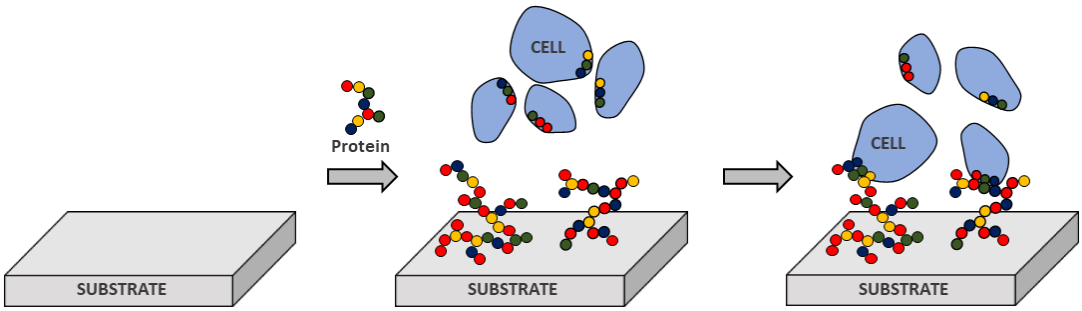

Figure 6. Cell-substrate interaction *via* integrin receptors

Integrins are dimeric transmembrane proteins existing as two noncovalently bound α– and β– subunits. There are known 18 α– and 8 β–subunits that combine to at least 24 integrin heterodimers. Each subunit of αβ–heterodimer consists of large 80-150 kDa extracellular domain responsible for interaction with ECM proteins, e.g. laminin, fibronectin, collagen or other biomolecules. The α–subunit also contains an additional domain for exclusive divalent metal cation (Mg^{2+}) and thus play an essential role in protein-ligand binding. Upon interaction, the signal is transduced through the short 25-29 amino acid transmembrane domain that forms an α–helical coiled coil. The intracellular part of integrin is generally unstructured heterodimer consisting of 10-70 amino acid residues. The role of the intracellular domain is the signalling *via* different intracellular proteins (e.g. talin, kindlin, vinculin) that play a crucial role in integrin activation and binding to the actin cytoskeleton.[72] The outside-in signalling is a dynamic process strongly influenced by cross-talk between growth-factors and other intracellular biomolecules. It is estimated that single integrin-matrix interaction activates signalling cascade to form complex focal adhesion assembly of more than 1500 different intracellular proteins. Cadherins also represent a large group of calcium-dependent adhesive molecules for cell-cell junction. They are responsible for cell communication by transferring mechanical stimulus to biochemical signals. This mechanotransduction is mediated by various cell junctions including gap-junction, tight-junction or anchoring-junction whose understanding is a significant challenge.[73]

2.3.2. Surface chemistry, morphology and topography

When designing a new scaffold for tissue engineering the structure and physicochemical properties which drives the cell-material interaction should be deeply understood.[74] It has been proven many times that energy, polarity and wettability of material surface play an essential role in cell adhesion.[75] Extremely hydrophobic neither hydrophilic materials are not suitable for cell growth due to weak interaction with adhesion-mediating proteins, e.g. fibronectin or vitronectin. However, such a statement is not entirely correct. Whereas hydrophilic materials do not allow proper surface-protein interaction, hydrophobic materials could often adsorb high amount of protein but in their unnatural geometrical conformation. It ultimately leads to a loss of selectivity towards membrane receptors responsible for cell binding. Materials are thus modified using dozens of physical or chemical techniques. One of a favourite and straightforward method for surface polarity enhancement is plasma treatment which found numerous applications across the scientific fields. Synthetic polymers with WCA higher than 100 ° can be easily modified to suit the requirements of scaffold for tissue engineering better. Unlike the chemical modifications, where retention of toxic substances often occurs, plasma treatment offers an interesting approach for material functionalization.[76] Moreover, newly created reactive sites on the surface can be used for immobilisation of various compounds and thus speed up the development of more suitable implants. Polymers can be modified 10 nm – 100 μm deep by ion bombardment. Such surface treatment leads to cleavage of C-C and C-H bonds to form conductive graphite-like structure. The degradation products also react with air oxygen resulting in polar groups (carbonyl, carboxyl, ester) introduction.[77–79] Newly created binding sites are thus commonly used for the connection of helpful molecules with a profound effect on the cell adhesion, proliferation or growth.

The surface charge can also significantly alter the performance of the substrate on cell-material interaction. Although the positive effect of NH_4^+ cation on the protein adhesion has been described, the proper spatial orientation of adsorbed proteins is considered as the most important predisposition.[80] This effect was compared between NH_2 and COOH embedded PP surface on endothelial cell growth.[81] Nevertheless, the importance of charge on the surface was experimentally verified with embryotic starfish cells, endothelial cells or platelets as well.[82,83] Despite the observed influence of surface wettability and polarity on the cell survival, negatively charged SO_3^- groups are normally introduced to protect the surface form protein adhesion and blood clotting.[84,85] Conductive materials for tissue engineering are also an important class of scaffolds with potential application in the field of medical devices. However, various compounds, e.g. carbon nanotubes must be grafted into the polymer structure to create suitable conductive material. Intrinsically conductive polymers have a profound effect on cell growth even without external electric stimulation. If the electric or magnetic stimulation is applied a selectivity of Ca^{2+} dependent receptors can also be influenced.[86,87]

Surface roughness and morphology can be described according to the size of irregularities. Roughness is generally measured as a peak to valley height although the exact mechanism of cell colonisation on the differently rough surfaces is still unclear.[88] The first problem is that only the peak to valley high is measured while the peak to peak distance, sharpness or shape of the peaks are not considered. Moreover, cell behaviour is strongly dependent on different physical and chemical parameters which are making this issue even more complex.[65] The results published by independent research groups are thus hardly comparable. The information about the positive influence of the macro-roughness (1 mm – 100 μm) on cell growth has been reported, but the size of surface irregularities is bigger than the cell diameter. A higher specific surface area is probably responsible for this occasionally seen influence. The situation is getting interesting with smaller surface irregularities in the range of 100 μm – 1 μm. Micro-roughness is considered as a controversial topic because several authors reported a positive influence on cell growth whereas the others negative effect.[89,90] But, it can be said that some bigger cells with the large spreading area, e.g. mammal cells are affected by surface roughness at the micrometre level. Sub-micro irregularities with a peak to valley height 1 μm – 100 nm have a dual effect and are strongly dependent on the material and corresponding cell line. Literature is inconsistent with the question of whether sub-micro roughness affects cell attachment and proliferation. General conclusions are thus still missing. The situation is different in the case of nano-roughness with surface irregularities lower than 100 nm. The scientific community unanimously confirmed the positive influence on cell colonisation. There are several reasons responsible for such an interesting phenomenon which is widely used in material research. Nanostructured surfaces are closely mimicking the native extracellular matrix and provide better cues for the interactions with adhesion-mediating proteins. These proteins are present on the surface in their native conformation and serve as a binding place for the interactions with many different types of membrane receptors. Such feature works synergistically with suitable surface energy, charge or wettability which was mention earlier. Therefore, even materials with optimal mechanical properties but a highly hydrophobic surface which is normally poor for cell colonisation can be improved by suitable grafting technique. Carl published an article where the polarity of hydrophobic planar PP was compensated by mixing of polymer with carbon nanotubes. The nanostructured surface affected the spatial conformation of adhesion-mediating proteins and as expected improved cell growth.[91] ELISA also confirmed the higher talin and vinculin expression. Osteoblasts prefer nanostructured surfaces whereas fibroblasts, chondrocytes and smooth muscle cells are less favourable.[92,93] It is caused by better adsorption of small and linear vitronectin in comparison with larger ECM proteins, e.g. laminin.[94] Vitronectin is preferred by osteoblasts where the cell-protein recognition is mediated by the interaction between heparin-sulphate proteoglycan and Lys-Arg-Ser-Arg (KRSR) through the heparin-binding domain of vitronectin.[95,96] Another possible way for the cell-protein interaction is *via* classic

Arg-Gly-Asp (RGD) amino acid sequence. This pathway is also responsible for interaction with other cell lines. The positive effect on the cell attachment and growth was observed for rat vascular endothelial cell as well for smooth muscle cells.[97] Also, nanostructured materials reduce the risk of negative immune reaction or inflammatory response to the new implant. It was found, that PLA nanofibrous scaffold exhibits lower secretion of macrophages in the medium if compared to the similar planar film.[98]

The rigidity and deformability of potential scaffold for tissue engineering are taken into account much less than surface chemistry (polarity, wettability, charge).[99] However, mechanical properties play a key role in the formation of material-adhesive complexes.[100] They are responsible for the assembly of the actin cytoskeleton and subsequent cell spreading, survival and growth. In this example, a general cellular behaviour can be seen because nature does not like extremes. It is hard to maintain a proper cell-material interaction *via* adhesion-mediating protein while the softness of the substrate is constantly disturbing the equilibrium between surface and the ECM. Such interaction finally leads to the expression of regulatory signalling proteins and suppression of the cell life cycle.[101] The analogy can be seen in the behaviour of cells cultured on the hydrophilic or soft matrices. There is a problem with the formation of stable protein adhesion either due to weak interaction of binding sites or by strong traction forces produced by cells. Stiffer substrates are thus favourable for the cell-material interaction and are better tolerated by various types of cell lines. Interestingly, material stiffness is a decisive factor directing cell differentiation towards certain phenotype.[102,103]

In order to create materials with changing the surface composition or physical properties, lithographic techniques, plasma polymerisation, 3D printing, laser beam writing can be commonly used today. Such micro- or nanopatterned surfaces are then utilised for the preparation of the novel drug-delivery system, biosensors, advanced genomic or cell microarrays. Thanks to modern methods we can tune material properties according to the desired application. Therefore, cell behaviour can be regulated by the type, number and distribution of surface-bound ligands. These binding places are then recognised by the specific integrin receptor located in the membrane of the certain cell which gives us another tool in the development of bio-mimicking scaffold. The most profound ligand for cell-material interaction enhancement is RGD amino acid sequence, although it is specific towards all cell types.[104] But, several examples of amino acid sequences with high selectivity are often used, e.g. REDV sequence for vascular endothelial cell or VAPG/KRSR which is specific towards vascular smooth muscle cells and osteoblasts. Mann and West published an interesting article[105] where fibroblasts metabolic activity decreased with the increasing concentration (0.2 nmol/cm^2 – 2 nmol/cm^2) of the surface-bound ligand. It was also found that even low concentration of amino acid ligand GRGDSY has a significant impact on cell proliferation and growth.[106] Therefore, nanopatterned materials can modulate the cell activity by tailor-made surface irregularities and exact distribution. It was postulated[107], that distance

between such irregularities should be 58 – 108 nm in order to achieve the best results. Apart from the precisely tuned surface structure of patterned materials, electrospun oriented fibrous scaffolds showed a great effect on the phenotype maturation and differentiation if compared to the random fibrous material.[63,108,109] The aligned fibres could force the filaments to order while the random fibres do not affect.

It is known that cells grow on the substrate surface thanks to interactions through the specific binding places. Based on the initial communication, the cell spreads over the surface which stimulates further proliferation. The biochemical or chemical pathway controls this process and are responsible for cell growth. Both possible mechanisms start with adsorption of cell-adhesion mediating proteins followed by the interaction of active binding places with integrin or non-integrin (proteoglycan based) membrane receptors. This interaction initiates a complex signalling cascade starting from membrane receptors which communicate with signalling proteins connected to the actin cytoskeleton. The biochemical pathway is initiated through the activation of signalling components in the focal adhesion plaques.[110] These regulatory signals are then transmitted into the cell core which ultimately leads to the DNA synthesis and cell division. Mechanical cues also influence the cell life cycle. Strong traction forces move with every cell organelle using actin filaments as a stimulation mediator.[111] Mitotically active cells typically do not have well-formed adhesive plaques. Therefore, thin active microfilament can be temporarily detached off the substrate which allows necessary cytoskeleton reorganisation before cell mitosis.

The conclusion of this chapter could be the statement, that artificial materials for tissue engineering have gone through an extensive development over the last few decades. Considering novel methods for scaffolds preparation, we can tune the physicochemical properties according to the desired application. The potential implant can also be functionalized with various active biomolecules which finally improve cell-material interaction or serve as a drug-delivery system with controllable release profile.

3. RESULTS AND DISCUSSION

3.1. Retrosynthesis of target compounds

The retrosynthetic approach leading to the target conjugates is described below (Scheme 3). We can start the retrosynthetic analysis of compound **A** with C-N bond disconnection. All mono substituted cyclodextrins **C**, **D** and **E** are easily accessible and can be synthesized from commercially available β−cyclodextrin **F**. Further, molecule **B** with tuneable carbon linker length can be prepared by extension of procedure published by Stefan et al.[112] First, pyrrole **J** is protected at nitrogen with bulky group and then compound **I** is selectively mono-brominated at position C3. Alkylation of compound **H** yields molecule **G** which is subsequently transformed into **B** using metal-halogen exchange reaction. The final conjugation between amino cyclodextrin **C** and activated ester of molecule **B** gives target molecule **A**. In the case of molecule **K**, a double C-N disconnection provides synthon **L** and the azido cyclodextrin **D** as was described before. Molecule **L** can be directly prepared from **G** by S_N2 substitution of halogen with acetylide anion. Conjugation of **K** and **L** is then carried out by CuAAC as a final synthetic step.

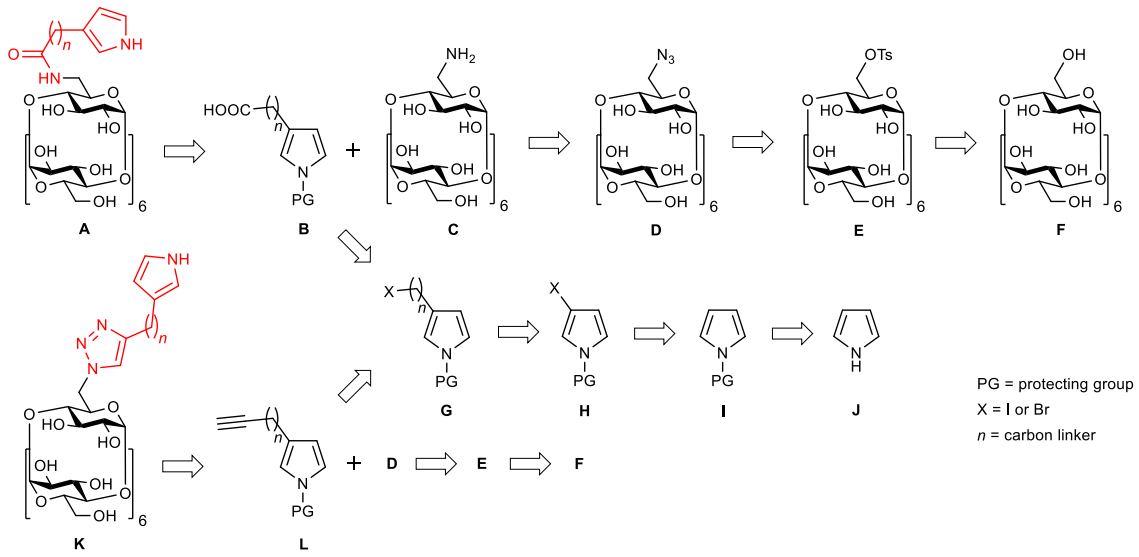

Scheme 3. Retrosynthetic analysis of target pyrrole-cyclodextrin conjugates

3.2. Synthesis of pyrroles for CD conjugation

3.2.1. Substitution of pyrrole at β–position

As was previously mentioned in the first part of the thesis, the β–substituted derivatives are not directly accessible by electrophilic aromatic substitution. Thus, pyrrole **1** was firstly protected at nitrogen with bulky TIPS group to enhance the selectivity of the next reaction step (Scheme 4). Treatment of pyrrole **1** with 1.1 eq. of sodium hydride in dry DMF at 0 °C for 2 hours under argon afforded product **2** in 68% yield after final vacuum distillation. This product is also available commercially. The selective derivatisation of compound **2** at the β–position was carried out in THF at -78 °C using 1.05 eq. of NBS as a brominating agent. After purification by vacuum distillation, the product **3** was obtained in 81% yield together with 5 % of α–isomer **4**.[10] It is generally known that bromo compounds are less reactive in Pd-catalysed cross-coupling reactions. Therefore, the corresponding iodo pyrrole derivative **5** was prepared by halogenation of **2** with 1 eq. of NIS at low temperature in excellent yield as well.[8]

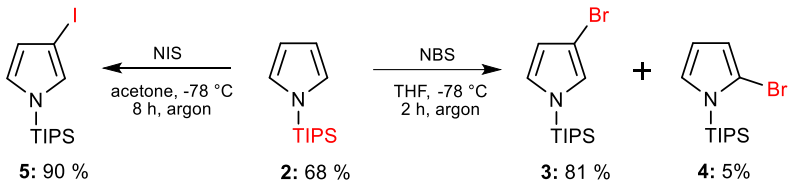

Scheme 4. Synthesis of mono halogenated pyrrole derivatives

Halogen substituted derivatives **3** or **5** were alkylated by 1,5-diiodopentane and 1,10-diiododecane. The starting compound was subjected to metal-halogen exchange reaction with *n*-BuLi in THF at room temperature and the *in situ* generated lithium intermediate was reacted with an excess of the alkylating agent (Scheme 5). Products **6** and **7** were isolated after column chromatography on silica gel in 67% and 43% yield respectively.

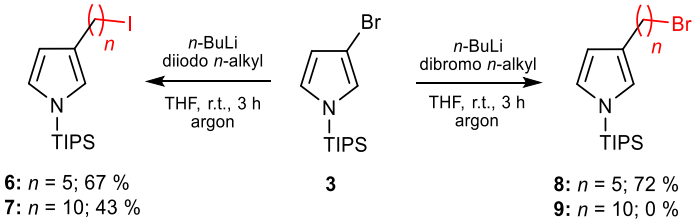

Scheme 5. Alkylation of β–substituted pyrrole **3**

Both new compounds were characterised by HRMS, 1D and 2D NMR spectroscopy. Three signals of corresponding hydrogen atoms in aromatic part of the ^{1}H NMR spectrum suggested the monosubstitution of the pyrrole ring. The rest of the signals were assigned to alkyl

chain with terminal iodine and the nitrogen protecting TIPS group. Combined information obtained from COSY, HSQC and HMBC spectra confirmed the structure of compounds **6** and **7**.

Because the 1,5-dibromopentane is roughly 15 times cheaper than the corresponding iodo compound, it can be used instead. Another benefit is that the excess of 1,5-dibromopentane can be easily distilled off after the reaction. Hence, the chromatography of crude product is more straightforward, and the unreacted alkylation agent can be recovered. The compound **8** was prepared in good yield, but low reactivity of 1,10-dibromodecane against lithiated intermediate was found despite the published literature.[112] Only a trace amount of product **9** was formed even when the reaction time was prolonged from 3 to 24 hours. Thus, a cheaper 1,5-dibromopentane was used for the synthesis of derivatives with five carbon linker, and the more reactive 1,10-diiododecane was used as an alkylating agent for the synthesis of derivatives with a longer linker.

3.2.2. Synthesis of pyrroles with the carboxylic group

Treatment of **3** with *n*-BuLi followed by addition of dry ice afforded pure compound **10** in 88% yield after recrystallization from EtOAc (Scheme 6).[10] Pyrrole-carboxylic acids **11** and **12** were synthesized by modified procedure published by Stefan et. al.[112] First, we took over their original protocol, where **8** was transformed into Grignard reagent and reacted with excess of CO_2. However, the reaction of Mg pellets catalysed with I_2 in dry etheric solvent failed. Thus, *t*-BuLi was used to generate reactive nucleophilic species at - 78 °C in THF and after that dry CO_2 was bubbled through the solution. Acidic workup afforded crude reaction product which was purified by column chromatography on silica gel with gradient elution. Pyrrole-carboxylic acids **11** and **12** were isolated in 64% and 51% yield respectively.

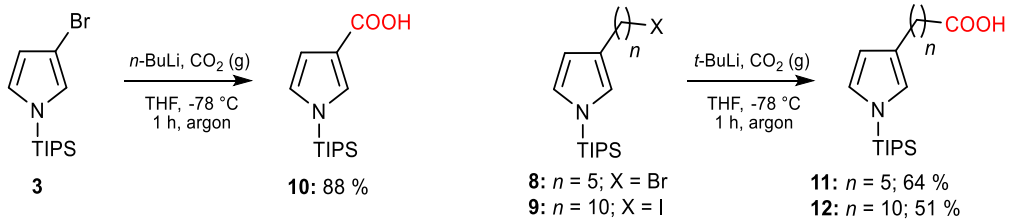

Scheme 6. Synthesis of pyrrole carboxylic acids

3.2.3. Synthesis of pyrroles with a triple bond

Despite the simplicity of the pyrrole structure only a few examples of triple bond substituted derivatives are published. It may be caused by instability of some molecules with a free terminal triple bond or unnecessary use of these compounds before the CuAAC reaction rediscovery.[113–115] Therefore, a new synthetic route for the synthesis of a triple bond substituted pyrroles with tuneable carbon linker length (0, 4 or 9 carbons) has been developed (Scheme 7).

First, the synthesis of pyrrole **15** with directly connected triple bond was examined. Starting from iodo derivative **5** the compound **13** was prepared using the Pd-catalysed Sonogashira cross-coupling reaction in 66% yield.[8,116] It was reported that deprotection of this compound with 1 eq. of TBAF provides unstable product **14** which spontaneously decomposes. Thus, selective deprotection of the TMS group by K_2CO_3 in methanol at room temperature was carried out to afford target molecule **15** in reasonable yield. Later, our synthetic protocol was improved, and compound **15** was synthesised directly from iodo pyrrole **5**. Coupling of compound **5** with ethynylmagnesium bromide under Kumada reaction conditions opened a straightforward way to the target molecule **15**.[117–119] A great advantage of this one-step procedure are high selectivity, mild reaction conditions and easy purification.

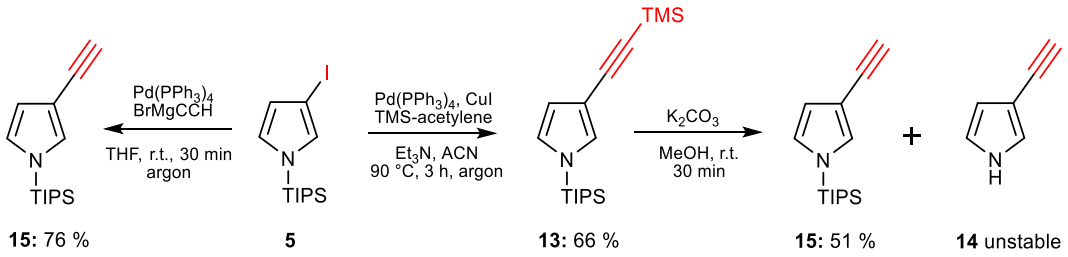

Scheme 7. Synthesis of TIPS-protected pyrroles with a directly connected triple bond

Further, the synthesis of pyrroles with triple bond on carbon linker was studied. Typically, molecules with the aliphatic triple bond are prepared by simple substitution of the corresponding I, Br, or Cl atom in the sense of nucleophilic substitution by acetylide anion. Surprisingly, the reaction of compound **6** or **7** with sodium acetylide, TMS-protected lithium acetylide, or lithium acetylide ethylenediamine complex in DMSO or THF afforded only a trace amount of desired product (Scheme 8).[120,121] If the ethynylmagnesium bromide was used as a nucleophilic agent an unexpected product of halogen exchange **8** was isolated in 82% yield instead of the desired molecule.

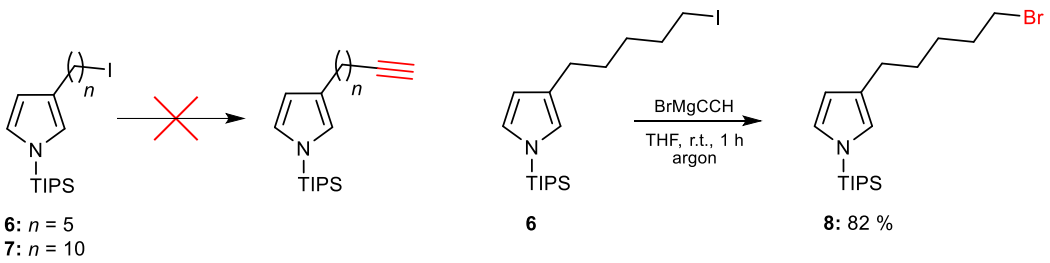

Scheme 8. Nucleophilic substitution of halogen atom with acetylide anion

Due to these unsuccessful attempts, another multistep synthetic procedure including Corey-Fuchs reaction[122] as a final transformation has been proposed (Scheme 9). The bromine atom was substituted with cyano group by reaction of **8** with NaCN in moderate yield. However, subsequent reduction of nitrile with DIBAH in toluene gave an only low yield of target aldehyde.[123,124] The key intermediate for the Corey-Fuchs reaction was finally prepared by Kornblum oxidation.[125] The reaction of pyrrole **6** or **7** with 2 eq. of $NaHCO_3$ in DMSO at 110 °C furnished crude products which were purified by column chromatography on silica gel. Aldehydes **16** and **17** were isolated in 71% and 58% yield respectively. The transformation of halogen to the carbonyl group was also carried out starting from bromopyrrole **8**, but the reaction must be further catalysed with 1.5 eq. of NaI.[126] Then, *in situ* generated iodo compound is converted into aldehyde **16**. It is interesting to mention that the Kornblum oxidation can be done in microwave reactor with high yields over 90 % as published by Bratulescu.[127] Next, geminal dibromo olefins **18** and **19** were prepared by reaction of aldehydes **16** or **17** with PPh_3, CBr_4 in DCM at 0 °C. The structure of these compounds was confirmed by NMR where the signal of the CHO group in ^{1}H NMR disappeared whereas triplet of vinyl hydrogen atom appeared around 6.40 ppm strongly influenced by two electron withdrawing bromine atoms. Finally, the triple bond substituted pyrroles **20** and **21** were prepared in almost quantitative yields by the elimination of bromines with 2 eq. of *n*-BuLi in THF at 0 °C.

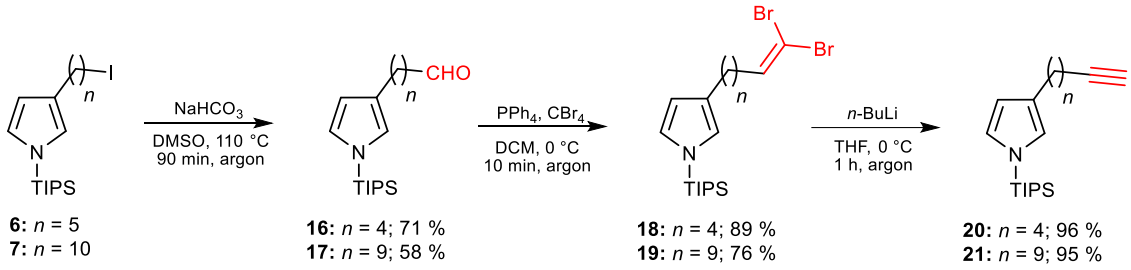

6: *n* = 5
7: *n* = 10

16: *n* = 4; 71 %
17: *n* = 9; 58 %

18: *n* = 4; 89 %
19: *n* = 9; 76 %

20: *n* = 4; 96 %
21: *n* = 9; 95 %

Scheme 9. Synthesis of pyrrole derivatives **20** and **21**

3.2.4. Synthesis of other β–substituted pyrroles

During our ongoing research on the synthesis of β–substituted pyrroles, several other useful derivatives have been prepared. Halogen atom of compound **6** or **7** can be easily transformed by nucleophilic substitution to the corresponding cyano or azido derivatives (Scheme 10). Treatment of **6** or **7** with sodium azide in dry DMF at room temperature afforded new derivatives **22**, **23** in very high yields. Azido compounds found numerous application in conjugation reaction, e.g. Huisgen dipolar cycloaddition or are frequently used as building blocks for the synthesis of amino compounds. Tuneable carbon linker length makes these pyrrole derivatives interesting for the design of novel polymeric materials. Similarly, cyano derivatives

24 and **25** were directly prepared by reaction of sodium cyanate with **6** or **7** in DMSO at elevated temperature.[128] Cyano derivatives are also useful compounds for the synthesis of carboxylic acids, aldehydes or amines.

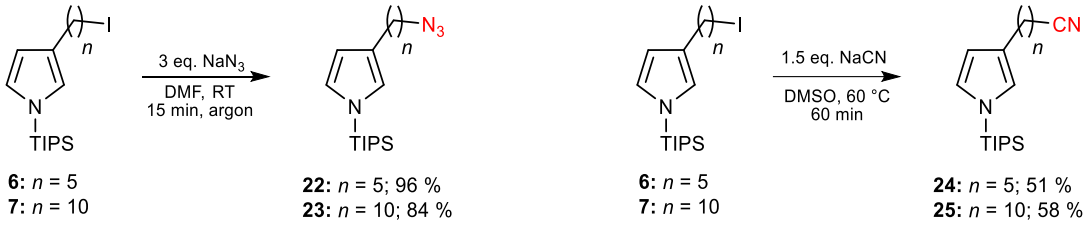

Scheme 10. Synthesis of azido and cyano derivatives **22-25**

NMR, MS and IR spectroscopy were used to characterise the structure of new pyrrole derivatives. Three signals in the aromatic part of the NMR spectra were assigned to hydrogens of the pyrrole ring and other signals to the aliphatic side chain. The characteristic sharp peak of azide in the IR spectra at 2095 cm^{-1} confirmed the successful introduction of this functional group (Figure 7). Relatively weak stretching vibration at 2247 cm^{-1} was assigned to cyano group in the case of derivatives **24** and **25**. Also, the increase of stretching vibration intensity of alkyl CH_2 groups for pyrrole derivatives **22**,**23** and **23**,**24** clearly show the difference in carbon linker length.

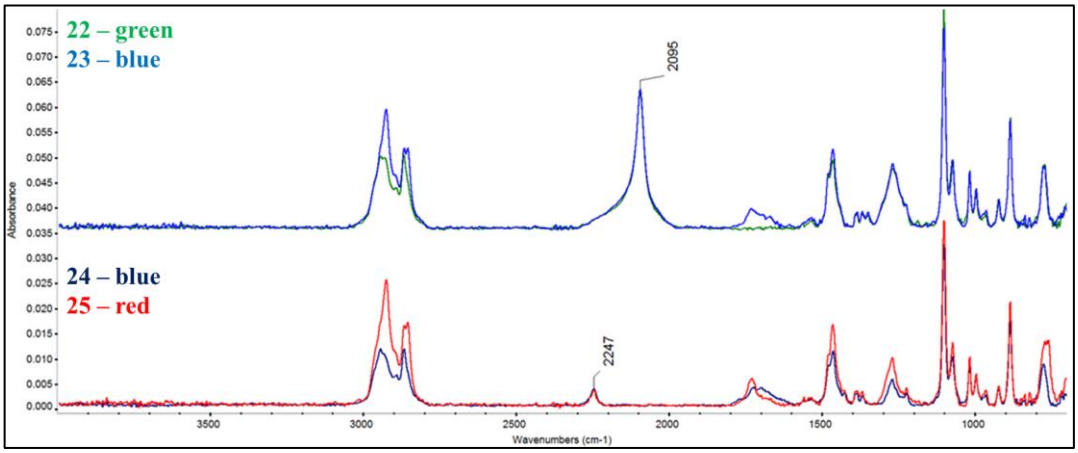

Figure 7. IR spectra of compounds **22-25** (characteristic vibrations of N_3 and CN group)

The pyrrole derivative **26** with aliphatic side chain have been prepared as well, the elimination of halogen from compound **8** afforded new derivative with a terminal double bond (Scheme 11). The reaction proceeded at elevated temperature to suppress competitive substitution. However, even when the large base (potassium *terc*-butanolate or lithium diisopropylamide) were used, the main product of elimination was extracted together with the

product of substitution. Compound **26** was separated from the reaction mixture using column chromatography on silica gel in 63% yield. Hydrogen H^3 of the double bond at 5.85 ppm has typical *cis* H^2-H^3 = 10.3 Hz and *trans*- H^1-H^3 = 16.9 Hz interaction constant in the ^{1}H NMR due to different torsion angle between interacting atoms. This signal is further split by two H^4 atoms (J = 6.7 Hz) into a doublet of the doublet of the triplet.

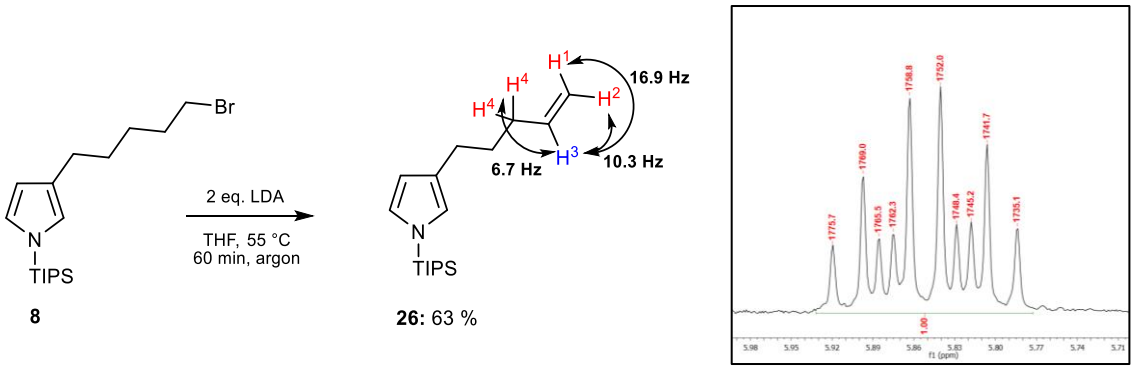

Scheme 11. Synthesis of compound **26** (the signal of H^3 atom in the ^{1}H NMR spectrum)

3.2.5. Deprotection of selected silylated pyrroles

Although many of β-substituted pyrrole derivatives without protecting group at the nitrogen atom are unstable, the possibility of TIPS cleavage from the compounds **10**, **11**, **12** and **15**, **20**, **21, 26** was examined.[8,10] The corresponding pyrroles could serve as essential intermediates on the way to tuneable polypyrrole coatings. While the pending carboxy group can be coupled with various biomolecules, e.g. growth factor or specific amino acid sequences *via* an amide bond, the multiple terminal bond offers even greater conjugation possibilities using one of many CLICK reactions. Is also generally agreed that *N*-substitution is lowering the polypyrrole conductivity due to substantial planarity disruption compared to β-substituted derivatives. The silyl protecting group was removed from all seven compounds using 1.05 eq of TBAF as a source of fluoride anion, and the crude reaction products were purified by column chromatography (Scheme 12). Three acids **27**, **28** and **29** were obtained in high yields as solids without any stability issues at standard conditions. Same reaction procedure has been used for the synthesis of pyrroles with a terminal triple bond. However, the pyrrole **14** with directly connected triple bond was subject of immediate decomposition as reported by Alvarez[8] while derivatives **30** and **31** were easily isolated after column chromatography in good yields. The pyrrole derivative **32** with a terminal double bond was synthesised by the same procedure as well.

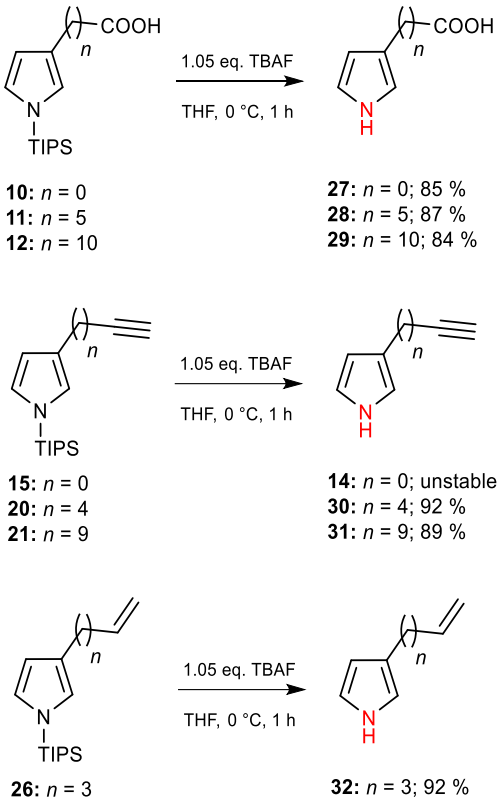

Scheme 12. The cleavage of silyl protecting group from the selected pyrroles

3.3. Synthesis of cyclodextrins

All cyclodextrin derivatives were synthesised according to published literature (Scheme 13).[129] Briefly, β–CD **33** was treated with an excess of NaOH and 1.5 eq. of *para*-toluenesulfonic anhydride in water for 2 hours. The crude reaction product was recrystallised 4 times from MeOH/H_2O mixture to afford exclusively monosubstituted compound **34**. Then, the tosyl group was substituted with azide by refluxing of **34** with 10 eq. of NaN_3 in water for 5 hours. The reaction mixture was poured into acetone, and the precipitate **35** was collected by filtration in 92% yield. Reduction of azido cyclodextrin **35** with PPh_3 and 25% aqueous ammonia in DMF rendered product **36** as a white powder in 86% yield.

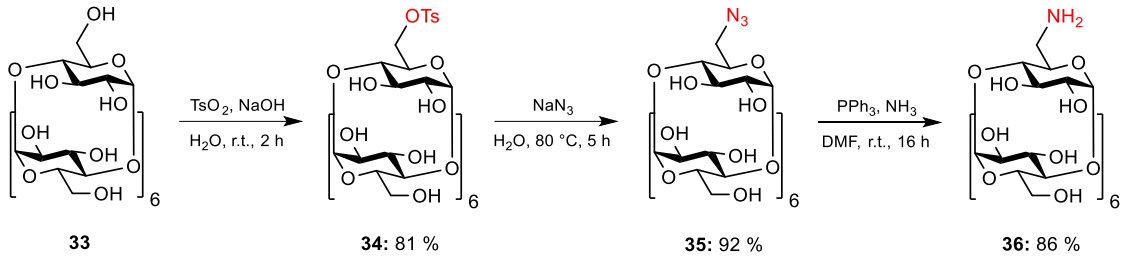

Scheme 13. Synthesis of β-cyclodextrin derivatives

The corresponding α– **37-40** and γ–cyclodextrins **41-44** were prepared by similar procedures with the only difference that the introduction of the tosyl group was carried out in dry pyridine with 1 eq. of *p*-toluenesulfonyl chloride (Scheme 14). Both tosylated products **38** and **42** were purified by precipitation and column chromatography on the C-18 silica gel. The corresponding azido and amino derivatives **39**, **40**, **43**, **44** were prepared as reported previously.

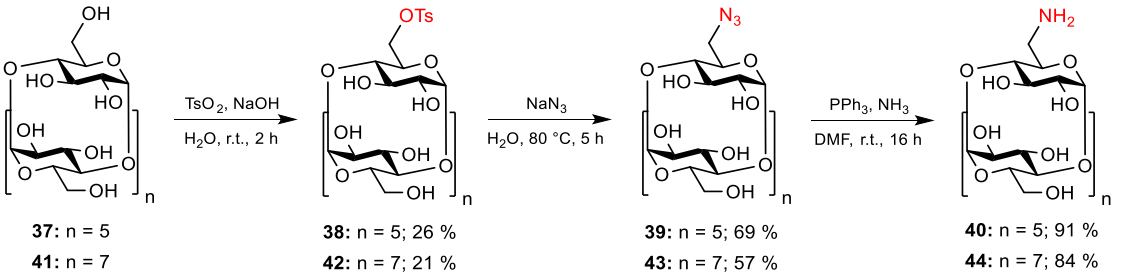

Scheme 14. Synthesis of α– and γ–cyclodextrin derivatives

3.4. Synthesis of Py-CD monomers

Two strategies for pyrrole-cyclodextrin conjugation were studied. First, pyrrole carboxylic acids **10**, **11** and **12** were directly connected with 6^A-deoxy-6^A-amino-β-CD **36** using amide bond. Activation of the carboxy group with EDC/NHS ester has proven to be a practical approach but without needed selectivity. The activated ester reacted with NH_2 group but also with other hydroxyl groups on cyclodextrin macrocycle to form an inseparable mixture of isomers. Therefore, a more selective type of activation with PyBOP/DIPEA in DMF was tested (Scheme 15).[130] After the full conversion of starting compound, a mixture of HF/Et_3N was added to cleave TIPS protecting the group. The solution of TBAF was also used as a deprotection agent, but purification was more complicated compared to the previous example. Three target molecules **45**, **46** and **47** with β-CD on different carbon linkers were successfully prepared in excellent yields without the need of chromatographic purification.

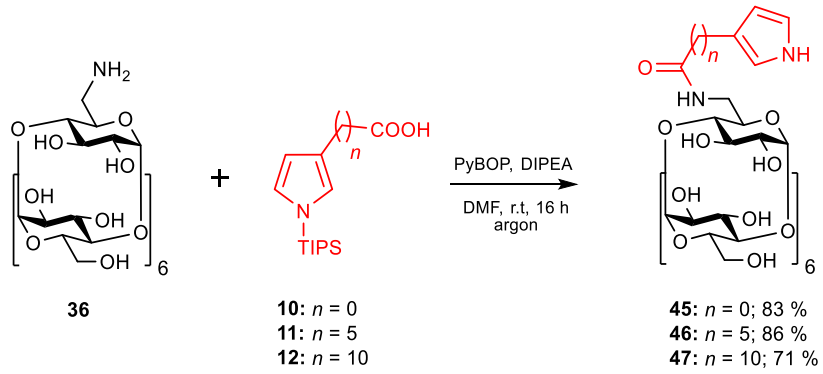

36

10: *n* = 0
11: *n* = 5
12: *n* = 10

45: *n* = 0; 83 %
46: *n* = 5; 86 %
47: *n* = 10; 71 %

Scheme 15. Conjugation of pyrrole with cyclodextrin *via* an amide bond

High selectivity of CuAAC was used for the synthesis of the second group of Py-CD conjugates **48-50** connected *via* triazole ring (Scheme 16). The reaction between pyrrole **15** and 6^A-deoxy-6^A-azido-β-CD **35** was catalysed by 5 mol% of CuI and 2 eq. of DIPEA in DMF at 100 °C. Then, the crude reaction mixture was treated with TBAF, and the target molecule **48** was isolated in 61% yield after column chromatography on C-18 silica gel. Surprisingly the same reaction conditions applied for the compounds **20** and **21** did not lead to desired products. Therefore, a modified procedure published by Chmursky et al. was used instead.[131] The Cu(I) catalyst was generated *in situ* by reducing $CuSO_4$ with ascorbic acid while the system was further stabilised with 0.2 eq. of TBTA. The reaction proceeded in DMSO/H_2O mixture at 60 °C, thus under milder conditions. Triazoles **48-50** were purified by simple precipitation and isolated after the final deprotection step in 79-88% yields.

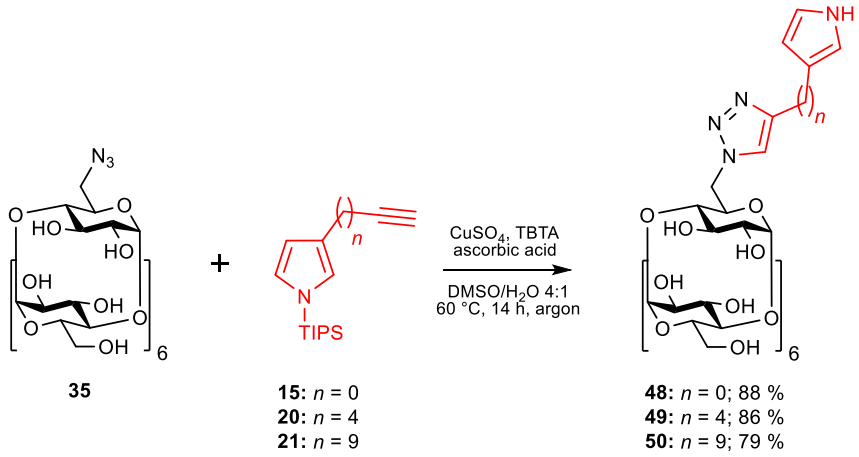

Scheme 16. Conjugation of pyrrole with cyclodextrin *via* triazole ring

3.5. Preparation of polypyrrole coating

3.5.1. Optimisation of pristine PPy layer formation

Synthesis of polypyrrole powder by chemical oxidation in the solution is a well-understood process. The influence of monomer concentration, oxidant/dopant ratio, type of solvent and polymerisation temperature was thoroughly studied over the last three decades. However, preparation of smooth polypyrrole layer on the material surface is a more significant challenge. Two main aspects (wettability/polarity and washing procedure) have to be precisely tuned. Otherwise, a product with many micro- and macroscopic defects is created. Further, defects at the micro- and nano- level are responsible for the lower conductivity of the final polypyrrole composite material.

Firstly, samples with oriented PCL microfibers were immersed in a water/methanol solution with freshly distilled pyrrole **1**. Then, a solution of $FeCl_3$ in water/methanol was added. The optimal concentration of pyrrole **1** in the final polymerisation mixture was estimated to 0.01 mmol/dm^3 with 2.4 eq. of the oxidising agent in order to create a smooth PPy layer **51**. The reaction was shaken (100 rpm) for three days at room temperature, and then the samples were washed with distilled water, methanol, sonicated and finally dried under vacuum. The original material changed colour into black which indicated the formation of a polymer layer on the surface. The morphology of resulting material **52** was studied using SEM and biocompatibility evaluated by *in-vitro* experiments on mouse 3T3 fibroblasts. In Figure 8, we can see images of PPy **51** coated PCL aligned microfibres with many structural defects (A) and smoothly coated material (B) after reaction conditions optimisation. The diffusion of the monomer **1** onto fibres before initialisation of polymerisation together with the optimal concentration of all reactants and intensive rinsing were essential parameters to obtain good PPy layer **51**.

Moreover, the utilisation of this procedure in the design of advanced molecular scaffold for tissue engineering was successfully demonstrated. The aligned fibrous scaffold improves the lengthwise proliferation of neural cells while inherently conductive PPy **51** enables electric stimulation. Though several papers dealing with stimulation of cell with electric filed have been published on PPy coated substrates, there is still plenty of space for improvement. One of the areas of interest is surface functionalization with helpful molecules which could alter material wettability, charge or other cues for cell growth. Therefore, several β-substituted pyrrole monomers were synthesised in order to introduce functionality onto the polymer surface. The indisputable benefit of β-substituted pyrroles compared to *N*-substituted analogues is their higher conductivity after polymerisation. It is caused by a smaller disruption of the conjugated system and thus better electron transport along the polymer backbone.

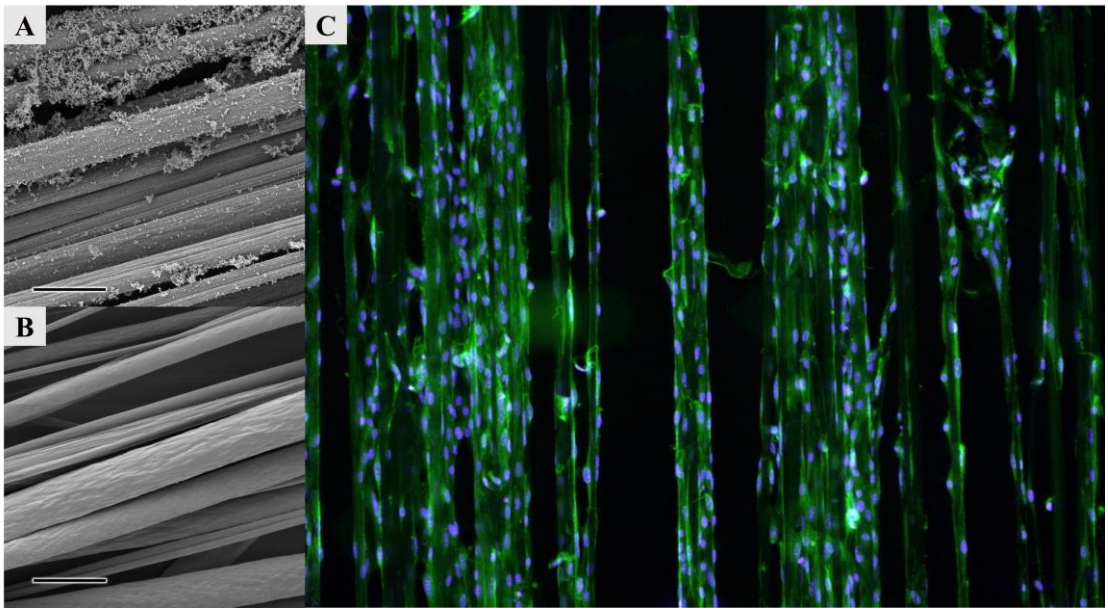

Figure 8. SEM and fluorescence images of the fibrous PPy-PCL material **52**; scale bar 50 μm

3.5.2. Preparation of PPy film with carboxy or alkyne terminal groups

Previously synthesised Py-CD conjugates, **45-50** were used for initial polymerisations. The PCL fibrous substrate was prepared by electrospinning technique instead of drawing from the polymer droplet (Figure 9). Although oriented fibres are better for neural cell guidance, random fibrous material with μm fibres diameter (1.13 ± 0.36 μm) was used in this study for several objective reasons. One of them is that several square meters of PCL sheet could be easily prepared using the Nanospider® device compared to the tedious drawing technique. Moreover, samples are more robust, and the polymerisation is easily repeatable. Our first idea was to copolymerize CD-decorated pyrrole **45-50** together with pyrrole **1** under optimised reaction condition mentioned in the previous chapter. However, the polymerisation rate was much higher for the pyrrole **1,** and thus the pristine polypyrrole was created as an only product. The monomers **45-50** were polymerised separately as well but only starting material was detected using LC-MS even with prolonged reaction time or elevated temperature.

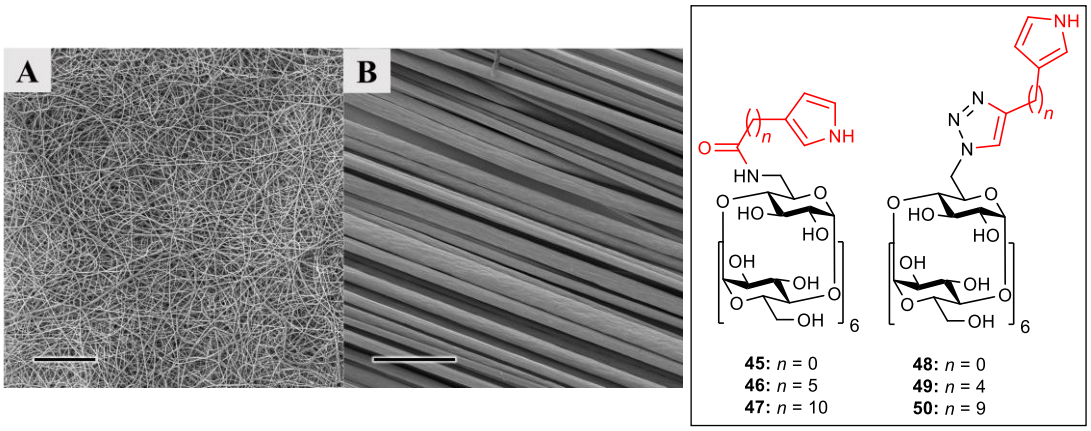

Figure 9. A, B) SEM image of PCL microfiber prepared by needless electrospinning and drawing technique (scale bar 100 μm); structures of β-substituted pyrrole monomers **45-50**

It is generally agreed, that substituted pyrroles polymerise slowly than unsubstituted analogues. It could be caused by steric demands of CD-Py monomer or interaction of the CD cavity with another molecule to form a stable supramolecular structure. For these reasons, we decided for the multistep procedure, where β-substituted pyrrole **28** or **30** with medium long carbon chain and various terminal group are deposited onto PCL surface, and then the cyclodextrin is connected using suitable conjugation reaction (Scheme 17). Derivatives **28** or **30** were oxidised by $FeCl_3$ together with pyrrole **1** (ratio 1:1) in aqueous methanol to form a grey-black coating on the PCL matrix. Unexpected reactivity of β-substituted pyrroles **28** and **30** have been found which formed a copolymer with **1** in ratio 10:1 according to elemental analysis. We concluded, that reaction rate is surprisingly high for pyrroles **28** or **30** and focused our efforts on the production of purely β-substituted conjugated polymers (Scheme 17) instead of polypyrrole copolymers. This approach led to the densely coated fibrous surface with a high amount of functional groups suitable for further derivatisation.

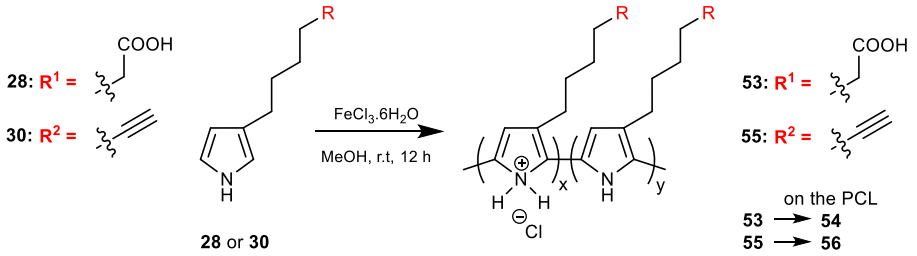

Scheme 17. Oxidation of pyrrole monomers **28** or **30** by $FeCl_3$ (PCL substrate omitted)

The next step was the optimisation of surface morphology of forming polypyrrole and its spectroscopic, elemental and biological analysis. The polymerisation rate is higher in water than alcoholic solvents due to better ions mobility. On the other hand, a suitable solvent which could wet material and still keep sufficient reaction rate has to be carefully selected. Thus, a mixture of H_2O/MeOH is typically used for aliphatic polyester like PCL. The polymerisation of pyrrole **28** was carried out in 60% aqueous MeOH (*v/v*) at room temperature, with monomer concentration 25 mM and 2.4 eq. of $FeCl_3$ as an oxidising agent. The reaction turned colour from bright orange to dark green/black in several hours which indicated a rapid formation of the polymer **53**. Therefore, 95% and 100% MeOH (*v/v*) were used as a solvent for the next experiment. The reaction rate was reasonable even when pure methanol was used, while similar polymerisation did not proceed with unsubstituted pyrrole **1**. Another surprising result was a dramatic change in the PCL-PPy-5C-COOH **54** surface morphology (Figure 10).

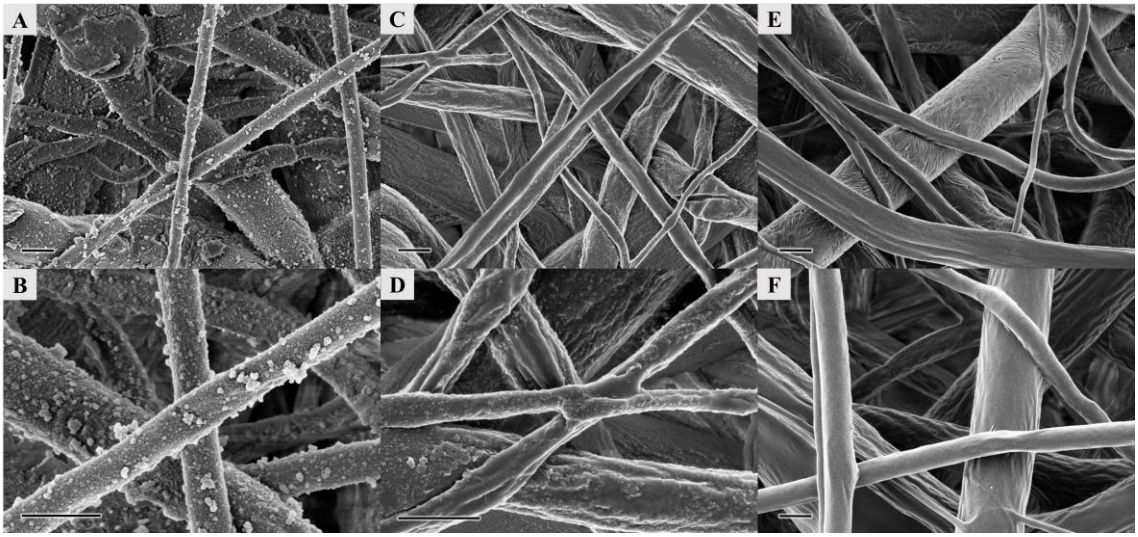

Figure 10. SEM image of the material **54**; **A, B)** 60% MeOH/H_2O (*v/v*); **C, D)** 95% MeOH/H_2O (*v/v*); **C, D)** 100% MeOH; scale bar 1 μm

As could be seen in the SEM pictures above, the resulting PPy layer **53** formed on the PCL microfibers using 60% MeOH had many structural defect and agglomerates on the surface. Even 5 % of water content had a significant impact on surface morphology. Better wettability of PCL in methanol rendered smoothly coated material which precisely follows the surface structure. The unexpected high reactivity of substituted pyrrole **28** in MeOH was found which was in contrast to the observed behaviour of CD-substituted pyrroles **45-50**, published examples from the literature or even the reactivity of simple pyrrole **1**.

The same reaction conditions have been applied for the polymerisation of pyrrole **30** with a triple bond. As we can see in Figure 11 minor structural defects, have been formed in 60% aqueous MeOH while the polymerisation in pure MeOH yielded excellent composite material PCL-PPy-4C-alkyne **56**. Interestingly, the polarity of terminal groups does not affect the quality of polymer film, and thus a thin layer of polymers **53** or **55** with useful functional groups could be introduced on the surface in one step. Moreover, these functional groups could later serve for the conjugation of different molecules. The second great benefit is the inherent conductivity of PPy films which could further enhance cell growth and survival.

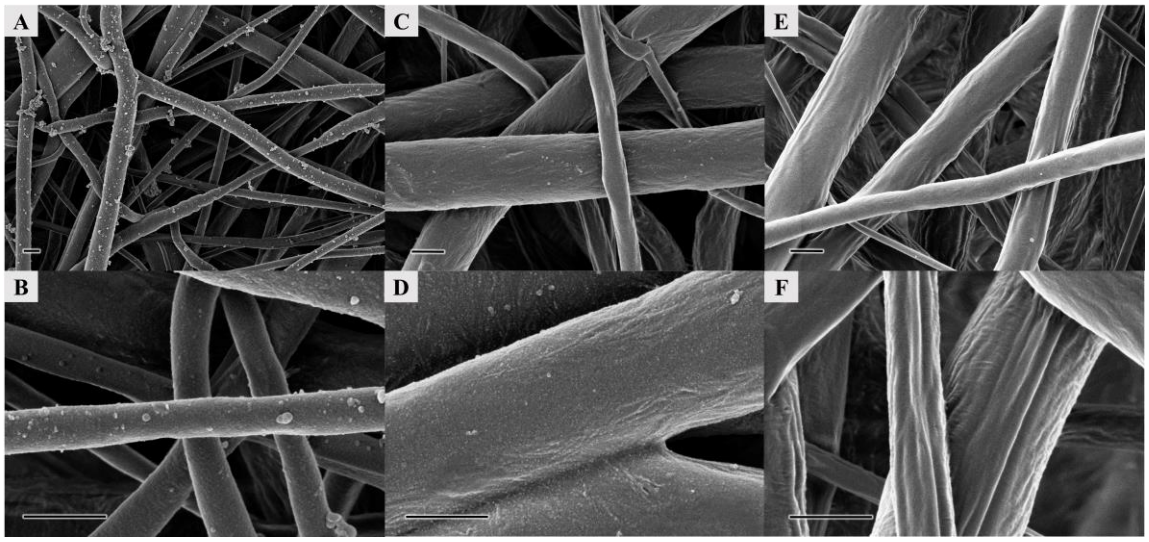

Figure 11. SEM image of the material **56**; **A, B)** 60% MeOH/H_2O (*v/v*); **C, D)** 95% MeOH/H_2O (*v/v*); **C, D)** 100% MeOH; scale bar 1 μm

After reaction conditions optimisation and evaluation of surface morphology by SEM, several spectroscopic methods have been used for the characterisation of the surface composition. Although the IR spectroscopy is a powerful tool for the study of material composition it is failing for nanometres thin layers. Depending on the energy used the penetration depth of IR spectroscopy is much higher than the thickness of our newly PPy coatings. Thus, the PCL matrix was rinsed from the 3D fibrous scaffold, and the resulting polymers **53** and **55** were characterised by IR, EDS and elemental analysis in powdered form.

The pristine polypyrrole **51** (blue line) has a limited number of characteristic vibrations in the IR if compared to its substituted analogues **53** and **55** (Figure 12). The first weak signal around 1700 cm^{-1} is probably vibration of conjugated π-system of the polymer backbone. It could be caused by the resonance of aromatic electrons to form imine like structures. The next signal at 1540 cm^{-1} is strong stretching vibrations of pyrrole ring followed by complicated deforming and skeletal vibrations at lower cm^{-1}. The red line in Figure 12 represents the IR spectrum of

PPy-5C-COOH **53**. A broad valence vibration of carboxylic O-H group between 3500 – 3050 cm^{-1} and characteristic strong symmetrical stretching vibration of the C=O group confirm the presence of carboxylic acid in the polymer structure. Moreover, we can find symmetric as well as asymmetric vibrations of corresponding alkyl CH_2 linker at 2932 cm^{-1} and 2859 cm^{-1}.

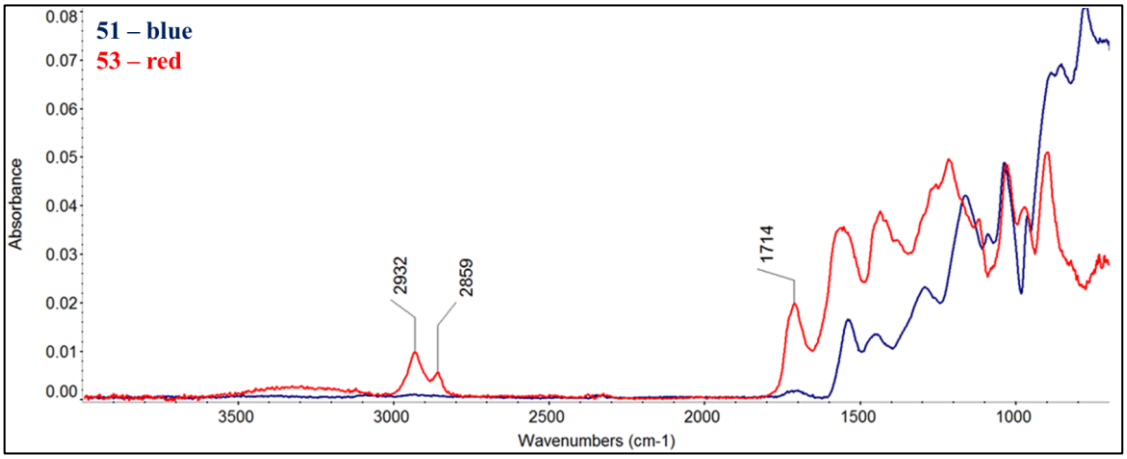

Figure 12. IR spectra of pristine PPy **51** and PPy **53** with carboxy groups

In Figure 13, we can see a significant difference between spectra of pristine **51** and substituted polypyrrole **55** with a triple bond. The hydrogen of the terminal triple bond has characteristic strong symmetrical valence vibration at 3292 cm^{-1} which can be assigned to triple bond together with weak carbon-carbon stretching vibration at 2114 cm^{-1}. The introduction of carbon linker is further confirmed by the corresponding valence vibrations of CH_2 groups at 2932 cm^{-1} and 2859 cm^{-1} respectively. Then, the vibrations of pyrrole around 1700 cm^{-1} and at 1530 cm^{-1} suggesting above mentioned ring vibration together with coupled deforming and skeletal vibrations of the whole conductive polymer.

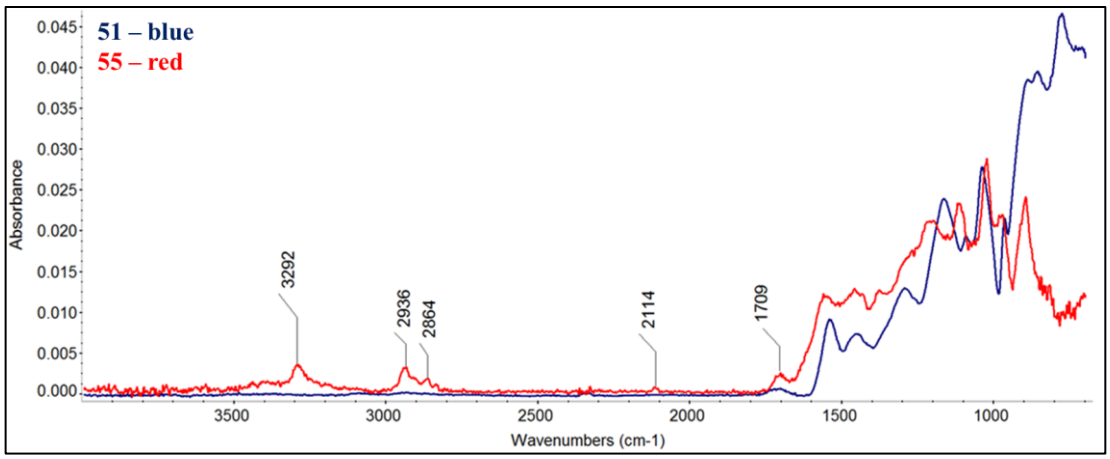

Figure 13. IR spectra of pristine PPy **51** and PPy **55** with a triple bond

The TGA has provided valuable information about thermal stability and behaviour of newly prepared polymers at elevated temperature (Figure 14). Generally, absorbed water is evaporated below 100 °C together with residual lower boiling organic solvents. Structurally bound water leaves at temperatures between 120 – 200 °C depending on the material structure. The pristine polypyrrole **51** degraded without any rapid change between 200 – 600 °C but substituted derivatives **53** and **55** were losing significant weight between 330 – 500 °C. The overall weight loss of polypyrrole **53** was higher than the weight loss of triple bond substituted polypyrrole **55**. It was in good agreement if we consider the fact that side chain with higher molecular weight contributes more to the thermal decomposition than the aliphatic counterpart.

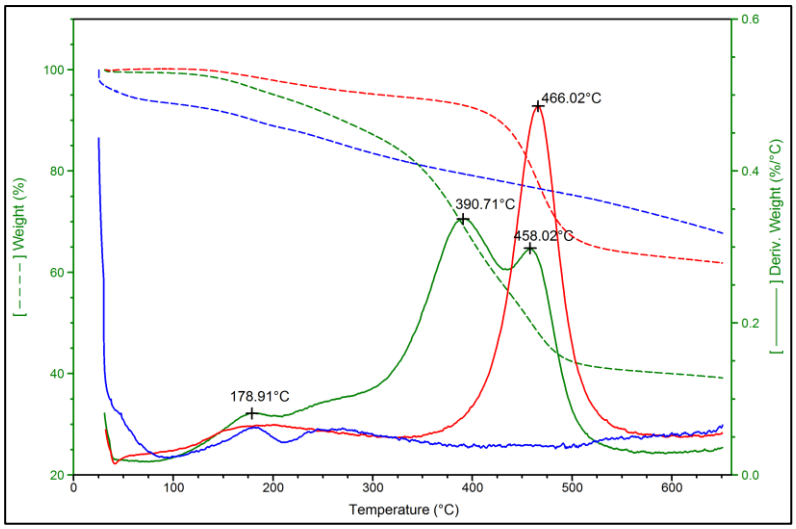

Figure 14. TGA spectra of pristine PPy **51** (**blue**), PPy **53** with carboxy groups (**green**) and PPy **55** with a triple bond (**red**)

Conjugated polymers like polypyrrole **51** are well-studied materials. They are investigated for several decades in the field of energy storage or biomedical devices. Huge application potential and inherent conductivity belong to the most precious feature of these materials. On a simple example, the conductivity of the surface PPy layer deposited on the PCL fibres could be demonstrated. In Figure 15, we can see SEM images of the fibrous scaffold **54**. Usually, nonconductive materials have to be gild before analysis. However, our material has sufficient conductivity for direct measurement due to its doped form. The conductivity can be tuned in several ways, for example by the level of doping, type of dopant or method of preparation. Although this qualitative proof of charge transport is straightforward, the area resistivity measurement should be used for precise conductivity measurement. Because this work is mainly focused on the preparation and spectral characterisation of novel PPy derivatives for tissue engineering, the conductivity measurements were not realised. It should be mentioned, that conductivity is an essential parameter of designed materials. However, the thickness of deposited

PPy layer, air sensitivity, doping level, type of dopant and the method of preparation significantly influence the overall conductivity.[132] Moreover, there are some issues regarding the structural defect in the polymer backbone which could further alter conductivity. Therefore, the emphasis was put onto synthesis, characterisation and biological experiments while the conductivity could be tailored according to a final application later.

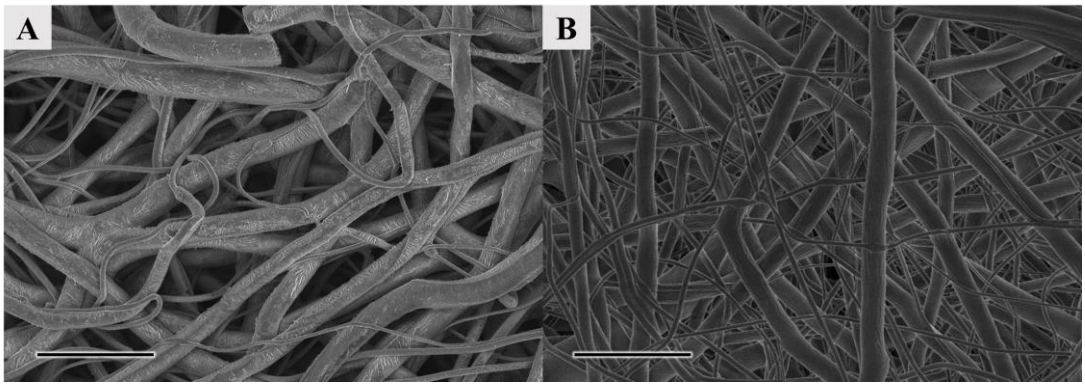

Figure 15. SEM images of PCL-PPy **54**; **(A)** pristine; (**B**) gold coated; scale bar 10 μm

The chemical composition of both newly prepared polymers was determined using elemental analysis (Table 1). The elemental composition was calculated without doping chlorine atoms, and the measured hydrogen content was affected by rapid air moisture absorption (up to 8 wt. % in the case of PPy **51** based on published literature). In the table below we can see that the resulting ratio of carbon to nitrogen corresponds accurately with the calculated values. Moreover, we were able to detect nitrogen in the both coated scaffolds **54** or **56** which confirmed the successful introduction of polypyrrole film on the surface of individual fibres.

Elemental analysis	**at% C** calcd / found	**at% H** calcd / found	**at% N** calcd / found	**C/N ratio** calcd / found
PPy 53	67.02 / 58.76	7.31 / 10.92	7.82 / 6.79	8.57 / 8.65
PPy 55	82.72 / 74.38	7.64 / 11.26	9.65 / 8.78	8.57 / 8.47

Table 1. Calculated and measured values of elemental composition for PPy **53** and **55**

Although the methods mentioned above provide valuable information about polymer composition, surface morphology and thermal properties, we still did not prove or estimated the amount of incorporated dopant. According to the published literature, this amount could vary significantly depending on the structure of doping agent, a method of polymer preparation. Small inorganic charged ions are incorporated more efficiently than large molecules, but the dopant exchange with moisture often occurs. For these reasons, various types of organic sulfonic acid are

commonly used for conductive polymers doping because of their improved environmental stability. However, the problem with the stability of dopant is more prominent in polyaniline than polypyrrole chemistry. Thus, we have prepared PCL-PPy composite materials using $FeCl_3$ as an oxidising agent in methanol to furnish coatings doped with chloride anion **53** or **55** based on EDS analysis (Figure 16). It is also generally agreed that some of the doped conductive polymers could find an application in tissue engineering. The interaction of CP with biological samples was described in several publications where the cytotoxicity was evaluated by extensive *in-vitro* and *in-vivo* experiments.[133–135]

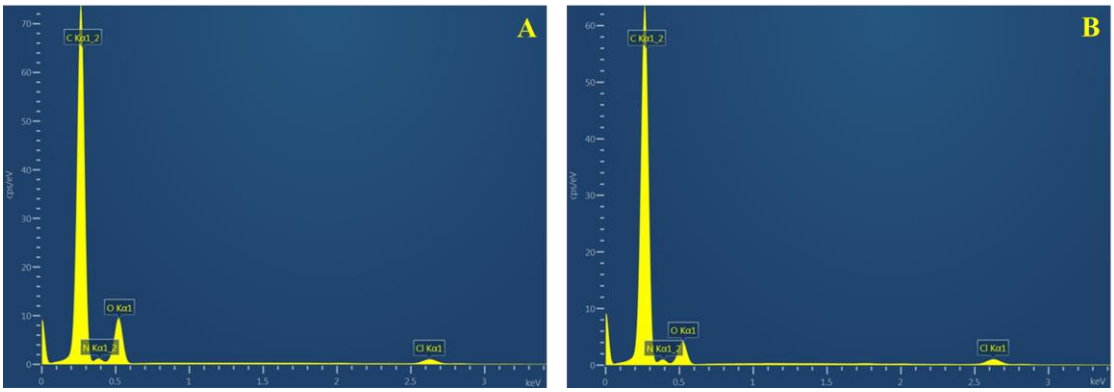

Figure 16. EDS spectra of polymers **A)** PPy **53** and **B)** PPy **55**

The chemical composition was affected by impurities caused by fast air moisture absorption, and thus oxygen could be found in both spectra. Although the overall values were shifted due to some impurities, the N/Cl ratio was independent on the material contamination and provided valuable information on the amount of dopant in the polymer structure (Table 2).

EDS	at% C	at% N	at% O	at% Cl	N/Cl molar ratio
PPy 53	79.02	5.40	14.85	0.73	7.40
PPy 55	83.84	6.66	8.62	0.89	7.48

Table 2. Elemental composition of PPy **53** and **55** measured by EDS

The level of doping was approximately one chlorine anion per every 7 – 8 pyrrole unit for the PPy **53**. The second sample **55** with aliphatic side chain had a similar level of doping. It means that we were able to prepare a series of polypyrrole composites with different side chains suitable for various types of conjugation reactions but with the same level of doping. Hence, the *in-vitro* experiments should reflect more precisely the changes of the surface functionalization while the surface morphology and the level of doping are kept similar as possible.

The chemical composition of PPy layer **53** on the fibrous scaffold **54** was further studied by XPS method (Figure 17). Due to the low penetration depth of the incident energy beam, even the nanometre size layer can be precisely characterised. Although XPS is a well-established technique for experiments on the metal surfaces, the polymeric fibrous scaffolds represent a more significant challenge. Generally, the tested samples are cleaned before the experiment by Ar^+ bombardment to remove traces of surface contamination. However, the low melting point of PCL and overall sensitivity to energy-rich incidental electrons do not allow surface spraying. Thus, samples were characterised as received using two primary sources to obtain a broad spectrum. Then, individual signals of the corresponding element were scanned separately with higher precision. As can be seen below, these signals are mostly a combination of the differently bound element. The blue line represents pristine PCL while the red lines are spectra of PCL-PPy-5C-COOH scaffold **54**. The oxygen and carbon spectra are similar for both samples because PCL substrate is measured together with thin PPy coating due to a higher penetration depth of incidental electrons. Even though, the oxygen and carbon spectra are not conclusive we can still rely on nitrogen spectrum because the nitrogen was not present in the pristine PCL. Although the polypyrrole typically has four binding modes in the nitrogen spectrum which correspond with the doped structure of the conductive polymer, we were able to distinguish only two modes. Nevertheless, despite the low intensity of measured spectrum the successful functionalization of PCL with PPy **53** has been confirmed. However, a more detailed study could shed light onto the binding modes of nitrogen and further describe a doping mechanism.

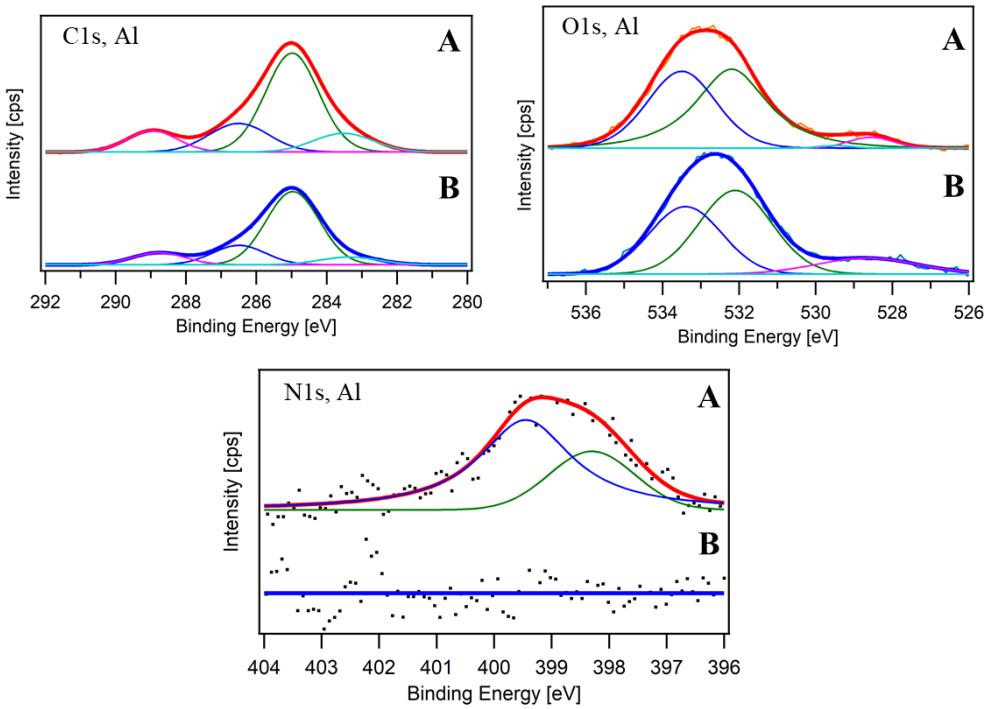

Figure 17. XPS spectra (C1s, O1s, N1s) of **A)** PPy **53**; **B)** pristine PCL

The chemical structure of PPy **53** in powder form was also studied by solid-state NMR (Figure 18). A similar molecule **57** was measured first as a standard (blue line) and compared with the sample of PPy **53** (red line). The solid-state ^{13}C NMR spectra were collected by rotating the sample under magic angle at 15 KHz. Both samples were measured at 303 K using a NMR machine operating at frequency 125.77 MHz. Then, expected chemical shifts were assigned to the corresponding carbon atoms. At 173.5 ppm the signal of COOH group could be found while the signals around 30 ppm are CH_2 carbons of the pyrrole aliphatic side chain. The carbons of the pyrrole ring are probably hidden under the signal between 155 – 95 ppm, where peak broadness is caused by a complicated conjugated system of double bonds in the polymer backbone. The chemical shift of the unassigned peak at 51.1 ppm suggests that this carbon is connected to the atom with higher electron density by a single bond. We could assume structure like -CH-NH- created on the α-carbons during doping but the chemical shift for carbocation should be significantly higher. The second explanation is based on the introduction of a particular structural defect, while the pyrrole ring is randomly connected with another heterocycle *via* the β-position.

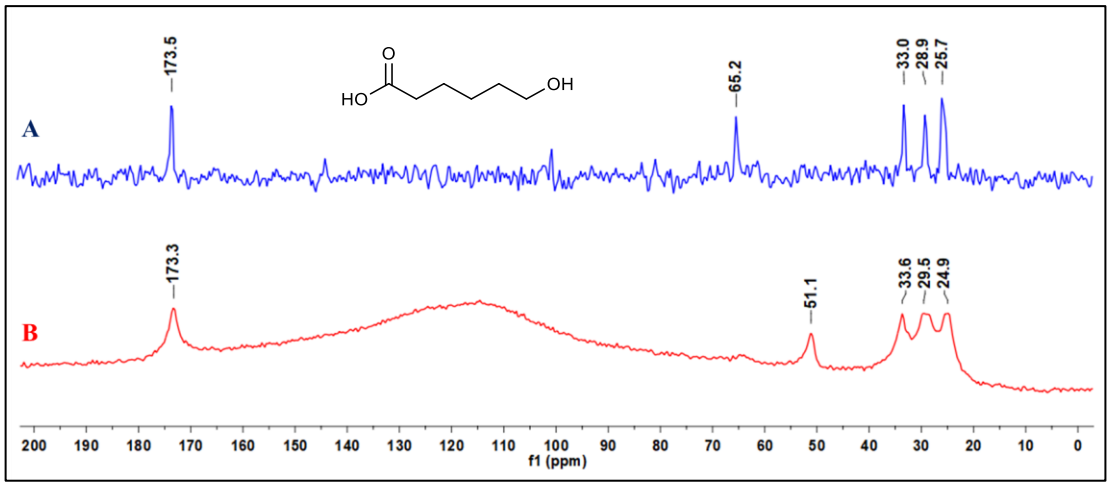

Figure 18. Solid-state ^{13}C MAS NMR spectra **A)** model compound; **B)** PPy **53**

For the summary, the structures of newly prepared polypyrrole derivatives were described and confirmed by several analytical techniques. Thermal properties of PPy **51**, **53**, **55** were studied, and the amount of deposited PPy on the PCL substrate was calculated based on TGA measurement for every sample. The polymerisation protocol for the deposition of PPy **53** or **55** was also optimised and the morphology of resulting scaffolds thoroughly examined using SEM.

3.5.3. Preparation of PCL-PPy scaffolds decorated with cyclodextrins

Over the past several decades, the organic chemist developed a vast variety of synthetic approaches for connecting molecules.[136] These methods involve the reaction of one functional group with another to form a covalent bond.[137] Nowadays we can choose from hundreds of commercially available activation and coupling agents. Perhaps the most utilised system for amine conjugation is carbodiimide chemistry (Scheme 18). Generally, carbodiimides are zero-length linkers which could mediate reactions between carboxylic acid with amino or phosphate groups. The water-soluble EDC can react with the carboxylic group to form very reactive *O*-acylisourea which is subsequently attacked by the nucleophile (e.g. primary NH_2 group) to form an amide bond and isourea byproduct. Whereas a new covalent bond is formed, the excess of water-soluble activation agent and isourea byproduct could be easily removed. In aqueous solution, the activation with EDC occurs mainly at pH 3.5 to 4.5, but the highest yield of amide bond can be achieved at pH 4 to 6. The leading competing reaction is the hydrolysis of the activated intermediate by water which results in the formation of isourea and a carboxylate anion. There are other side reaction pathways which could occur after activation of the carboxylic group. Besides the hydrolysis of activated ester, the excess of EDC can mediate the formation of *N*-acylisourea derivative. Further, the reaction between the second molecule of carboxylic acid and *O*-acylisourea intermediate forms an anhydride. This reactive species could react with an amino group to form the target amide bond or hydrolyse to starting carboxylic acid.

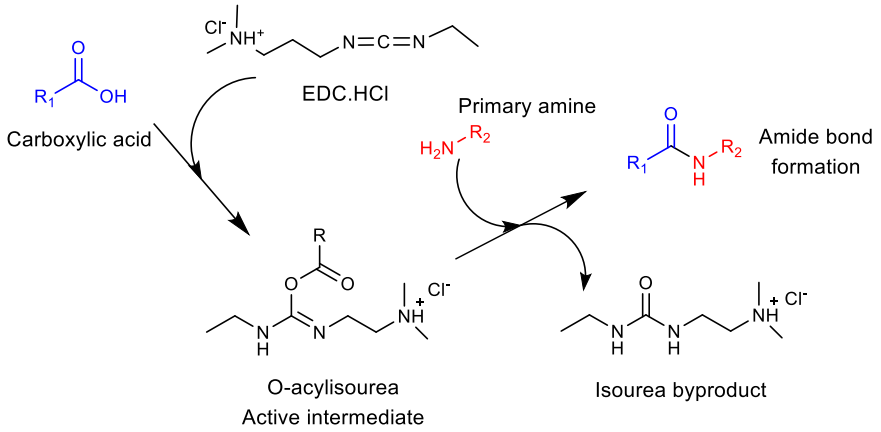

Scheme 18. Amide bond formation using carbodiimide chemistry

Similar reaction procedure can be applied for the functionalization of inorganic, organic or polymeric surfaces. Our composite material **54** was decorated with cyclodextrins according to Scheme 19. The first step was the activation of carboxyl groups on the surface using EDC/NHS. It is generally agreed, that NHS forms a stable intermediate which is more resistant against

hydrolysis but retains its reactivity and selectivity towards molecules containing amino groups. The reaction proceeded in MES buffer at pH 6 to keep high reactivity of activated ester and slow down the unwanted hydrolysis. After 3 hours of activation, the buffer was removed, and monosubstituted amino cyclodextrin **40**, **36** or **44** was added in 20 ml of fresh buffer. Finally, the activated substrate was shaken in aqueous buffer with the corresponding NH_2-CD at room temperature for 12 hours to yield functionalized materials. The washing procedure removed the excess of unreacted cyclodextrin together with some byproducts using an ultrasonic bath. All newly prepared materials PCL-5C-CONH- with immobilised α-CD **58**, β-CD **59** or γ-CD **60** on the surface were characterised and further used in biological experiments.

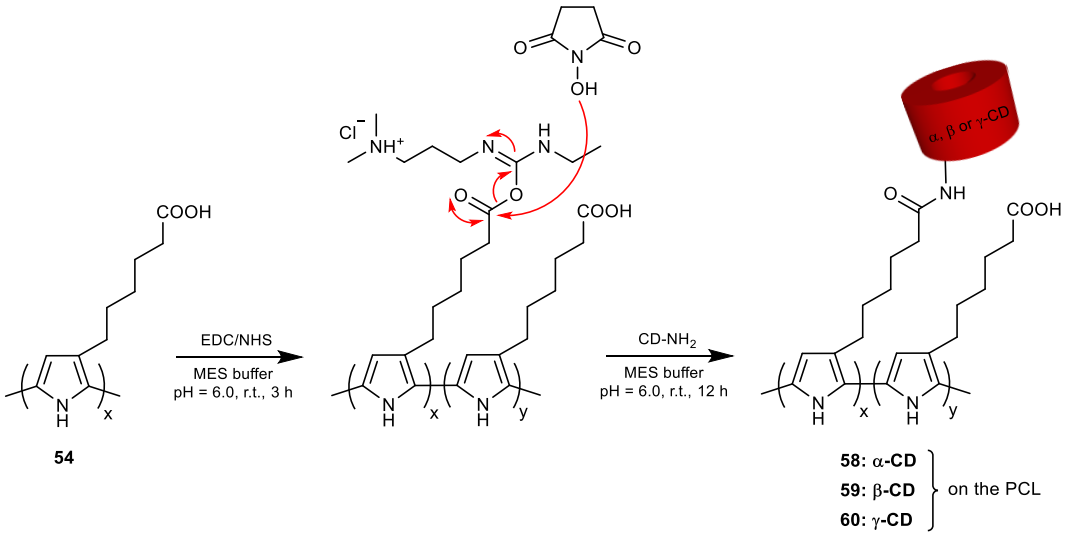

Scheme 19. Immobilisation of various CD using EDC/NHS (PCL substrate and doping agent omitted for better clarity)

Because of the low density of CD molecules on the surface, we had limited direct spectroscopic methods for its characterisation. However, the inherent ability of cyclodextrins to form inclusion complexes with lipophilic molecules can be utilised. First, the surface-bound cyclodextrins are labelled with an appropriate tag, and then the number of immobilised molecules is calculated. Methyl orange was selected as a guest molecule with a known binding constant of MO and β-CD between 10^{-3} and 10^{-4} [M^{-1}] according to published literature. The calibration curve of MO in water was measured using UV/VIS spectroscopy. Then, 10 ml of MO solution with the lowest concentration which can be measured without significant error was incubated with approximately 50 mg of CD-coated material **59** for 30 minutes. Next, the supernatant was measured again, but unfortunately, the number of surface bond cyclodextrins was probably several times lower than we can detect by UV/VIS spectroscopy. Despite this unsuccessful experiment, the surface concentration of immobilised CD was finally estimated using fluorescence spectroscopy.

The fluorescence spectroscopy is more sensitive than UV/VIS, but suitable fluorescence label has to be selected first. One option was the synthesis of adamantyl labelled guest compound, or we could use directly one of many commercially available fluorescence tags. Based on literature research, Rhodamine B seemed to be the best candidate for our study. It has linear dependence at low concentrations below 10^{-3} mol/dm^3 and provides high quantum yield upon excitation. Moreover, it is well soluble in methanol or water. Thus, stability constant and complexation ratio between Rhodamine B and β-CD **33** was verified experimentally to see if it agrees with published data. The isothermal titration calorimetry was used to investigate thermodynamics behind host-guest interaction. Therefore, the guest molecule of Rhodamine B was dissolved in water and titrated in 20 aliquots into a solution of the macrocycle **33** at 25 °C. The resulting heat response upon each addition was plotted and the binding constant together with complexation ratio calculated (see the experimental part). The blind heat signature was deducted before calculation, and the measurement repeated three times. The results were in a good agreement with published literature and confirmed the expected interaction constant around 10^4 [M^{-1}].

The experimental setup for the estimation of surface-bound β-CD **36** using fluorescence spectroscopy can be seen in Scheme 20. First, the fluorescence of Rhodamine B in the series of solutions was measured for the concentrations between 10^{-2} – 10^{-9} mol/dm^3. The fluorescence had a linear dependence in the concentration range between 10^{-4} – 10^{-9} mol/dm^3, which was in good agreement with published literature. Next, the theoretical surface density of immobilised β-CD **36** on the PCL-PPy-5C-CONH-CD scaffold **59** was calculated based on results from BET analysis. The sample for BET analysis was outgassed at 40 °C for 24 hours and then measured using krypton gas with the resulting value of specific surface area 2.747 m^2/g. Thanks to this analysis we were able to accurately calculate the maximum theoretical surface coverage of scaffold **59** by β-CD molecules and therefore choose the optimal concentration of Rhodamine B for subsequent host-guest interaction.

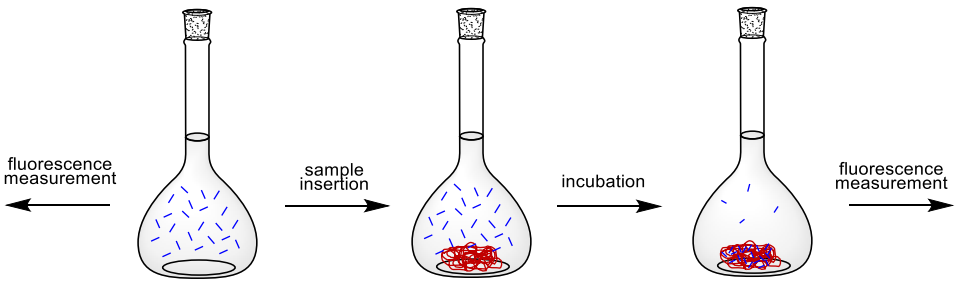

Scheme 20. Host-guest interaction of Rhodamine B and surface-bound β-CD

The data from the fluorescence measurement are summarised in the experimental part of this thesis. Not only a successful introduction of β-CD **36** on the fibrous surface has been proven, but we also calculated the surface density of immobilised cyclodextrins. It was estimated that the density of attached cyclodextrins on the PCL-PPy-5C-CONH-CD **59** was approximately 800 times lower than the maximal theoretical value. Although, this approach provided valuable information for the β-CD coated material **59** we were unable to determine the surface density of α- and γ-CD covered materials **58** and **60**. The reason was, that only β-CD interacts with Rhodamine B, while cavity of α-CD is too small for complexation and conversely inner space of γ-CD is broader than is necessary for strong host-guest interaction. At this point I would allow an approximation, that surface density of bound α-, β- or γ-CD is about the same. If steric repulsion of CD is omitted due to low surface concentration and the reactivity of NH_2-CDs is roughly the same, the approximation as mentioned above is reasonable.

Further, the surface morphology of samples (PCL, PCL-PPy-5C-COOH **54**, PCL-PPy-5C-CONH-CD **58**, **59** and **60**) for *in-vitro* experiments were examined using SEM. We can see in Figure 19, that PCL matrix was coated with polypyrrole **53** without any significant surface defects. However, the longer polymerisation time (72 hours) had a slight impact on the mechanical properties of the final material, while a shorter reaction time (12 hours) afforded smoothly coated material without any surface defects or damaged fibres. The subsequent surface functionalization with cyclodextrins had no visible effect on the scaffold quality.

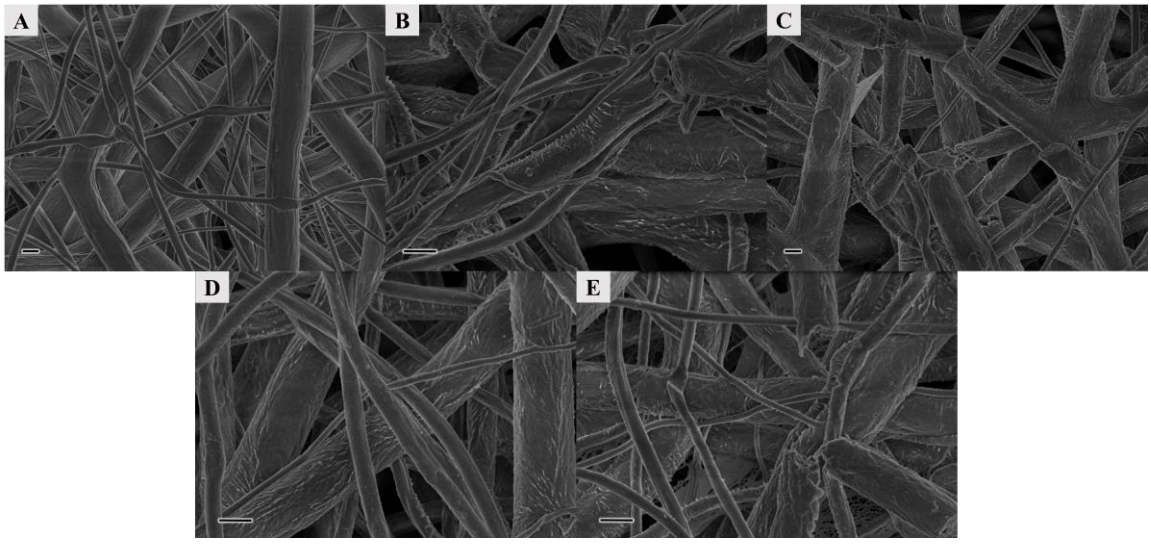

Figure 19. SEM image of **A)** PCL; **B)** PCL-PPy-5C-COOH **54**; **C)** PCL-PPy-5C-CONH-α-CD **58**; **D)** PCL-PPy-5C-CONH-β-CD **59**; **E)** PCL-PPy-5C-CONH-γ-CD **60**; scale bar 1 μm

Strongly hydrophobic neither hydrophilic materials are not favourable for cell adhesion and growth. Thus, we measured the water contact angle as an important parameter for all new materials. However, it can be found in the literature, that WCA is ranging by tens of degrees even for pristine fibrous PCL. It was difficult to distinguish whether the material morphology or surface chemistry has a stronger effect on WCA. Although we would like to compare WCA of tested materials, a small difference cannot be distinguished for the nonwoven scaffolds. The interpretation of such results is difficult due to variable fibres density which significantly affects the value of measured contact angle. Thus, we have focused our attention on the parameters, which could be measured more precisely for the given materials.

3.5.3.1. Biological experiments on functionalized PCL scaffolds

The main goal of this thesis is design, preparation, characterisation and biological evaluation of new molecular scaffold for tissue engineering. While properties of PCL-PPy fibrous materials were thoroughly described in the previous chapter, this part will be focused on cell-material interaction. At this point, we will focus on the *in-vitro* experiments to study the biocompatibility of newly prepared materials. Later it will be necessary to investigate the degradation profiles, byproducts formation or potentially toxic compounds leaching as well. Despite the promising *in-vitro* studies with different cell lines it is often problematic to transfer these results into more complex living systems. However, we were more interested in the fundamental aspects of the cell interaction with CD decorated PPy surface using PCL fibrous scaffold as a model substrate. Such conclusions could be transferred into the design of advanced material for the target application, e.g. neural tissue regeneration.

Five fibrous materials **A-E** were subjected to an *in-vitro* experiment with NHDF cell line, and the cell metabolic activity was determined using the MTT assay over two weeks (Graph 1). This assay is based on the transformation of yellow tetrazolium dye by mitochondrial reductase enzyme into purple formazan. Then, the absorbance is measured at a specific wavelength, and the number of viable cells is quantified according to the calibration curve. The data clearly show, that PPy coating **53** is not only biologically compatible but also significantly improves cell growth. Moreover, the introduction of cyclodextrins further increases overall performance. On the other hand, only a minor change in cell viability can be seen between materials bearing different types of cyclodextrins on the surface.

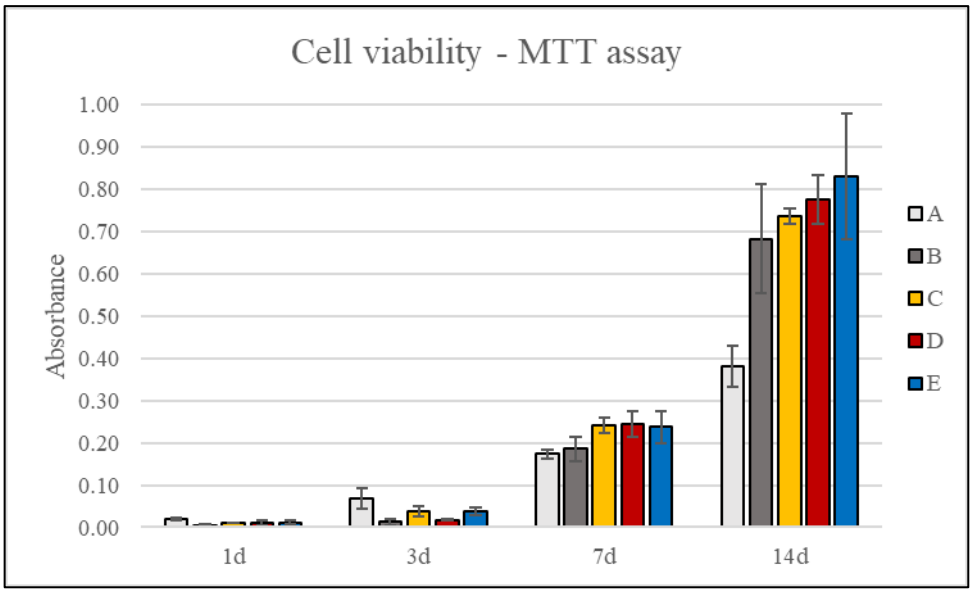

Graph 1. Cell metabolic activity (MTT assay) **A)** PCL; **B)** PCL-PPy-5C-COOH **54**; **C)** PCL-PPy-5C-CONH-α-CD **58**; **D)** PCL-PPy-5C-CONH-β-CD **59**; **E)** PCL-PPy-5C-CONH-γ-CD **60**

Thanks to these results our original goal of creating material combining cues for cell adhesion, proliferation and growth has been pushed forward. The introduction of cyclodextrin macrocycles onto a polymer surface probably worked thanks to host-guest interaction between the CD cavity and ECM synergistically. Although these non-bonding interactions are relatively weak, they have a dramatic impact on protein adhesion and subsequent cell viability. For the first few days, a higher cellular activity has been seen on the pristine PCL if compared to other tested samples. Cells were well spread on the fibres which had a direct effect on their growth based on the SEM images. Although cell activity was better on pristine PCL during the first days of the *in-vitro* experiment, later there was a sharp increase in the number of cells on the functionalized substrates. The first reason could be the interaction of ECM with charged PPy surface and thus better cell-cell communication *via* conductive polymer backbone. Secondly, inclusion complexes of serum proteins with lipophilic CD cavity could provide binding sites for cell adhesion and boost the cell-material interaction. Hence, the importance of surface chemistry was demonstrated on protein absorption experimentally. Generally known fact, that material surface is covered with adhesive protein before cell attachment leads us to such specifically designed scaffold at the first place. While many different proteins were already present in the culturing media, we just exploited CD ability to form inclusion complexes and to pull up proteins onto the surface. This action was followed by dynamic surface layer remodelling and later to cell adhesion *via* specific receptors. Although surface coating with RGD amino acid sequence[104] represents the most

common strategy, our approach relies on spontaneous interaction of the CD cavity with proteins to form a tissue mimicking environment.

The promising results from the *in-vitro* experiment showed that surface functionalization has a dramatic impact on cell proliferation, maturation and growth. Although there are many factors which simultaneously influence the overall cell response we focused our attention on the protein adhesion. It is known, that adhesion-mediating proteins like fibronectin, vitronectin or laminin adsorb onto the material surface, and the specific cell membrane receptors then recognise their presence. After this initial phase, the attached cells begin to feel the surface chemistry, topography and roughness and adapt their life cycle according to the given stimulus.

The absorption of bovine serum albumin onto the pristine PCL and scaffold **54**, **58**, **59** and **60** was measured to understand the protein-surface interaction better. The samples were incubated with a model BSA protein, and SDS-PAGE with liquid chromatography quantified the concentration after protein desorption. Although the original idea was to create an advanced conductive fibrous scaffold with CD decorated surface for better interaction with adhesion-mediating proteins, the data indicate that the pristine PCL is superior for the protein absorption. The spatial conformation of adsorbed proteins is far more critical than the total amount. According to previously published articles, hydrophobic surfaces with the WCA higher than 100 ° absorb proteins in a more considerable amount than hydrophilic materials. Proteins are absorbed on these materials in a denatured form and thus unable to provide specific binding sites for the interactions with the cell membrane. However, the composite materials **58**-**60** with immobilised various cyclodextrins on the surface support cell growth significantly better, although the total amount of initially absorbed proteins is lower than on the pristine PCL.

Interestingly, even the low concentration of CD on the surface dramatically improves cell proliferation, spreading, differentiation and growth. This phenomenon could be caused by the favourable interaction with the adhesion-mediating proteins which are absorbed on the surface in non-denatured conformation. Such naturally organised surface is more favourable for cell attachment which ultimately improves scaffold performance.

3.5.4. Preparation of PCL-PPy composites with the tuneable linker

In the next stage of our research, the influence of carbon linker length on cell growth was examined. Before the biological experiment, the polymerisation of pyrrole **27**-**29** was studied (Scheme 21). While the oxidation of pyrrole **28** and **29** proceeded smoothly, the pyrrole derivative **27** with carboxyl group connected directly to the heterocycle did not react under similar conditions. However, if the water was used as a solvent, the monomer **27** was finally deposited onto PCL at 45 °C. At this temperature the reaction was tedious, and it took 3 days before some visual change was visible. Moreover, the reaction worked swiftly at 95 °C, but the PCL substrate would be melted at this temperature.

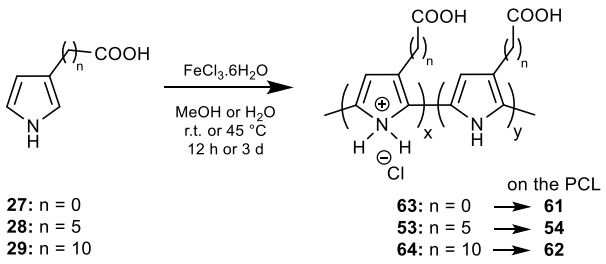

Scheme 21. Oxidation of pyrrole monomers **27-29** by $FeCl_3$ (PCL substrate omitted)

The morphology of PCL-PPy scaffolds **61** (Figure 20), **54**, **62** (Figure 23) were examined using SEM and the deposited PPy layers **53**, **63** and **64** were characterised by elemental analysis, IR or TGA in powdered form. A surprising structure of PCL-PPy-OC-COOH **61** can be seen in the picture below. While pristine PCL fibrous scaffold represents material with a regular surface, the morphology of resulting composite **61** after PPy **63** deposition has changed considerably. This example clearly illustrates how the type of solvent, the reaction temperature or minor change in monomer structure could influence the quality of final material. Probably a different wettability of PCL in water/methanol or the polymerisation rate were responsible for this unexpected outcome. Moreover, a significant amount of hematite side product was incorporated in the material structure despite an extensive washing procedure. Regularly, PPy coated substrates have grey-black colour, but sample **61** was reddish-brown (hematite). Moreover, EDS analysis confirmed a presence of residual Fe in the spectrum which also corresponded with the TGA analysis.

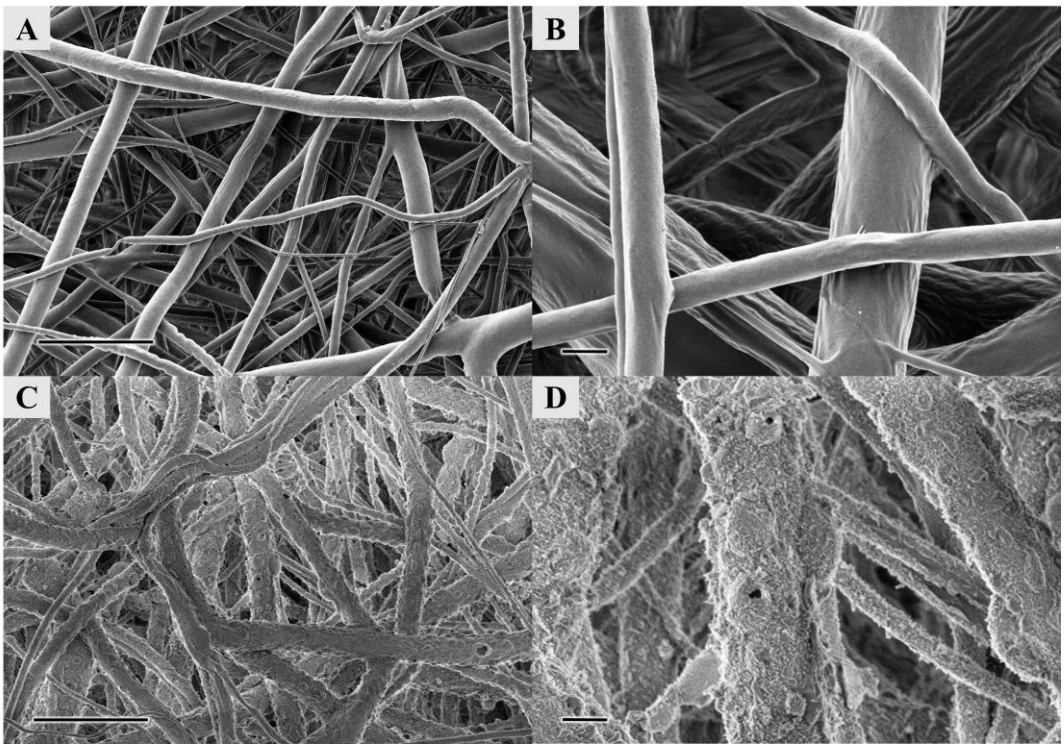

Figure 20. SEM images of **A, B)** pristine PCL; **C, D)** PCL-PPy-OC-COOH **61**; scale bar 1 μm

The chemical composition of deposited polypyrrole layers **53** and **64** was determined by elemental analysis (Table 3). Although the values of the elemental composition are influenced by moisture absorption and varying doping level, the carbon to nitrogen ratio nicely correlates with calculated values for conjugated polypyrroles (without dopant). The elemental composition of PPy **63** was inaccurate because of inseparable impurities in the polymer structure, especially the hematite.

Elemental analysis	**at% C** calcd / found	**at% H** calcd / found	**at% N** calcd / found	**C/N ratio** calcd / found
PPy 53	67.02 / 58.76	7.31 / 10.92	7.82 / 6.79	8.57 / 8.65
PPy 64	72.25 / 61.64	9.30 / 11.35	5.62 / 4.76	12.86 / 12.95

Table 3. Calculated and measured values of the elemental composition of PPy **53** and **64**

The last two methods used for the description of newly prepared materials were IR spectroscopy and TGA. In Figure 21 three overlapped IR spectra of PPy **53**, **63**, **64** with carboxyl group connected to the pyrrole ring *via* different carbon linkers are shown. The intensive peak of C=O bond valence vibration at 1696 cm^{-1} and broad O-H vibration between 3600 cm^{-1} and 3000 cm^{-1} prove the presence of the carboxyl group in sample **63**. Slightly shifted vibration energy

of carboxyl C=O bond can be found in the polymer **53** and **64** probably because of the lower electronic influence of pyrrole ring. The introduction of carbon linkers was further confirmed by the corresponding valence vibrations of CH_2 groups at 2934 cm^{-1} and 2858 cm^{-1} together with their deforming vibrations at 1461 cm^{-1} and 1436 cm^{-1}. Other peaks are mostly coupled deforming and skeletal vibrations which are commonly very complicated for proper assignment.

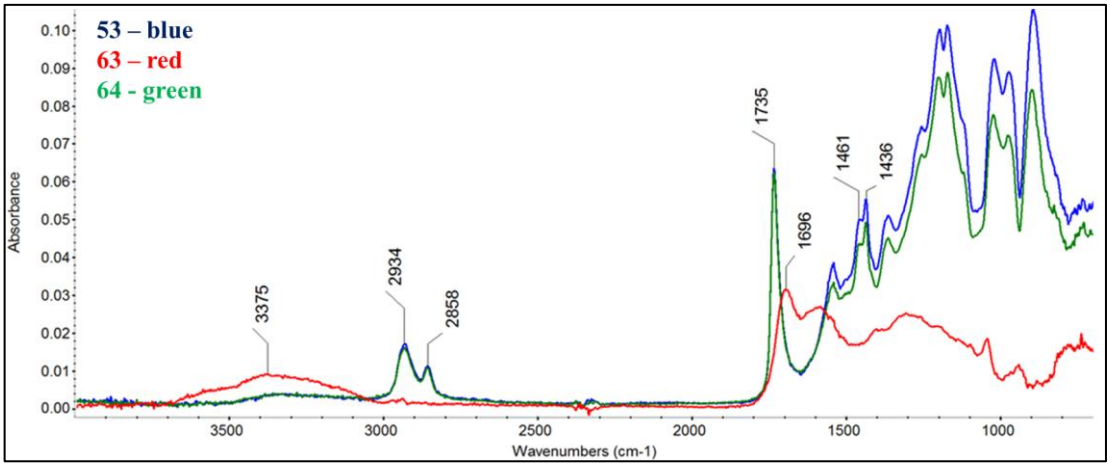

Figure 21. IR spectra of β-substituted PPy **53**, **63** and **64** with different carbon linkers

Thermal properties were investigated only for polypyrroles **53** and **64** with carbon linkers (Figure 22). Our goal was to prove the presence of PPy on the surface and also calculate the amount of deposited PPy. Although, the majority of weight loss was the contribution of PCL we could still calculate the amount of deposited polypyrrole from residual weights. Thus, pristine PCL, PCL-PPy scaffold (**54** or **62**) and powdered PPy (**53** or **64**) were measured separately. The difference in residual weights of pristine PCL and functionalized materials were 1.98 % (PCL-PPy-5C-COOH **54**) and 2.46 % (PCL-PPy-10C-COOH **62**). If some approximations were taken into account, the PCL-PPy scaffolds **54** and **62** contained 5.0 wt% of PPy **53** and 7.9 wt% of PPy **64** on the surface (see experimental part). This conclusion correlated with observed reactivity of monomer **29** which provided darker PCL fibrous material **62** if compared to other samples. Although such a method could not tell us about the thickness of PPy layer without known density, we have established fast and reliable proof of PPy deposition. Moreover, the amount of surface-bound PPy from different experiments can be easily compared.

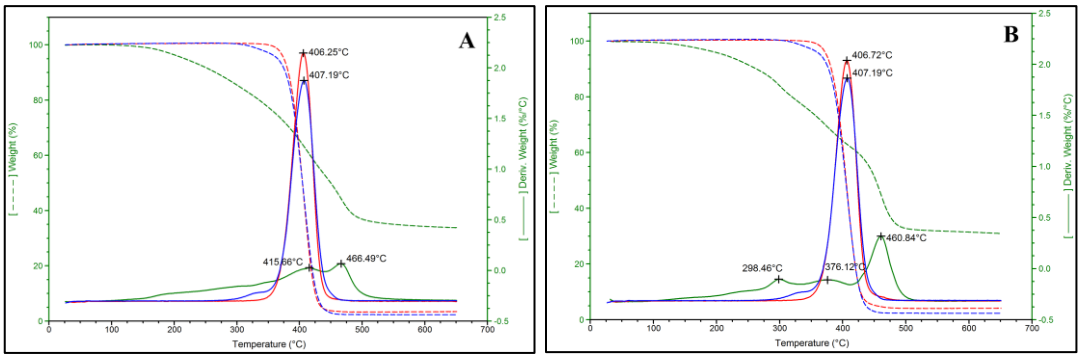

Figure 22. TGA spectra of **A)** PCL (blue), PCL-PPy **54** (red), PPy **53** (green); **B)** PCL (blue), PCL-PPy **62** (red), PPy **64** (green)

Further, composite scaffolds **54** and **62** were functionalized with β-CD **36** while the reaction conditions for CD immobilisation were taken over the previous experiment (Scheme 22). First, all available surface bound carboxyl groups were activated using EDC/NHS, then the β-CD **36** was added to furnish the desired materials. Although the main product should be an amide, the competing reaction is always hydrolysis, especially in more acidic water solution. Even though some activated carboxyl groups were hydrolysed the successful introduction of CDs onto PPy surface was confirmed by fluorescence spectroscopy using host-guest labelling technique as mentioned previously. The surface density of immobilised CDs was similar for both samples (see experimental part) which allowed us to study cell viability on the CD decorated materials connected to the surface *via* differently long carbon linkers.

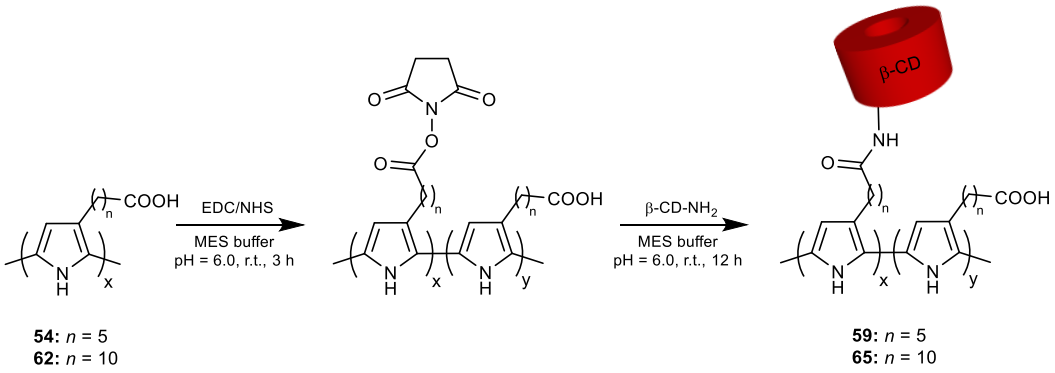

Scheme 22. Immobilisation of β-CD using EDC/NHS in MES buffer (PCL substrate and the doping agent were omitted for better clarity)

The structure and surface morphology of samples **59** and **65** were studied using scanning electron microscopy and compared with PCL-PPy **54**, **62** before functionalization. All individual fibres were smoothly coated without any defects as can be seen in the images below (Figure 23). For a summary, the protocol for CD connection utilising the classical carbodiimide chemistry can be also applied for the connection of CD onto PPy **62**. Although a longer carbon linker could interact with CD lipophilic cavity and thus hinder conjugation *via* an amide bond, the surface density of immobilized β-CD was similar for both samples **54** or **62**.

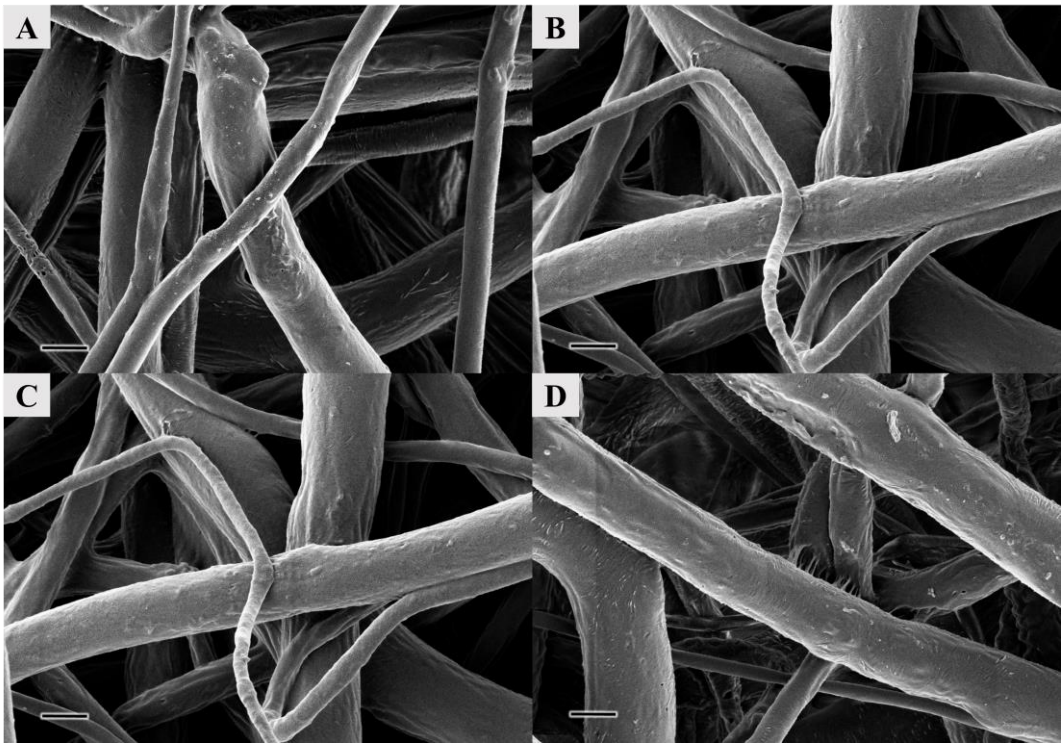

Figure 23. SEM images of **A)** PCL-PPy-5C-COOH **54**; **B)** PCL-PPy-5C-CONH-β-CD **59**; **C)** PCL-PPy-10C-COOH **62**; **D)** PCL-PPy-10C-CONH-β-CD **65**; scale bar 1 μm

There is a question if flexible carbon linker increases CD ability to form inclusion complexes with serum protein and thus improves cell adhesion, or its more lipophilic character hampers desirable molecular recognition. Therefore, the *in-vitro* experiment was carried out to further understand the behaviour of our new material in contact with biological matter. The experiment was carried out for 14 days with NHDF cells complementary to the previous *in-vitro* experiment. The results of cell viability are summarized in Graph 2 below where the same pattern as before (Graph 1) could be seen. Although the cell metabolic activity of NHDF on the pristine PCL seemed better during the first days of the *in-vitro* experiment, it was greatly surpassed by functionalized materials later.

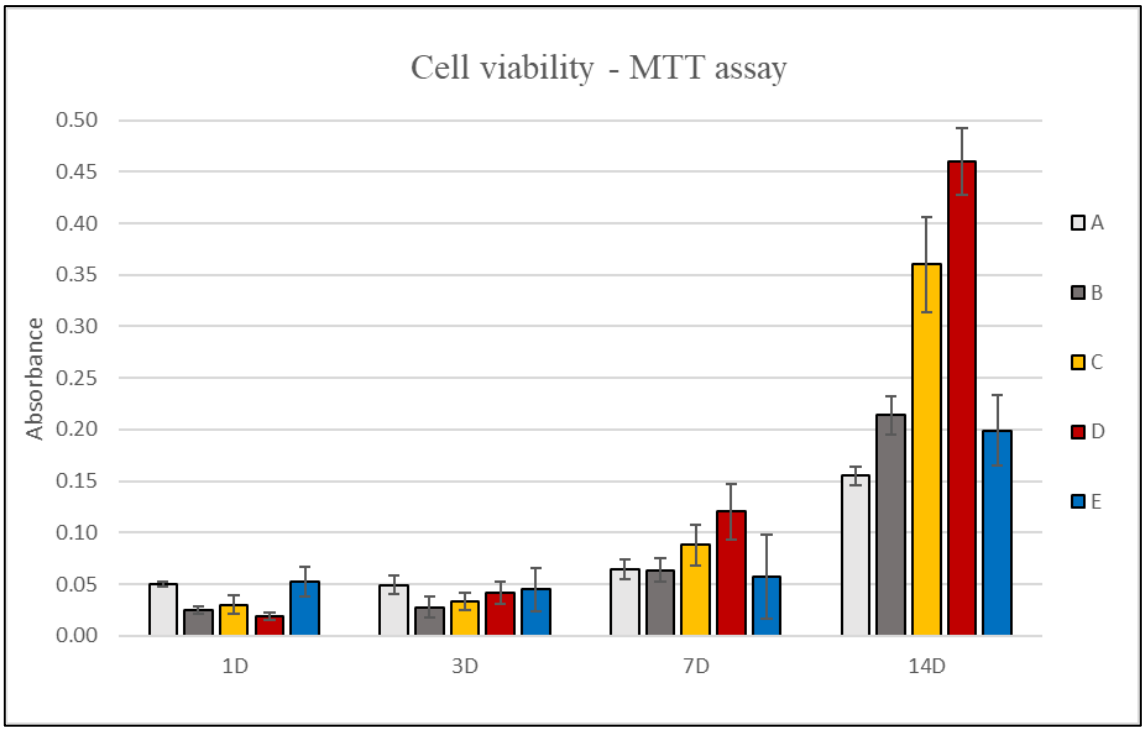

Graph 2. Cell metabolic activity (MTT assay) **A)** PCL; **B)** PCL-PPy-5C-COOH **54**; **C)** PCL-PPy-10C-COOH **62**; **D)** PCL-PPy-5C-CONH-β-CD **59**; **E)** PCL-PPy-10C-CONH-β-CD **65**

If the results are analysed, several conclusions about cell interaction with the fibrous scaffolds can be formulated. Generally, all functionalized materials have a positive effect on the cell adhesion, proliferation and growth. Based on SEM images, cells were well spread and also incorporated in the fibrous structure (Figure 24). Similar data have been obtained from two separate *in-vitro* experiments for PCL, PCL-5C-COOH **54** and PCL-PPy-5C-CONH-β-CD **59** scaffolds. Further, an unexpected behaviour was found for the β-CD functionalized material **65** where its performance was only 28 % better than pristine PCL but surprisingly 81% worse than PCL-PPy composite **62** without β-CD on the surface. On the other hand, in the case of sample **59**, there was almost 200 % increase in cell metabolic activity compared to PCL. Although the cell growth was also better (38 %) on the PCL-PPy **54** compared to PCL the decisive positive influence of β-CD on the cell adhesion and growth has been proved. This result is also fascinating because the attached cyclodextrins have a significant effect on cell activity even in at low surface concentration.

Moreover, the importance of CD distance from the surface has also been described, but we can only speculate what the reasons behind such unexpected behaviour are. One explanation may be that CDs interact with surrounding side chains of pyrrole rings to form rotaxane like supramolecular structures. Therefore, the cavity is occupied and not available for the interaction

with adhesion-mediating proteins. The second reasonable explanation for the surprisingly poor performance of scaffold **65** is that more flexible carbon linker could prevent proper CD-protein interaction or influence the spatial conformation of already attached adhesion proteins.[138] These proteins could be present in high amount but in their unnatural form similarly to lipophilic surfaces with WCA over 100°.

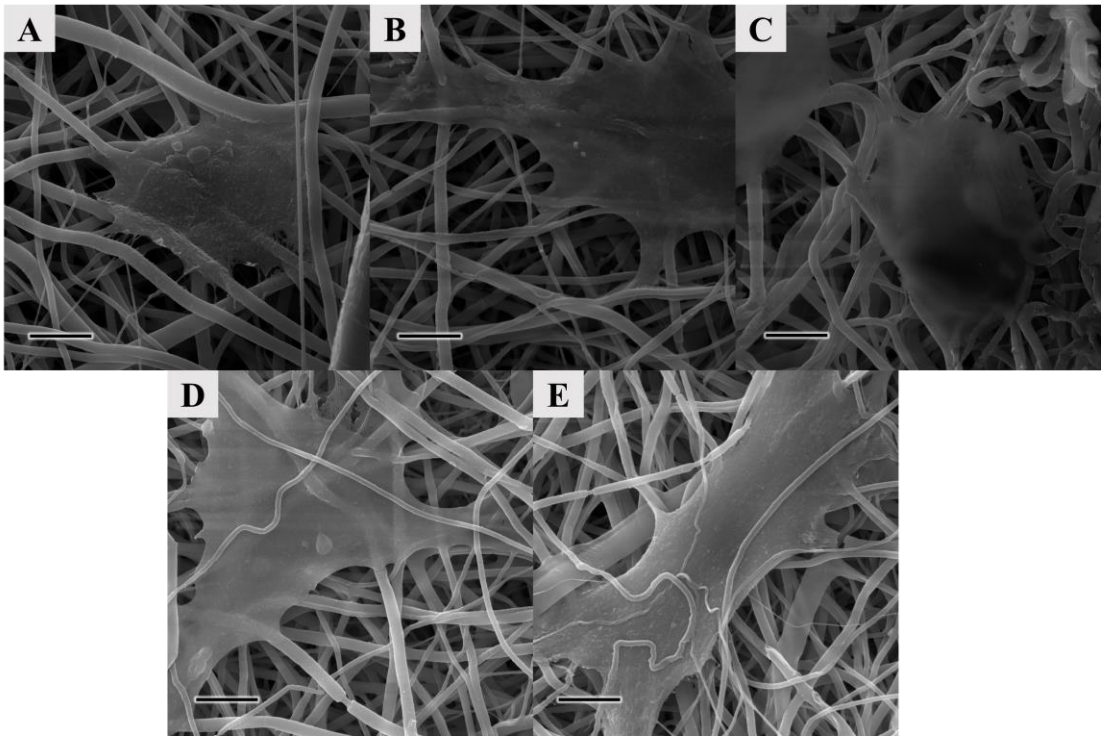

Figure 24. SEM images of NHDF cells on tested materials after 7 days of incubation **A)** PCL; **B)** PCL-PPy-5C-COOH **54**; **C)** PCL-PPy-10C-COOH **62**; **D)** PCL-PPy-5C-CONH-β-CD **59**; **E)** PCL-PPy-10C-CONH-β-CD **65**; scale bar 10 μm

3.6. The extension of research

3.6.1. Possible conjugation methods for CD connection

The copper-free Huisgen dipolar cycloaddition represents the most popular version of CLICK reaction but the classic Cu^+ catalysed protocol can be utilised as well (Scheme 23). The PCL fibrous scaffold was thus functionalized with PPy layer **55** containing a terminal triple bond on the carbon spacer as mentioned earlier in this work. The morphology of newly prepared material PCL-PPy **56** was studied using SEM (Figure 11) and the deposited PPy **55** analysed by IR (Figure 13). Further, the amount of deposited PPy **55** on the PCL fibres was determinate using TGA (Figure 25). The results were consistent with the previous experiments conducted on the complementary PPy derivatives with a carboxy group. However, the amount of deposited PPy **55** was lower even the polymerisation was carried out under similar reaction conditions.

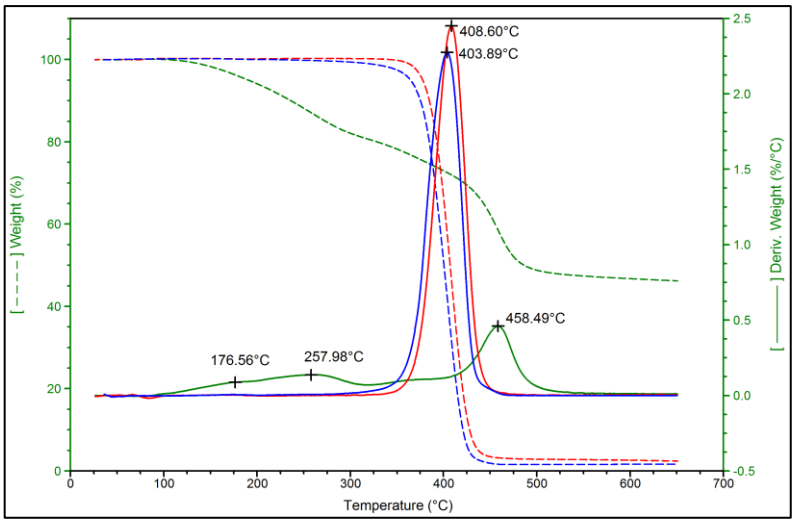

Figure 25. TGA spectra of pristine PCL (**blue**), PPy **55** (**green**) and PCL-PPy **56** (**red**)

It would be interesting to compare if a different type of CD connection (amide bond or triazole ring)[139] have some impact on cell growth. It was also published, that conjugation *via* triazole has many similarities with the classical amide bond, especially the bond length. Such general platform could extend the possibilities of surface functionalization and help us in the development of advanced materials for tissue engineering.

The azido β-CD **35** could be used as a second reaction partner while the Cu^+ catalyst is generated *in situ* by reduction of $CuSO_4$ with ascorbic acid.[140] The water-soluble THTA could be used instead of classical TBTA as a co-catalyst to stabilise the transition state and further improve the overall reaction performance.[141] Finally, the host-guest interaction between Rhodamine B and the CD lipophilic cavity can be exploited as a confirmation and quantification of the immobilised β-CD on the PCL-PPy-4C-triazole-β-CD **66**.

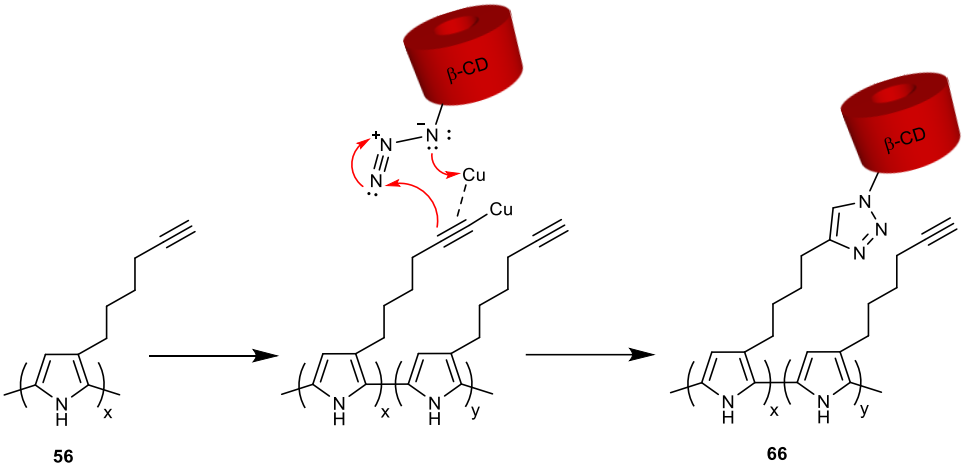

Scheme 23. Possible synthetic route for the immobilisation of CD using copper catalysed Huisgen dipolar cycloaddition

To further extend the possibilities of CD immobilisation the PPy **67** with terminal double bond was deposited onto PCL to produce PCL-PPy-3C-alkene scaffold **68**. The polymerisation of monomer **32** was carried out in methanol with $FeCl_3$ at room temperature as reported previously. Although this material could be functionalized by metathesis reaction, an advanced approach using photo-induced thiol-ene/yne reaction could be examined as well (Scheme 24).[142] It is known that thiol-ene/yne reactions represent an excellent tool for material derivatization.[143,144] Especially mild reaction conditions, high selectivity and almost no side products classify this type of conjugation technique as a cutting edge approach.[145,146] In our research focused on the immobilisation of CD on the fibrous materials such photo-induced reactions could be utilised because the monosubstituted CDs with a thiol group at position C6 are readily available.[147,148] It would be interesting to compare the number of attached CD molecules based on the conjugation technique used e.g. Huisgen dipolar cycloaddition or thio-ene/yne reactions.[149] However, the optimal reaction conditions with suitable initiator have to be found first and resulting materials with immobilised CD thoroughly investigated.

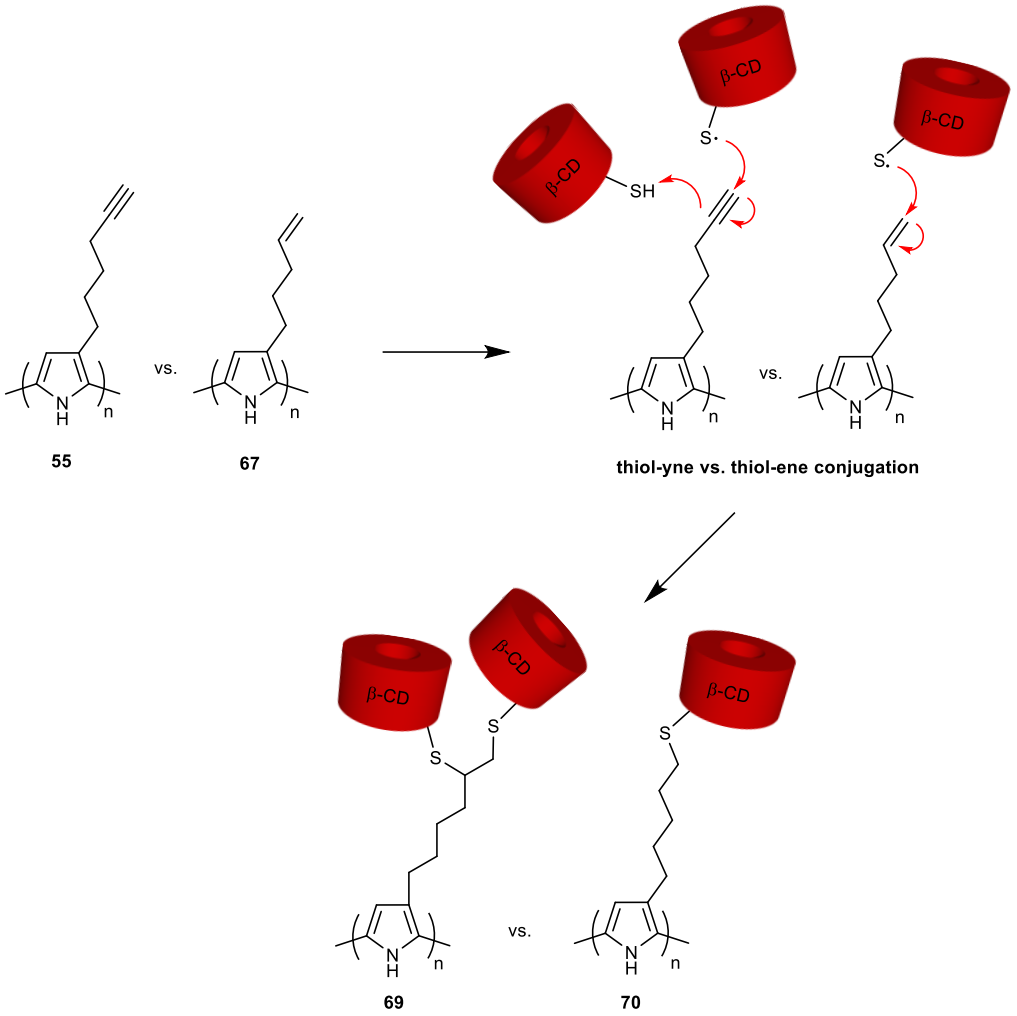

Scheme 24. Comparison of possible CD immobilisation using photo-induced radical thiol-ene or thiol-yne reactions (dopants omitted for better clarity)

Powdered PPy coatings **55** and **67** were measured by IR spectroscopy, and the characteristic peaks have been assigned according to expected polymer structures (Figure 26). In the case of sample **55**, a strong symmetrical valence vibration at 3289 cm^{-1} of single C-H bond at the terminal triple bond and carbon-carbon stretching vibration of multiple bond at 2116 cm^{-1} proved the successful introduction of this functional group. Moreover, the corresponding CH_2 valence vibrations of the carbon linker at 2933 cm^{-1} and 2857 cm^{-1} confirmed the desired structure. Also, PPy **67** featured characteristic vibrations of the terminal double bond in the IR spectrum. The vibrations of C-H on the double bond at 3072 cm^{-1} together with the relatively weak signal of C=C double bond at 1642 cm^{-1} and valence vibration of CH_2 hydrogens at 2933 cm^{-1} and 2857 cm^{-1}confirmed the presence of expected functional groups in the structure of PPy **67**.

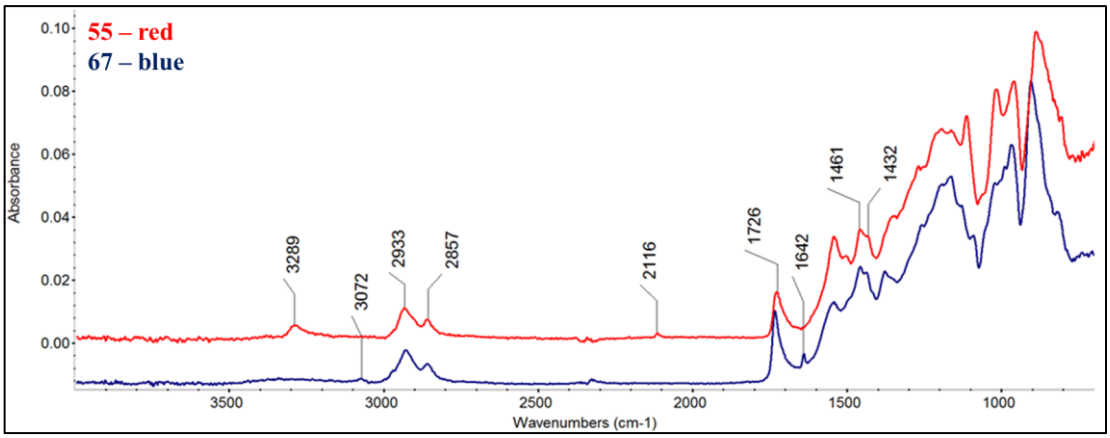

Figure 26. IR spectra of PPy **55** with a triple bond and PPy **67** with a double bond

3.6.2. Series of PPy coatings on the various fibrous scaffolds

Until this moment, all surface functionalization was done on the fibrous PCL. In order to show the usefulness of our deposition protocol, several other polymers have also been coated with PPy **53**. The reaction conditions were the same as previously reported, and the polymers PDX, P4HB, PA6, PVDF used as received. Although PCL is considered as a slowly degrading polymer, some applications require a material which degrades faster in order of weeks or several months. Thus, PDX and PH4B with fibres diameter (0,61 ± 0.38 μm, 0,50 ± 0.32 μm) were functionalized on the surface, and the amount of deposited PPy **53** was calculated based on the TGA measurements (Figure 27). The pristine PDX or P4HB (blue curves) were measured before and after PPy **53** deposition (red curves) representing the TGA spectra of samples PDX-PPy-5C-COOH **71** and P4HB-PPy-5C-COOH **72**. As described in the previous chapters, the amount of PPy **53** deposited on the fibres can be estimated by the difference of the residual weights. During the heating process up to 650 °C, the pristine fibrous materials lost 99.9 % of their weight, while powdered PPy **53** weight loss was only 60.5 %. Therefore, a higher residual weight of functionalized materials can be expected thanks to the PPy **53** surface layer. Moreover, this analysis qualitatively and also quantitatively confirmed the successful introduction of PPy **53** on both polymers. Although the diameter of fibres was approximately the same for PDX and P4HB, the amount of deposited PPy **53** was three times higher in the case of PDX. Also, the thermal properties showed significant change after PPy **53** deposition with the shift of mean decomposition temperature by 28 °C for the sample **71** and 28 °C in the case of material **72**. The morphology of both pristine and coated samples was almost identical. There were none visible structural defects on the surface of the fibres and the materials did not show any changes in their mechanical properties (Figure 28).

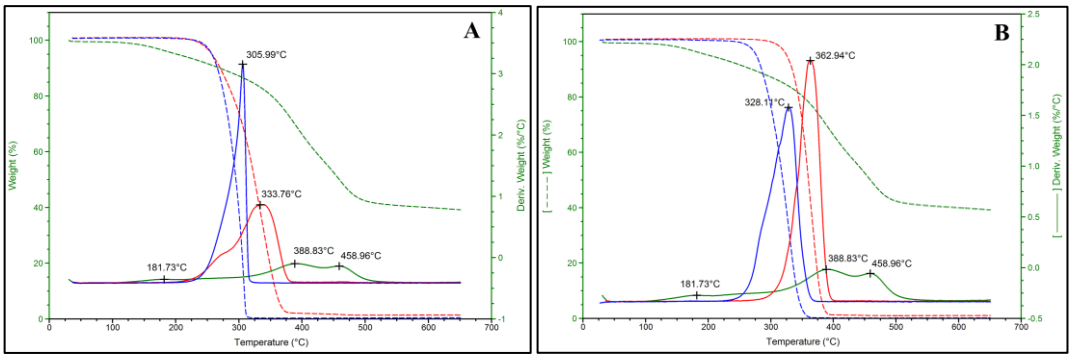

Figure 27. TGA spectra of **A)** PDX (blue), PDX-PPy **71** (red), PPy **53** (green); **B)** P4HB (blue), P4HB-PPy **72** (red), PPy **53** (green)

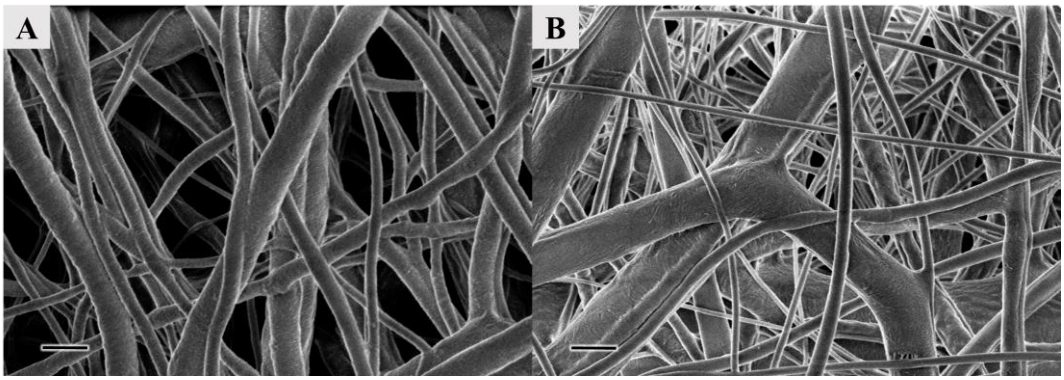

Figure 28. SEM images of **A)** PDX-PPy **71**; **B)** P4HB-PPy **72**; scale bar 1 μm

Two other fibrous scaffolds PA6 and PVDF with fibres diameter (0,15 ± 0.05 μm, 0,28 ± 0.06 μm) were functionalized with PPy **53** as well. These polymers found several applications in tissue engineering for their superior mechanical properties and good environmental stability. However, for the lack of proper biological effect on cell growth and viability, they are often used as blends with other biocompatible polymers. Therefore, the composite scaffolds PA6-PPy-5C-COOH **73** and PVDF-PPy-5C-COOH **74** were prepared as previously reported to extend the scope of this work further. Based on TGA curves and residual weights, the amount of deposited PPy **53** was calculated (Figure 29). Whereas the thickness of PPy layer is difficult to measure on fibrous materials, we can compare the amount of deposited polymer on the surface using TGA. Scaffolds **73** and **74** contained 7.5 % and 7.0 % of PPy **53** according to measured residual weights (see experimental part). Although such a relatively high amount of deposited PPy suggest that PA6 and PVDF have preferable polarity or wettability if compared to P4HB and PDX, the diameter of the fibre should be considered as well. It means that a higher amount of PPy is deposited on the thinner fibres if the thickness of PPy layer is about the same. Nevertheless, the successful introduction of PPy **53** onto PA6 and PVDF fibrous scaffold

could be easily confirmed by TGA. This functionalization also resulted in a smooth coating on both fibrous samples **73** and **74** as shown in Figure 30.

To summarise the last chapter, the β-substituted pyrrole derivative **53** can be quickly deposited onto various fibrous scaffold with high efficiency. Moreover, such a general platform can be tailored according to the desired application by further derivatisation utilising suitable conjugation technique.[150]

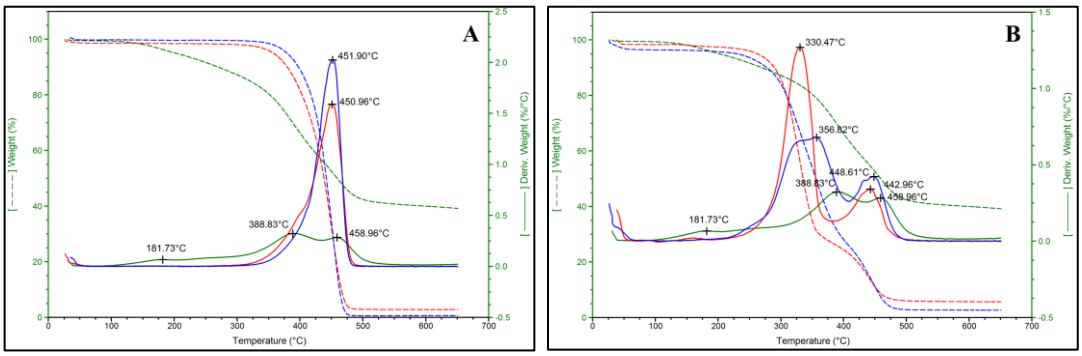

Figure 29. TGA spectra of **A)** PA6 (blue), PA6-PPy **73** (red), PPy **53** (green); **B)** PVDF (blue), PVDF-PPy **74** (red), PPy **53** (green)

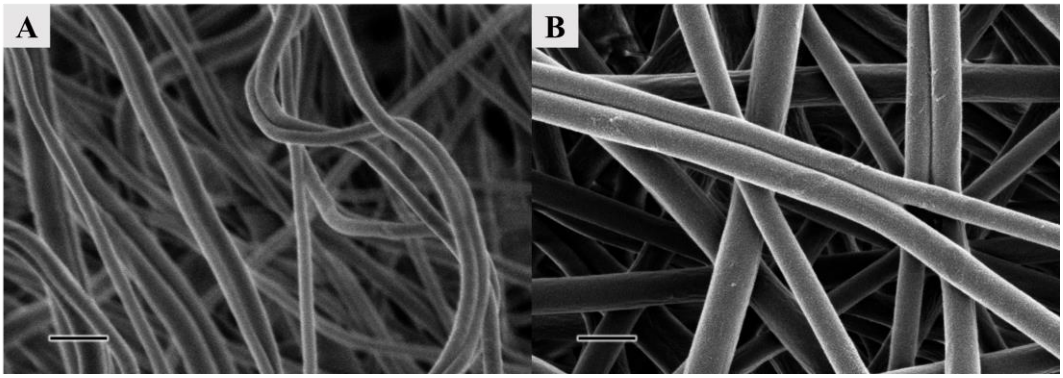

Figure 30. SEM images of **A)** PA6-PPy **73**; **B)** PVDF-PPy **74**; scale bar 500 nm

4. EXPERIMENTAL PART

All the reagents were obtained from standard commercial sources, and the solvents were used as obtained unless otherwise noted. NMR spectra were recorded using Agilent 400-MR DDR2 399.94 MHz for ^{1}H and 100.58 MHz for ^{13}C or JEOL JNM-ECZR 500.16 MHz for ^{1}H and 125.77 MHz for ^{13}C. Samples were measured as solutions in deuterated solvents and referenced to a residual solvent peak. Chemical shifts are given in δ-scale, and coupling constants *J* are given in Hz. HRMS spectra were recorded using GC-MS Autospec Ultima (EI) or LC-MS LTQ-Orbitrap Velos (ESI^+, ESI^- or $APCI^+$). Silica gel 60 and silica gel 60 F254-coated aluminium sheets (both Merck, Germany) were used for column and thin layer chromatography, respectively. Spots were detected under UV or by spraying with 50% aqueous H_2SO_4 solution and carbonisation with a heat-gun.

Pyrrole derivatives **2, 3**, **5**, **8, 10, 13** and (α, β, γ)-CDs **33-44** were prepared according to the published literature.[8,10,129]

4.1. Synthesis of pyrrole derivatives

4.1.1. General procedure for the synthesis of iodoalkylpyrroles 6 and 7

A dry argon-flushed flask was charged with **5** (302 mg, 1 mmol) and anhydrous THF (18 ml). The solution was cooled to 0 °C, and *n*-BuLi (1.18 ml, 2 mmol, 1.7 M solution in THF) was added dropwise over 10 min, and the reaction mixture was stirred for 1 hour. In a second flask 1,5-diiodopentane or 1,10-diiododecane (6 mmol) was dissolved in 3 ml of dry THF and added to the solution of lithiated species *via* a cannula. The reaction mixture was allowed to reach room temperature and stirred for 3 hours before quenched with a saturated solution of NH_4Cl (30 ml). The aqueous layer was extracted with hexane (3 x 25 ml). The combined organic layers were washed with brine (1 x 50 ml), water (1 x 50 ml), dried over $MgSO_4$ and filtered. Solvents were evaporated under reduced pressure and the crude reaction mixture was purified by column chromatography on silica gel using hexane:EtOAc as the mobile phase with gradient elution (20:1, 10:1, 5:1).

3-(5-iodopent-1-yl)-1-(triisopropylsilyl)pyrrole (6)

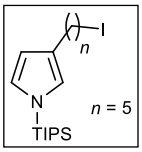

^{1}H NMR (400 MHz, $CDCl_3$) δ 6.70 (t, *J* = 2.4 Hz, 1H), 6.52 (s, 1H), 6.14 (dd, *J* = 2.5, 1.4 Hz, 1H), 3.19 (t, *J* = 7.1 Hz, 2H), 2.50 (t, *J* = 7.4 Hz, 2H), 1.86 (quint, *J* = 7.4 Hz, 2H), 1.60 (quint, *J* = 7.3 Hz, 2H), 1.49-1.37 (m, 5H), 1.09 (d, *J* = 7.4 Hz, 18H); ^{13}C NMR (100 MHz, $CDCl_3$) δ 126.0, 124.2, 121.2, 110.7, 33.7, 30.4, 30.0, 26.9, 18.0, 11.8, 7.5; HRMS ($APCI^+$): calcd for $C_{18}H_{34}INSi$ 420.15780 [$(M+H)^+$)]; found *m/z* 420.15796 [$(M+H)^+$)]; Yield 281 mg (67 %).

3-(10-iododec-1-yl)-1-(triisopropylsilyl)pyrrole (7)

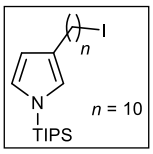

^{1}H NMR (400 MHz, $CDCl_3$) δ 6.69 (t, J = 2.4 Hz, 1H), 6.51 (s, 1H), 6.14 (dd, J = 2.4, 1.3 Hz, 1H), 3.19 (t, J = 7.1 Hz, 2H), 2.47 (t, J = 7.5 Hz, 2H), 1.82 (quint, J = 7.4 Hz, 2H), 1.50-1.18 (m, 17H), 1.09 (d, J = 7.5 Hz, 18H); ^{13}C NMR (100 MHz, $CDCl_3$) δ 126.5, 124.0, 121.1, 110.7, 33.7, 31.2, 30.7, 29.7, 29.61, 29.57, 29.56, 28.7, 27.1, 18.0, 11.9, 7.5; HRMS (APCI$^+$): calcd for $C_{23}H_{44}INSi$ 490.23605 [(M+H)$^+$)]; found *m/z* 490.23645 [(M+H)$^+$)]; Yield 211 mg (43 %).

4.1.2. General procedure for the synthesis of acids 11 and 12

An oven-dried flask was charged with **6** or **7** (1 mmol) and anhydrous THF (5 ml) under argon atmosphere. The solution was cooled to -78 °C and *t*-BuLi (1.09 ml, 1.85 mmol, 1.7 M solution in THF) was added dropwise over 10 min. The reaction mixture was stirred for 1 hour at low temperature before bubbled with CO_2 for 30 minutes. The reaction was quenched with a saturated NH_4Cl solution (30 ml) and acidified with 1M HCl to neutral pH. The aqueous layer was extracted with $CHCl_3$ (3 x 30 ml), the combined organic layers were washed with water (1 x 50 ml), dried over $MgSO_4$ and filtered. Solvents were evaporated under reduced pressure and the crude reaction mixture was purified by column chromatography on silica gel using $CHCl_3$:MeOH with a gradient elution mixture (40:1, 20:1, 5:1).

6-[(1-triisopropylsilyl)pyrrol-3-yl)]hexanoic acid (11)

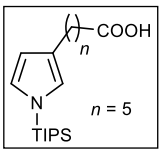

^{1}H NMR (400 MHz, $CDCl_3$) δ 6.68 (t, J = 2.4 Hz, 1H), 6.50 (m, 1H), 6.13 (dd, J = 2.5, 1.4 Hz, 1H), 2.49 (t, J = 7.4 Hz, 2H), 2.34 (t, 7.4 Hz, 2H), 1.66 (quint, J = 7.42 Hz, 2H), 1.59 (quint, J = 7.42 Hz, 2H), 1.50-1.33 (m, 5H), 1.08 (d, J = 7.5, 18H); ^{13}C NMR (100 MHz, $CDCl_3$) δ 180.1, 126.1, 124.1, 121.2, 110.7, 34.2, 30.8, 29.0, 26.9, 24.7, 18.0, 11.8; HRMS (ESI$^-$): calcd for $C_{19}H_{35}NO_2Si$ 336.2364 [(M-H)$^-$)]; found *m/z* 336.2365 [(M-H)$^-$)]; Yield 216 mg (64 %).

11-[(1-triisopropylsilyl)pyrrol-3-yl)]undecanoic acid (12)

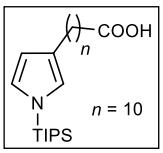

^{1}H NMR (400 MHz, $CDCl_3$) δ 6.68 (t, J = 2.3 Hz, 1H), 6.51 (m, 1H), 6.14 (dd, J = 2.3, 1.2 Hz, 1H), 2.47 (t, J = 7.5 Hz, 2H), 2.34 (t, J = 7.5 Hz, 2H), 1.63 (quint, J = 7.4 Hz, 2H), 1.56 (quint, J = 7.4 Hz, 2H), 1.41 (m, J = 7.5 Hz, 3H), 1.35-1.24 (m, 6H), 1.09 (d, J = 7.5 Hz, 18H); ^{13}C NMR (100 MHz, $CDCl_3$) δ 179.7, 126.5, 124.0, 121.2, 110.7, 34.1, 31.2, 29.8, 29.63, 29.59, 29.58, 29.4, 29.2, 27.2, 24.8, 18.0, 11.9; HRMS (ESI$^-$): calcd for $C_{24}H_{45}NO_2Si$ 406.3147 [(M-H)$^-$)]; found *m/z* 406.3147 [(M-H)$^-$)]; Yield 208 mg (51 %).

4.1.3. Synthesis of pyrrole with a directly connected triple bond

3-ethynyl-1-(triisopropylsilyl)pyrrole (15)

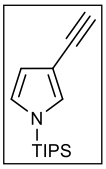

An oven dried flask was charged with the starting compound **5** (166 mg, 0.475 mmol), $Pd(PPh_3)_4$ (28 mg, 23.8 umol) and 2.5 ml of anhydrous THF under argon atmosphere. Ethynylmagnesium bromide (1.4 ml, 0.713 mmol, 0.5 M solution in THF) was added dropwise over 5 minutes, and the stirring was continued for an additional 30 minutes at room temperature. The reaction mixture was quenched with 10 ml of distilled water, and the aqueous phase was extracted with Et_2O (3 x 10 ml). The combined organic layers were dried over $MgSO_4$ and filtered. All volatiles were removed under reduced pressure, and the residual yellowish slurry was purified by column chromatography on silica gel using hexane:EtOAc (10:1) to afford 82 mg of compound **15** as a colourless oil in 75% yield.
^{1}H NMR (400 MHz, $CDCl_3$) δ 7.03 (dd, J = 1.8, 1.5 Hz, 1H), 6.66 (dd, J = 2.6, 2.2 Hz, 1H), 6.41 (dd, J = 2.7, 1.4 Hz, 1H), 2.97 (s, 1H), 1.43 (m, J = 7.5 Hz, 3H), 1.09 (d, J = 7.5 Hz, 18H); ^{13}C NMR (100 MHz, $CDCl_3$) δ 129.4, 124.2, 114.1, 105.2, 79.9. 75.9, 17.8, 11.7; GC-HRMS (EI^+): calcd for $C_{15}H_{25}NSi$ 247.17563 [(M^+)]; found *m/z* 247.17605 [(M^+)].

4.1.4. General procedure for the synthesis of aldehydes 16 and 17

Iodoalkylpyrrole **6** or **7** (2 mmol) was dissolved in 10 ml of DMSO and heated to 110 °C. Sodium bicarbonate (336 mg, 4 mmol) was then added in one portion. The reaction mixture was stirred at this temperature for 90 minutes and monitored by TLC. The excess of DMSO was evaporated under reduced pressure, and the residue was dissolved in Et_2O before washed with H_2O. The aqueous phase was extracted three times with Et_2O (3 x 30 ml), the combined organic phases were extracted with brine (1 x 50 ml), dried over $MgSO_4$ and filtered. All volatiles were removed under reduced pressure, and the crude product was purified by column chromatography on silica gel using hexane:$CHCl_3$ with a gradient elution mixture (1:1, 1:2, 1:4).

5-[(1-triisopropylsilyl)pyrrol-3-yl)]-pentan-1-al (16)

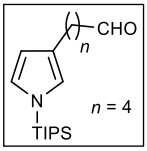

^{1}H NMR (400 MHz, $CDCl_3$) δ 9.74 (t, J = 1.9 Hz, 1H), 6.69 (t, J = 2.3 Hz, 1H), 6.51 (m, 1H), 6.12 (dd, J = 2.3, 1.5 Hz, 1H), 2.51 (t, J = 7.3 Hz, 2H), 2.43 (dt, J = 7.1, 1.9 Hz, 2H), 1.74-1.55 (m, 4H), 1.41 (m, J = 7.5 Hz, 3H), 1.08 (d, J = 7.5, 18H); ^{13}C NMR (100 MHz, $CDCl_3$) δ 203.2, 125.6, 124.5, 121.3, 110.6, 44.0, 30.6, 26.8, 22.0, 18.0, 11.8; HRMS ($APCI^+$): calcd for $C_{18}H_{33}NOSi$ 308.24042 [($M+H)^+$)]; found *m/z* 308.24104 [($M+H)^+$)]; Yield 437 mg (71 %).

10-[(1-triisopropylsilyl)pyrrol-3-yl)]-decan-1-al (17)

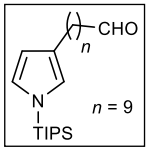

^{1}H NMR (400 MHz, $CDCl_3$) δ 9.76 (t, J = 1.9 Hz, 1H), 6.68 (t, J = 2.3 Hz, 1H), 6.51 (s, 1H), 6.14 (dd, J = 2.3 Hz, 1.4 Hz, 1H), 2.47 (t, J = 7.5 Hz, 2H), 2.41 (dt, J = 7.4, 1.9 Hz, 2H), 1.62 (quint, J = 7.4 Hz, 2H), 1.56 (quint, J = 7.5 Hz, 2H), 1.42 (m, J = 7.5 Hz, 3H), 1.35-1.23 (m, 10H), 1.09 (d, J = 7.5 Hz, 18H); ^{13}C NMR (100 MHz, $CDCl_3$) δ 203.2, 126.5, 124.0, 121.2, 110.7, 44.1, 31.2, 29.58, 29.56, 29.5, 29.3 overlap, 27.1, 22.3, 18.04. 11.86; HRMS (APCI$^+$): calcd for $C_{23}H_{43}NOSi$ 378.31867 [(M+H)$^+$)]; found *m/z* 378.31776 [(M+H)$^+$)]; Yield 438 mg (58 %).

4.1.5. General procedure for the synthesis of pyrroles 18 and 19

Tetrabromomethane (665 mg, 2 mmol) was dissolved in 6 ml of dry CH_2Cl_2, and the solution was cooled to 0 °C using an ice-water bath. Triphenylphosphine (1.05 g, 4 mmol) was added under stirring which resulted in a change of colour from colourless to orange-yellow. After 10 minutes, the aldehyde **16** or **17** (1 mmol) was added as a solution in dry CH_2Cl_2 (2 ml). The reaction mixture was stirred for an additional 30 minutes and then filtered through the plug of silica gel. All volatiles were evaporated under reduced pressure and the residue purified by column chromatography on silica gel (hexane:CH_2Cl_2 5:1) to afford the target compound in good yield.

1-(triisopropylsilyl)-3-(6,6-dibromohex-5-en-1-yl)pyrrole (18)

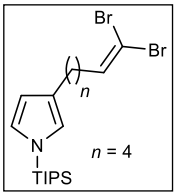

^{1}H NMR (400 MHz, $CDCl_3$) δ 6.69 (t, J = 2.3 Hz, 1H), 6.52 (s, 1H), 6.38 (t, J = 7.3 Hz, 1H), 6.14 (dd, J = 2.4, 1.5 Hz, 1H), 2.50 (t, J = 7.3 Hz, 2H), 2.12 (q, J = 7.4 Hz, 2H), 1.60 (quint, J = 7.5 Hz, 2H), 1.45 (quint, J = 7.5 Hz, 2H), 1.43 (m, J = 7.5 Hz, 3H), 1.09 (d, J = 7.5 Hz, 18H); ^{13}C NMR (100 MHz, $CDCl_3$) δ 139.1, 125.9, 124.2, 121.3, 110.8, 88.5, 33.1, 30.5, 27.6, 26.8, 18.05, 11.9; GC-HRMS (EI$^+$): calcd for $C_{19}H_{33}Br_2NSi$ 463.07294 [(M$^+$)]; found *m/z* 463.07294 [(M$^+$)]; Yield 412 mg (89 %).

1-(triisopropylsilyl)-3-(11,11-dibromoundec-10-en-1-yl)pyrrole (19)

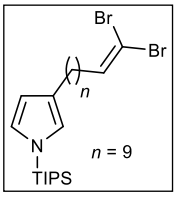

^{1}H NMR (400 MHz, $CDCl_3$) δ 6.68 (t, J = 2.4 Hz, 1H), 6.50 (s, 1H), 6.38 (t, J = 7.3 Hz, 1H), 6.14 (dd, J = 2.4 Hz, 1.4 Hz, 1H), 2.47 (t, J = 7.5 Hz, 2H), 2.08 (q, J = 7.3 Hz, 1H), 1.55 (quint, J = 7.3 Hz, 2H), 1.48-1.36 (m, 5H), 1.35-1.23 (m, 10H), 1.09 (d, J = 7.5 Hz, 18H); ^{13}C NMR (100 MHz, $CDCl_3$) δ 139.1, 126.5, 124.0, 121.2, 110.7, 88.5, 33.2, 31.2, 29.7, 29.61, 29.57, 29.5, 29.2, 28.0, 27.2, 18.0, 11.9; HRMS (APCI$^+$): calcd for $C_{24}H_{43}Br_2NSi$ 534.15838 [(M+H)$^+$)]; found *m/z* 534.15894 [(M+H)$^+$)]; Yield 405 mg (76 %).

4.1.6. General procedure for the synthesis of compounds 20 and 21

A solution of dibromoalkene **18** or **19** (1 mmol) in dry THF (4 ml) was treated with *n*-BuLi (1.18 ml, 2 mmol, 1.7 M solution in hexane) at -78 °C under argon atmosphere. After being stirred for 1 hour at -78 °C, the reaction mixture was allowed to reach room temperature, and the stirring was continued for an additional hour. The reaction was quenched with a saturated solution of NH_4Cl (30 ml) followed by extraction with $CHCl_3$ (3 x 25 ml), combined organic phases were washed with distilled water (1 x 50 ml), dried over $MgSO_4$, filtered and concentrated. The product was purified by column chromatography on silica gel using hexane:$CHCl_3$ (5:1) as a mobile phase.

1-(triisopropylsilyl)-3-(hex-5-yn-1-yl)pyrrole (20)

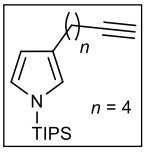

^{1}H NMR (400 MHz, $CDCl_3$) δ 6.69 (t, *J* = 2.4, 1H), 6.52 (m, 1H), 6.14 (dd, *J* = 2.5, 1.4, 1H), 2.51 (t, *J* = 7.3 Hz, 2H), 2.20 (dt, *J* = 7.1, 2.6 Hz, 2H), 1.93 (t, *J* = 2.6 Hz, 1H), 1.75-1.51 (m, 4H), 1.42 (m, *J* = 7.5 Hz, 3H), 1.09 (d, *J* = 7.5 Hz, 18H); ^{13}C NMR (100 MHz, $CDCl_3$) δ 125.9, 124.2, 121.2, 110.7, 85.0, 68.1, 30.2, 28.4, 26.6, 18.4, 18.0, 11.9; HRMS (APCI$^+$): calcd for $C_{19}H_{33}NSi$ 304.24550 [$(M+H)^+$)]; found *m/z* 304.24601 [$(M+H)^+$)]; Yield 291 mg (96 %).

1-(triisopropylsilyl)-3-(undec-5-yn-1-yl)pyrrole (21)

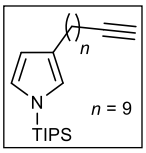

^{1}H NMR (400 MHz, $CDCl_3$) δ 6.69 (t, *J* = 2.4 Hz, 1H), 6.51 (m, 1H), 6.13 (dd, *J* = 2.4, 1.4 Hz, 1H), 2.47 (t, *J* = 7.5 Hz, 2H), 2.17 (dt, *J* = 7.1, 2.6 Hz, 2H), 1.93 (t, *J* = 2.6 Hz, 1H), 1.60-1.48 (m, 2H), 1.46-1.36 (m, 5H), 1.34-1.24 (m, 10H), 1.09 (d, *J* = 7.5 Hz, 18H); ^{13}C NMR (100 MHz, $CDCl_3$) δ 26.5, 124.0, 121.2, 110.7, 85.0, 68.16, 31.6, 29.66, 29.61, 29.58, 29.3, 28.9, 28.7, 27.1, 18.6, 18.0, 11.9; HRMS (APCI$^+$): calcd for $C_{24}H_{43}NSi$ 374.32375 [$(M+H)^+$)]; found *m/z* 374.32419 [$(M+H)^+$)]; Yield 354 mg (95 %).

4.1.7. General procedure for the synthesis of azido derivatives

The round bottom flask was charged with iodoalkylpyrroles **6** or **7** (0.5 mmol), 3 eq. of NaN_3 (1.5 mmol) and 4 ml of dry DMF under argon. The reaction mixture was stirred at room temperature for 15 minutes before quenched with 10 ml of distilled H_2O. The crude product was extracted with Et_2O (3 x 15 ml), the combined organic phases were washed with distilled water (1 x 25 ml), dried over $MgSO_4$, filtered and concentrated under reduced pressure. The product was purified by column chromatography on silica gel using hexane:$CHCl_3$ (7:1) as the mobile phase.

1-(triisopropylsilyl)-3-(5-azidopent-1-yl)pyrrole (22)

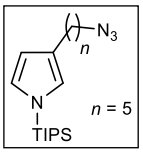

^{1}H NMR (400 MHz, $CDCl_3$) δ 6.69 (t, *J* = 2.4 Hz, 1H), 6.52 (dd, *J* = 2.2, 0.6 Hz, 1H), 6.13 (dd, *J* = 2.5, 1.4 Hz, 1H), 3.52 (t, *J* = 7.1 Hz, 2H), 2.50 (t, *J* = 7.6 Hz, 2H), 1.67-1.56 (m, 4H), 1.47-1.35 (m, 5H), 1.09 (d, *J* = 7.5 Hz, 18H); ^{13}C NMR (100 MHz, $CDCl_3$) δ 126.0, 124.2, 121.2, 110.7, 51.7, 30.7, 28.9, 27.0, 26.6, 18.0, 11.9; HRMS (APCI$^+$): calcd for $C_{18}H_{34}N_4Si$ 335.26255 [(M+H)$^+$)]; found *m/z* 335.26285 [(M+H)$^+$)]; Yield 119 mg (96 %). (hexane:$CHCl_3$ 5:1, R_f = 0.34)

1-(triisopropylsilyl)-3-(10-azidodec-1-yl)pyrrole (23)

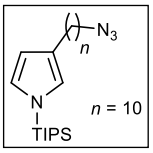

^{1}H NMR (400 MHz, $CDCl_3$) δ 6.69 (t, *J* = 2.4 Hz, 1H), 6.51 (s, 1H), 6.14 (dd, *J* = 2.4, 1.4 Hz, 1H), 3.25 (t, *J* = 7.1 Hz, 2H), 2.47 (t, *J* = 7.5 Hz, 2H), 1.65-1.52 (m, 4H), 1.47-1.23 (m, 17H), 1.09 (d, *J* = 7.5 Hz, 18H); ^{13}C NMR (100 MHz, $CDCl_3$) δ 126.5, 124.0, 121.1, 110.7, 51.7, 31.2, 29.70, 29.62 (overlap), 29.58, 29.3, 29.0, 27.1, 26.9, 18.0, 11.9; HRMS (APCI$^+$): calcd for $C_{23}H_{44}N_4Si$ 405.34080 [(M+H)$^+$)]; found *m/z* 405.34112 [(M+H)$^+$)]; Yield 140 mg (84 %). (hexane:$CHCl_3$ 5:1, R_f = 0.38)

4.1.8. General procedure for the synthesis of cyano derivatives

A flask was charged with pyrrole **6** or **7** (0.5 mmol) and 4 ml of DMSO. In a second flask, 1.5 eq. of sodium cyanide (0.75 mmol) was dissolved in 2 ml of DMSO at elevated temperature. The nucleophilic agent was added dropwise to the first flask over 5 minutes. The course of the reaction was monitored by TLC. After complete conversion of starting compound, a distilled water (30 ml) was added and the crude product extracted with Et_2O (4 x 20 ml). The combined organic fraction was washed with brine (1 x 40 ml), water (1 x 40 ml) and dried over $MgSO_4$. The solvent was evaporated under reduced pressure and the product purified by column chromatography on silica gel using hexane:EtOAc (20:1) as a mobile phase. The target molecules were isolated as a colourless oil which turns brown over time.

1-(triisopropylsilyl)-3-(5-cyanopent-1-yl)pyrrole (24)

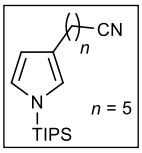

^{1}H NMR (400 MHz, $CDCl_3$) δ 6.70 (t, *J* = 2.4 Hz, 1H), 6.52 (dd, *J* = 1.9, 0.6 Hz, 1H), 6.13 (dd, *J* = 2.5, 1.4 Hz, 1H), 2.50 (t, *J* = 7.6 Hz, 2H), 2.32 (t, *J* = 7.2 Hz, 2H), 1.67 (quint, *J* = 7.5 Hz, 2H), 1.60 (quint, *J* = 7.6 Hz, 2H), 1.49 (quint, *J* = 7.4 Hz, 2H), 1.42 (m, *J* = 7.5 Hz, 3H), 1.09 (d, *J* = 7.5 Hz, 18H); ^{13}C NMR (100 MHz, $CDCl_3$) δ 125.7, 124.3, 121.2, 110.6, 30.3, 29.9, 28.5, 26.8, 25.4, 18.0, 11.8; HRMS (APCI$^+$): calcd for $C_{19}H_{34}N_2Si$ 319.25640 [(M+H)$^+$)]; found *m/z* 319.25678 [(M+H)$^+$)]; Yield 81 mg (51 %). (hexane:EtOAc 15:1, R_f = 0.22)

1-(triisopropylsilyl)-3-(5-azidodec-1-yl)pyrrole (25)

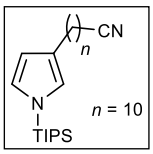

^{1}H NMR (400 MHz, $CDCl_3$) δ 6.69 (t, *J* = 2.4 Hz, 1H), 6.51 (s, 1H), 6.14 (dd, *J* = 2.4, 1.4 Hz, 1H), 2.47 (t, *J* = 7.6 Hz, 2H), 2.33 (t, *J* = 7.2 Hz, 2H), 1.65 (quint, *J* = 7.4 Hz, 2H), 1.45-1.25 (m, 17H), 1.09 (d, *J* = 7.5 Hz, 18H); ^{13}C NMR (100 MHz, $CDCl_3$) δ 126.5, 124.0, 121.1, 120.0, 110.7, 31.2, 29.64, 29.57, 29.55, 29.43, 28.91, 28.82, 27.13, 27.07, 25.5, 18.0, 11.9; HRMS (APCI$^+$): calcd for $C_{19}H_{34}N_2Si$ 389.33465 [(M+H)$^+$)]; found *m/z* 389.33509 [(M+H)$^+$)]; Yield 113 mg (58 %). (hexane:EtOAc 15:1, R_f = 0.24)

4.1.9. Synthesis of alkenyl pyrroles

1-(triisopropylsilyl)-3-(pent-4-en-1-yl)pyrrole (26)

A round-bottom flask was charged with compound **8** (186 mg, 0.5 mmol), sealed with rubber septum, evacuated and filled with argon three times. Then 4.5 ml of dry THF (freshly distilled form Na/benzophenone) was added *via* cannula under argon. The reaction mixture was heated to 55 °C before 2 eq. of LDA (758 µl of 1M solution in THF) were added dropwise. After 60 minutes the flask was allowed to reach room temperature and 10 ml of saturated aqueous solution of NH_4Cl was added. The product was extracted with $CHCl_3$ (3 x 15 ml), combined organic phases were washed with distilled water (30 ml), dried over $MgSO_4$ and concentrated. Column chromatography on silica gel (mobile phase hexane:$CHCl_3$ 5:1, R_f = 0.45) afforded title compound **26** in 63% yield.

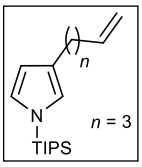

^{1}H NMR (400 MHz, $CDCl_3$) δ 6.70 (t, *J* = 2.4 Hz, 1H), 6.53 (s, 1H), 6.15 (dd, *J* = 2.4, 1.4 Hz, 1H), 5.86 (ddt, *J* = 16.9, 10.3, 6.7 Hz, 1H), 5.06-4.92 (m, 2H), 2.51 (t, *J* = 7.6 Hz, 2H), 2.10 (quart, *J* = 7.6 Hz, 2H), 1.68 (quint, *J* = 7.6 Hz, 2H), 1.42 (m, 3H), 1.09 (d, *J* = 7.4 Hz, 18H); ^{13}C NMR (100 MHz, $CDCl_3$) δ 139.4, 126.1, 124.1, 121.3, 114.4, 110.7, 33.7, 30.4, 29.9, 26.6, 18.0, 11.9; HRMS (APCI$^+$): calcd for $C_{18}H_{33}NSi$ 292.24674[$(M+H)^+$)]; found *m/z* 292.24691 [$(M+H)^+$)]; Yield 72 mg (63 %).

3-(pent-4-en-1-yl)pyrrole (32)

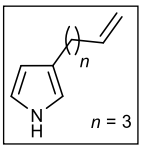

The solution of 1 M TBAF in THF (515 µl, 0.515 mmol) was added to a stirred solution of compound **26** (143 mg, 0.49 mmol) in dry THF at 0 °C under argon. The reaction turned yellow and was stirred for 60 minutes. All volatiles were evaporated under reduced pressure and the oily residue purified by column chromatography on silica gel (mobile phase hexane:$CHCl_3$ 1:1, R_f = 0.33) to afford 61 mg of compound **32** as colourless oil in 92% yield.

^{1}H NMR (500 MHz, $CDCl^3$) δ 7.99 (br s, 1H), 6.73 (tdt, *J* = 2.7, 2.0, 0.3 Hz, 1H), 6.59 (dddt, *J* = 2.4, 2.0, 1.6, 0.8, 1H), 6.11 (tdt, *J* = 2.7, 1.6, 0.5 Hz, 1H), 5.87 (ddtt, *J* = 17.1, 10.2, 6.7, 0.3 Hz, 1H), 5.04 (ddt, *J* = 17.1, 2.2, 1.7 Hz, 1H), 4.97 (ddt, *J* = 10.2, 2.2, 1.3 Hz, 1H), 2.52 (t, *J* = 7.7 Hz, 2H), 2.13 (quart, *J* = 7.2 Hz, 2H), 1.70 (quint, *J* = 7.6 Hz, 2H); ^{13}C NMR (126 MHz, $CDCl_3$) δ 139.2, 124.3, 117.8, 115.1, 114.5, 108.7, 33.7, 30.5, 26.5; HRMS (APCI$^+$): calcd for $C_9H_{13}N$ 136.11219 [$(M+H)^+$)]; found *m/z* 136.11213 [$(M+H)^+$)]; Yield 61 mg (92 %).

4.1.10. Synthesis of pyrrolyl carboxylic acid

An oven-dried flask was charged with (6 mmol) of compound **11** or **12**, evacuated and refilled with argon three times. Dry THF (29 ml) was added *via* cannula, and the reaction mixture was cooled to 0 °C using NaCl/H_2O bath. The reaction mixture was treated with 1.05 eq. of 1 M TBAF (6.3 ml) at low temperature and stirred for 60 minutes. Then, all volatiles were evaporated under reduced pressure, and the semi-solid residue was purified by column chromatography on silica gel with gradient elution strength ($CHCl_3$:MeOH 40:1, 20:1, 5:1, 1:1). Target compounds **28** and **29** were isolated as grey solids in good yields.

6-[pyrrol-3-yl)]hexanoic acid (28)

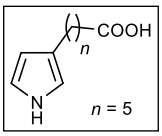

^{1}H NMR (500 MHz, $CDCl_3$/DMSO-d^6) δ 9.24 (br s, 1H), 6.36 (ddd, *J* = 2.6, 2.0, 0.2 Hz, 1H), 6.23 (ddd, *J* = 2.5, 2.0, 1.6, 0.8 Hz, 1H), 5.70 (ddd, *J* = 2.7, 1.6, 0.5 Hz, 1H), 2.17 (t, *J* = 7.6 Hz, 2H), 1.97 (t, *J* = 7.6 Hz, 2H), 1.34 (quint, *J* = 7.3 Hz, 2H), 1.29 (quint, *J* = 7.4 Hz, 2H), 1.10 (quint, *J* = 7.7 Hz, 2H); ^{13}C NMR (126 MHz, DMSO-d^6) δ 175.6, 122.9, 116.8, 114.2, 107.2, 33.6, 30.4, 28.4, 26.2, 24.2; HRMS (APCI$^+$): calcd for $C_{10}H_{15}NO_2$ 182.11756 [(M+H)$^+$)]; found *m/z* 182.11757 [(M+H)$^+$)]; Yield 946 mg (87 %). ($CHCl_3$:MeOH 5:1, R_f = 0.18).

11-[pyrrol-3-yl)]undecanoic acid (29)

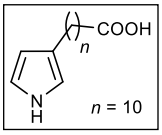

^{1}H NMR (500 MHz, DMSO-d^6) δ 11.94 (br s, 1H), 10.35 (br s, 1H), 6.59 (ddd, *J* = 2.7, 2.6, 2.0 Hz, 1H), 6.47 (dddt, *J* = 2.5, 2.0, 1.6, 0.8 Hz, 1H), 5.84 (dddt, *J* = 2.6, 2.6, 1.6, 0.5 Hz, 1H), 2.35 (t, *J* = 7.5 Hz, 2H), 2.18 (t, *J* = 7.4 Hz, 2H), 1.52-1.42 (m, 4H), 1.29-1.21 (m, 12H); ^{13}C NMR (126 MHz, DMSO-d^6) δ 174.5, 122.5, 117.2, 114.5, 107.4, 33.7, 31.0, 29.0, 28.94, 28.92, 28.91, 28.74, 28.55, 26.6, 24.5.

HRMS (APCI$^+$): calcd for $C_{15}H_{25}NO_2$ 252.19581 [(M+H)$^+$)]; found *m/z* 252.19558 [(M+H)$^+$)]; Yield 1,27 g (84 %). ($CHCl_3$:MeOH 5:1, R_f = 0.21).

4.1.11. Synthesis of alkynyl pyrroles

The solution of 1 M TBAF in THF (525 µl, 0.525 mmol) was added to a stirred solution of compound **20** or **21** (0.5 mmol) dissolved in dry THF at 0 °C under argon. The reaction turned yellow and was stirred for 60 minutes. All volatiles were evaporated under reduced pressure and the oily residue purified by column chromatography on silica gel (mobile phase hexane:$CHCl_3$ 1:1, 1:2, 1:5) to afford desired compounds in high yields.

3-(hex-5-yn-1-yl)pyrrole (30)

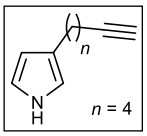

^{1}H NMR (400 MHz, $CDCl_3$) δ 8.01 (br s, 1H), 6.73 (br t, *J* = 2.7 Hz, 1H), 6.59 (br s, 1H), 6.11 (br t, *J* = 2.7 Hz, 1H), 2.54 (t, *J* = 7.5 Hz, 2H), 2.22 (td, *J* = 7.2, 2.7 Hz, 2H), 1.96 (t, *J* = 2.7 Hz, 1H), 1.72 (quint, *J* = 7.6 Hz, 1H), 1.62 (quint, *J* = 7.4 Hz, 2H); ^{13}C NMR (100 MHz, $CDCl_3$) δ 124.1, 117.8, 115.1, 108.6, 84.9, 68.3, 30.3, 28.4, 26.5, 18.4; HRMS (APCI$^+$): calcd for $C_{10}H_{13}N$ 148.11208 [(M+H)$^+$)]; found *m/z* 148.11215 [(M+H)$^+$)]; Yield 68 mg (92 %). (hexane:$CHCl_3$ 1:1, R_f = 0.25).

3-(undec-10-yn-1-yl)pyrrole (31)

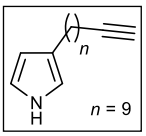

^{1}H NMR (400 MHz, $CDCl_3$) δ 7.98 (br s, 1H), 6.72 (dd, *J* = 4.8, 2.5 Hz, 1H), 6.57 (dd, *J* = 2.4, 1.6 Hz, 1H), 6.09 (dd, *J* = 2.5, 1.7 Hz, 1H), 2.48 (t, *J* = 7.8 Hz, 2H), 2.18 (dt, *J* = 7.1, 2.6 Hz, 2H), 1.94 (t, *J* = 2.6 Hz, 1H), 1.62-1.48 (m, 4H), 1.43-1.25 (m, 10H); ^{13}C NMR (100 MHz, $CDCl_3$) δ 124.8, 117.7, 114.9, 108.7, 85.0, 68.2, 31.4, 29.65, 29.63, 29.62, 29.26, 28.91, 28.65, 27.08, 18.55; HRMS (APCI$^+$): calcd for $C_{15}H_{23}N$ 218.19033 [(M+H)$^+$)]; found *m/z* 218.19045 [(M+H)$^+$)]; Yield 97 mg (89 %). (hexane:$CHCl_3$ 1:1, R_f = 0.29).

4.2. Synthesis of Py-CD conjugates

4.2.1. General procedure for the synthesis of compounds 45-47

Acids **10**, **11**or **12** (0.662 mmol), 6^A-deoxy-6^A-amino-β-CD (500 mg, 0.441 mmol) and PyBOP (275 mg, 0.529 mmol) were dissolved in 11 ml of dry DMF. Then DIPEA (154 µl, 0.882 mmol) was added, and the reaction mixture was stirred for 16 hours at room temperature under argon atmosphere. Triethylamine (614 µl, 4.41 mmol) together with HF (44 µl, 0.882 mmol, 35% solution in H_2O) was added, and the reaction mixture was stirred for an additional hour. All volatiles were evaporated under reduced pressure, and the oily residue precipitated with acetone (100 ml). The white solid was collected by filtration on sintered glass funnel, washed with acetone, dichloromethane and ethyl acetate.

***N*-(6^A-Deoxy-β-cyclodextrin-6^A-yl)-1H-pyrrole-3-carboxyamide (45)**

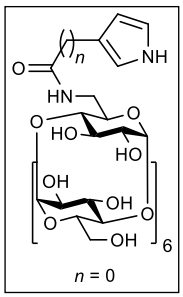

^{1}H NMR (400 MHz, DMSO-d_6) δ 11.05 (s, 1H), 7.44 (t, J = 5.4 Hz, 1H), 7.28 (m, 1H), 6.71 (dd, J = 4.6, 2.2 Hz, 1H), 6.42 (m, 1H), 6.01-5.39 (m, 14H), 4.95-4.65 (m, 7 H), 4.61-4.28 (m, 6H), 4.14-3.02 (m, 42H, overlap H_2O); ^{13}C NMR (100 MHz, DMSO-d_6) δ 164.3, 120.4, 119.4, 118.3, 107.2, 102.4-101.7, 101.2, 84.3, 81.9-81.3, 80.6, 73.5, 73.3-71.6, 70.3, 60.3-59.3; HRMS (ESI$^+$): calcd for $C_{47}H_{74}N_2O_{35}$ 1249.3964 [(M+Na)$^+$)]; found *m/z* 1249.3961 [(M+Na)$^+$)]; Yield 449 mg (83 %).

***N*-(6^A-Deoxy-β-cyclodextrin-6^A-yl)-6-(1H-pyrrol-3-yl)hexanamide (46)**

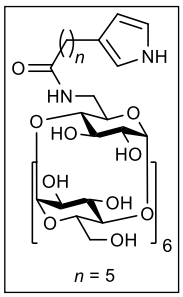

^{1}H NMR (400 MHz, DMSO-d_6) δ 10.34 (s, 1H), 7.57 (t, J = 5.2 Hz, 1H), 6.60 (dd, J = 4.5, 2.3 Hz,), 6.49 (m, 1H), 6.11-5.25 (m, 15H), 5.04-4.71 (m, 7H), 4.62-4.32 (m, 6H), 3.94-3.02 (m, 42H, overlap H_2O), 2.36 (t, J = 7.5 Hz, 2H), 2.08 (m, 2H), 1.57-1.39 (m, 4H), 1.26 (m, 2H); ^{13}C NMR (100 MHz, DMSO-d_6) δ 172.5, 122.5, 117.2, 114.5, 107.4, 102.3-101.6, 81.7-81.2, 73.2-71.8, 72.0, 60.2-59.5, 35.2, 30.7, 28.6, 26.6, 25.2; HRMS (ESI$^+$): calcd for $C_{52}H_{84}N_2O_{35}$ 1319.4747 [(M+Na)$^+$)]; found *m/z* 1319.4743 [(M+Na)$^+$)]; Yield 492 mg (86 %).

***N*-(6^{A}-Deoxy-β-cyclodextrin-6^{A}-yl)-11-(1H-pyrrol-3-yl)undecanamide (47)**

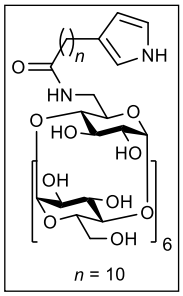

^{1}H NMR (400 MHz, DMSO-d_6) δ 10.33 (s, 1H), 7.56 (t, J = 5.2 Hz, 1H), 6.59 (dd, J = 4.7, 2.4 Hz, 1H), 6.48 (m, 1H), 6.03-5.43 (m, 15H), 4.95-4.71 (m, 7H), 4.56-4.32 (m, 6H), 3.91-3.00 (m, 42H, overlap H_2O), 2.36 (t, J = 7.4 Hz, 2H), 2.08 (m, 2H), 1.56-1.36 (m, 4H), 1.35-1.04 (m, 12H); ^{13}C NMR (100 MHz, DMSO-d_6) δ 172.5, 122.5, 117.2, 114.5, 107.4, 102.3-101.6, 83.6, 81.7-81.2, 73.1-72.9, 60.1-59.7, 35.1, 31.0, 29.05, 29.00, 28.96, 28.92, 28.78, 28.71, 26.6, 25.2; HRMS (ESI^{+}): calcd for $C_{52}H_{84}N_2O_{35}$ 1389.5529 [(M+Na)$^{+}$)]; found *m/z* 1389.5522 [(M+Na)$^{+}$)]; Yield 428 mg (71 %).

4.2.2. General procedure for the synthesis of compounds 48-50

A flask was charged with 6^{A}-deoxy-6^{A}-azido-β-CD (500 mg, 0.431 mmol), pyrrole **15**, **20** or **21** (0.647 mmol) and ascorbic acid (11 mg, 64.7 μmol as a solution in 0.5 ml of H_2O). Subsequently, a mixture of DMSO/H_2O (4:1, 38 ml) was added, and argon was bubbled through the solution for 20 minutes. Next, TBTA (46 mg, 86.2 μmol) was added, and the reaction mixture was heated to 60 °C under argon atmosphere. Finally, $CuSO_4$ (3.5 mg, 21.6 μmol as a solution in 500 μl of H_2O) was added *via* a cannula over 5 minutes and the stirring was continued for 16 hours. The solvents were evaporated under reduced pressure, and the solid residue was precipitated with acetone (100 ml), filtered and vacuum-dried. The TIPS-protected intermediate was dissolved without further purification in DMF (10 ml), and triethylamine (600 μl, 4.31 mmol) together with HF (43 μl, 0.862 mmol, 35% solution in H_2O) were added. The reaction mixture was stirred for 1 hour before poured into acetone (150 ml). The white precipitate was collected by filtration on sintered glass funnel, washed with acetone, dichloromethane, ethyl acetate and dried.

6^{A}-Deoxy-6^{A}-[4-(1H-pyrrol-3-yl)-1,2,3-triazol-1-yl]-β-cyclodextrin (48)

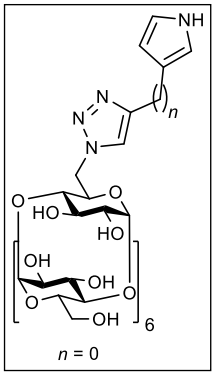

^{1}H NMR (400 MHz, DMSO-d_6) δ 10.85 (s, 1H), 8.06 (s, 1H), 7.11 (m, 1H), 6.76 (m, 1H), 6.34 (m, 1H), 5.85-5.47 (m, 14H), 5.05 (d, J = 3.4 Hz, 1H), 4.90-4.73 (m, 6H), 4.64-4.39 (m, 6H), 4.23 (m, 1H), 4.10 (m, 1H), 3.96-2.90(m, 40H); ^{13}C NMR (100 MHz, , DMSO-d_6) δ 143.7, 128.7, 119.8, 118.4, 114.9, 114.0, 105.8, 102.3-101.7, 101.0, 83.6, 82.2, 81.5, 81.4, 81.2, 80.5, 73.3-71.7, 69.8, 60.4-60.2, 60.0-59.4, 58.4; HRMS (ESI^{+}): calcd for $C_{48}H_{74}N_4O_{34}$ 1273.4077 [(M+Na)$^{+}$)]; found *m/z* 1273.4075 [(M+Na)$^{+}$)]; Yield 475 mg (88 %).

6^{A}-Deoxy-6^{A}-{4-[4-(1H-pyrrol-3-yl)-but-1-yl]-1,2,3-triazol-1-yl}-β-cyclodextrin (49)

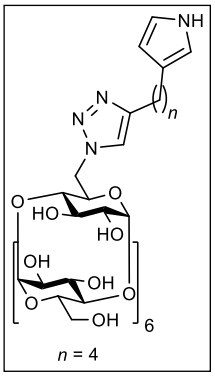

^{1}H NMR (400 MHz, DMSO-d_6) δ 10.35 (s, 1H), 7.74 (s, 1H), 6.60 (dd, J = 4.6, 2.3 Hz, 1H), 6.50 (m, 1H), 5.90-5.55 (m, 15H), 5.03 (d, J = 3.3 Hz, 1H), 4.89-4.72 (m, 6H), 4.63-4.38 (m, 6H), 4.29 (m, 1H), 4.06-2.79 (m, 41H), 2.59 (t, J = 7.4 Hz, 2H), 2.41 (t, J = 7.3 Hz, 2H), 1.68-1.47 (m, 4H); ^{13}C NMR (100 MHz, DMSO-d_6) δ 146.8, 122.7, 122.4, 117.2, 114.6, 107.5, 102.3-101.8, 101.1, 83.5, 82.0, 81.6-81.3, 80.7, 73.3-72.8, 72.6-71.7, 70.0, 62.5, 60.2-59.7, 58.8, 30.7, 28.8, 26.4, 24.9; HRMS (ESI^{+}): calcd for $C_{52}H_{82}N_4O_{34}$ 1329.4703 [(M+Na)$^{+}$)]; found *m/z* 1329.4681 [(M+Na)$^{+}$)]; Yield 485 mg (86 %).

6^{A}-Deoxy-6^{A}-{4-[9-(1H-pyrrol-3-yl)non-1-yl]-1,2,3-triazol-1-yl}-β-cyclodextrin (50)

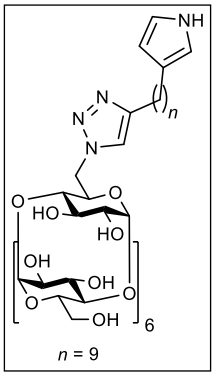

^{1}H NMR (400 MHz, DMSO-d_6) δ 10.33 (s, 1H), 7.75 (s, 1H), 6.59 (dd, J = 4.7, 2.4 Hz, 1H), 6.48 (m, 1H), 6.03-5.37 (m, 15H), 5.03 (d, J = 3.5 Hz, 1H), 4.92-4.72, (m, 6H), 4.61-4.35 (m, 6H), 4.28 (t, J = 5.8 Hz, 1H), 4.13-2.82 (m, 41H), 2.56 (t, J = 7.6 Hz, 2H), 2.36 (t, J = 7.6 Hz, 2H), 1.58 (m, 2H), 1.48 (m, 2H), 1.43-1.03 (m, 10H); ^{13}C NMR (100 MHz, DMSO-d_6) δ 146.8, 122.7, 122.5, 117.2, 114.5, 107.4, 102.2-101.7, 101.1, 83.5, 82.2-81.9, 81.6-81.3, 80.7-80.6, 73.3-71.7, 70.0, 60.2-59.7, 58.9-58.8, 31.0, 29.08, 28.95, 28.94, 28.93, 28.81, 28.78, 26.6, 25.0; HRMS (ESI^{+}): calcd for $C_{57}H_{92}N_4O_{34}$ 1399.5485 [(M+Na)$^{+}$)]; found *m/z* 1399.5489 [(M+Na)$^{+}$)]; Yield 469 mg (79 %).

4.3. Polymerisation of pyrrole and its derivatives

4.3.1. Preparation of pristine polypyrrole

Test tubes were attached to the self-made PS holder and fit in a shaker Figure 31. Each test tube was charged with 4 ml of MeOH/H_2O 3:2 v/v mixture and freshly distilled pyrrole (4.16 µl, 60 µmol). Aligned PCL fibres clamped on the PMMA circlet were immersed in the monomer solution for 60 minutes. Then, 2.4 eq. (38.9 mg, 0.144 mmol) of $FeCl_3.6H_2O$ was added as a solution in 2 ml of MeOH/H_2O 3:2 v/v mixture. All test tubes were sealed with a rubber septum and shaken at 150 rpm for 3 days. The samples were rinsed with a copious amount of distilled water, methanol and sonicated five times in the MeOH/H_2O 3:2 *v/v* mixture for 10 minutes. In the end, the PCL fibres were allowed to air dry, dried under reduced pressure and stored in the desiccator.

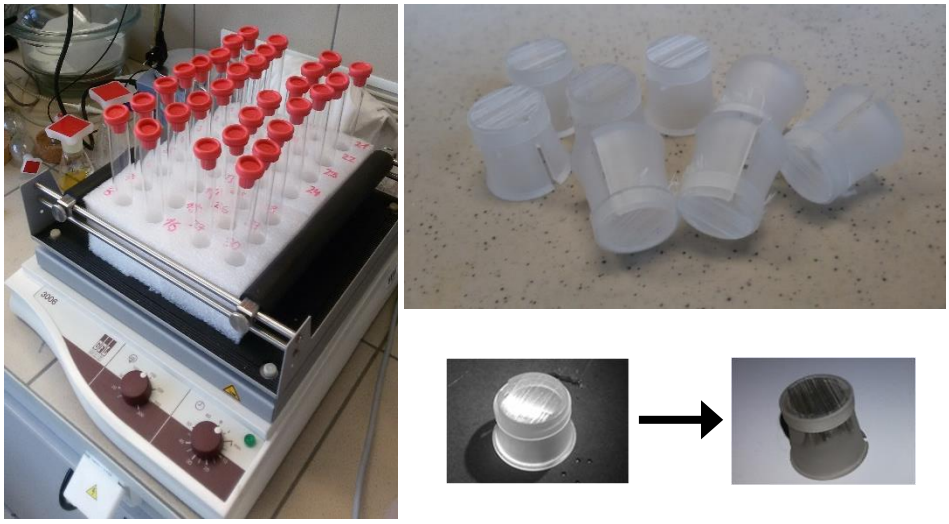

Figure 31. Self-made holder with test-tubes and PCL samples

4.3.2. Polymerization of pyrrole monomers 27, 28, 29

A glass vial with polypropylene cap was charged with 0.1 mmol of corresponding pyrrole monomer dissolved in 3.2 ml of methanol. The PCL sheet made by electrospinning with area weigh of 5.23 mg/cm^2 was cut into circles with a diameter of 0.9 cm and immersed for 60 minutes into the monomer solution. Then, 2.4 eq. of $FeCl_3.6H_2O$ (65 mg, 0.24 mmol) was added as a solution in 0.8 ml of methanol. After addition, the target concentration 2.5 mM of pyrrole monomer was achieved, and the polymerisation shook (150 rpm) at room temperature for 12 hours. The reaction became green/black which indicated the formation of insoluble polypyrrole (Figure 32). All samples were rinsed with a copious amount of methanol and sonicated five times in the MeOH for 5 minutes. Eventualy the PCL fibres were allowed to air dry, dried under reduced pressure and stored in the desiccator.

Figure 32. Images of PCL samples after soaking with the solution of pyrrole **28**, **29** and **27** (**left**), immediately after addition of $FeCl_3$ (**middle**); samples after 12 hours at RT (**right**)

4.3.2.1. Immobilisation of α- β- or γ-NH_2-cyclodextrin onto material 54 or 62

Corresponding samples from the previous experiment were sonicated in MES buffer (c = 10 mM, pH = 6) until they were completely soaked with the solvent. Then, they were transferred to 12 ml of fresh buffer solution. EDC (200 mg, 1.04 mmol) was dissolved together with NHS (300 mg, 2.6 mmol) in 8 ml of MES buffer and added in one portion to the reaction chamber. The reaction vessel was closed with a cap and gently shaken at 150 rpm for 3 hours at room temperature. After activation of carboxy groups, the solvent was removed, and 20 ml of the fresh buffer with 41.6 μmol dissolved NH_2-CD (**36**, **40** or **44**) was added. The functionalization proceeded for 12 hours before the buffer was removed and the samples rinsed with copious amount distilled water, sonicated 6 times for 5 minutes in water and allowed to air dry. Finally, all samples were dried under vacuum and stored in a desiccator.

4.3.3. Polymerisation of pyrroles 30 and 32

An inert polypropylene reaction vessel was charged with 3.2 ml of methanol and (0.1 mmol) of oily compound **30** or **32**. The solution turned slightly brown after addition of pyrrole monomer, but no precipitation occurred. The PCL scaffold with submicron fibres diameter and area weigh of 5.23 mg/cm2 was cut into circles and immersed for 60 minutes into the monomer solution. Then, 2.4 eq. of $FeCl_3.6H_2O$ (65 mg, 0.24 mmol) was added as a solution in 0.8ml of methanol. After addition, the target concentration 2.5 mM of pyrrole monomer was achieved, and the polymerisation continued (150 rpm) at room temperature for 12 hours. Then, all samples were removed and thoroughly washed with methanol, sonicated five times in the MeOH for 5 minutes to remove dispersed polypyrrole and excess of an oxidation agent. Eventually the end the PCL fibres were allowed to air dry, dried under reduced pressure and stored in the desiccator before use.

4.4. Characterisation of PPy coated fibrous scaffolds

4.4.1. Thermogravimetric analysis

The thermogravimetric analyser Q500 (TA Instruments, USA) was used for all experiments. The sample was placed on the platinum pan, and the thermal properties were analysed under a nitrogen atmosphere with a flow rate of 60 ml/min. The analysis ran from room temperature to 650 °C with a gradient of 10 °C / min. Temperature and weight loss were not correlated, and the TA Universal Analysis software was used for data processing.

Calculation of the amount of deposited PPy derivatives on the fibrous scaffolds:

A – PPy derivative

B – fibrous scaffold-PPy derivative

C – pristine fibrous scaffold

m_{105} - sample weight at 105 °C

m_{650} - sample weight at 650 °C

$m_{deposited}$ – the amount of PPy on the PCL

equation 1:
$$m_{deposited} = \frac{mB_{650°C} - mC_{650°C}}{\frac{mA_{105°C}}{mA_{650°C}}} mg$$

equation 2:
$$PPy_{deposited} = \frac{m_{deposited}}{mB_{105°C}} \%$$

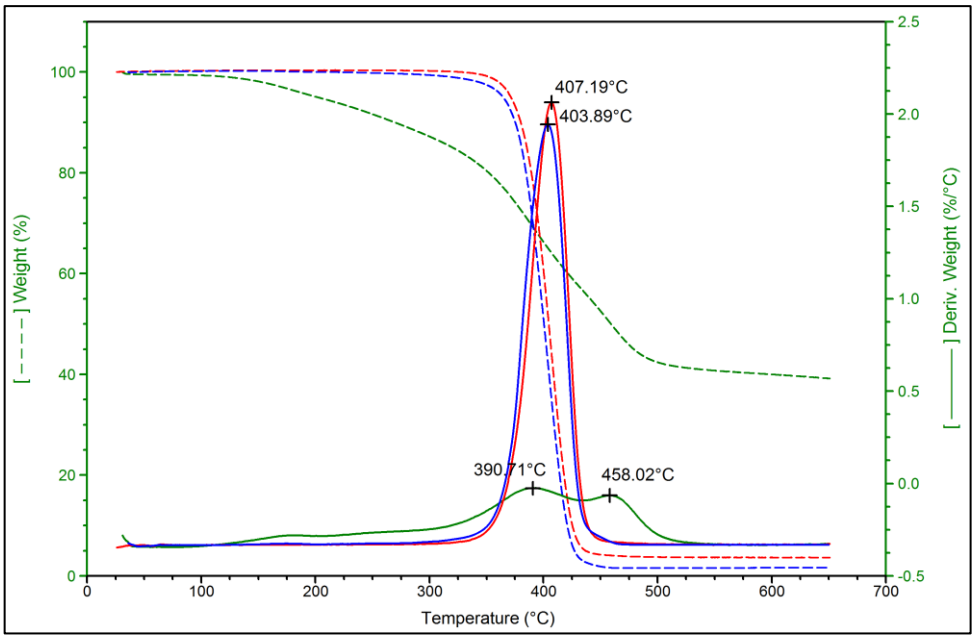

Figure 33. TGA spectra of PCL (blue line), PPy-5C-COOH **53** (green line) and PCL-PPy-5C-COOH **54** (red line) scaffolds

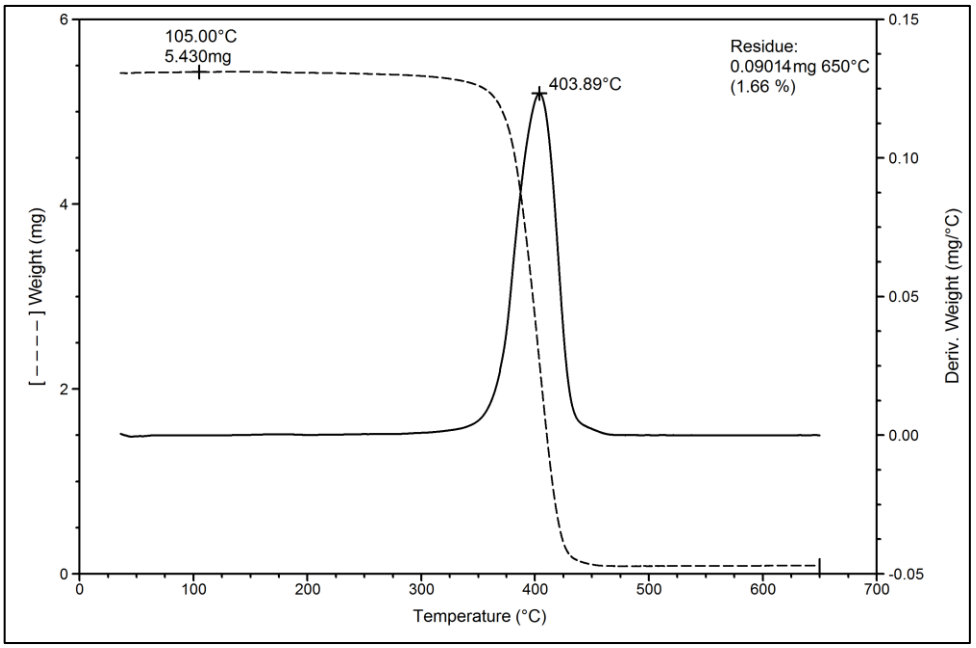

Figure 34. TGA spectrum of pristine PCL fibrous scaffold

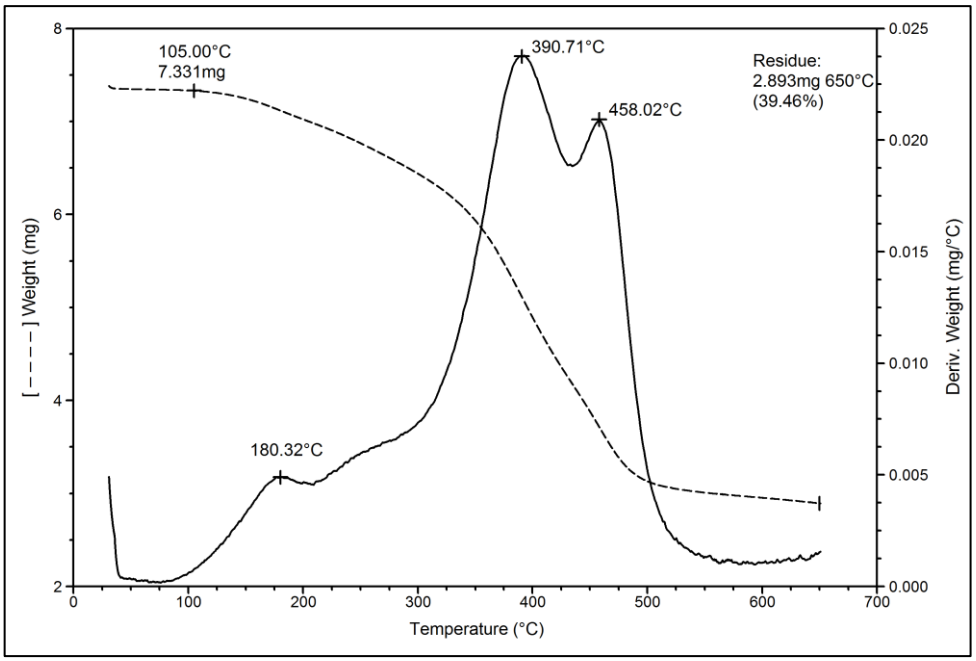

Figure 35. TGA spectrum of PPy-5C-COOH **53** in powdered form

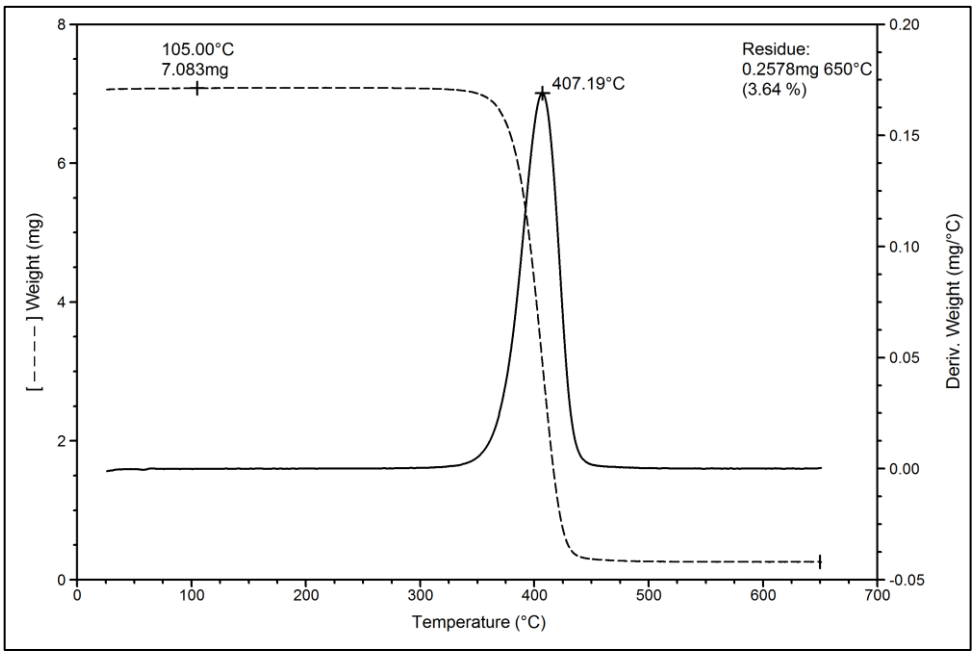

Figure 36. TGA spectrum of material PCL-PPy-5C-COOH **54**

Sample	$m_{105°C}$ [mg]	$m_{650°C}$ [mg]	residue %	$PPy_{deposited}$ %
PPy-4C-alkyne **55**	5.885	2.723	46.27 %	1.61 %
PCL-PPy-4C-alkyne **56**	6.241	0.150	2.41 %	
PCL	5.430	0.090	1.66 %	
PPy-5C-COOH **53**	7.331	2.893	39.46 %	4.99 %
PCL-PPy-5C-COOH **54**	7.083	0.258	3.64 %	
PCL	5.430	0.090	1.66 %	
PPy-10C-COOH **64**	5.148	1.601	31.10 %	7.88 %
PCL-PPy-10C-COOH **62**	4.933	0.203	4.12 %	
PCL	5.430	0.090	1.66 %	
PPy-5C-COOH **53**	7.331	2.893	39.46 %	1.51 %
PDX-PPy-5C-COOH **71**	5.677	0.034	0.60 %	
PDX	6.189	0.000	0.00 %	
PPy-5C-COOH **53**	7.331	2.893	39.46 %	0.53 %
P4HB-PPy-5C-COOH **72**	5.938	0.012	0.21%	
P4HB	5.822	0.000	0.00 %	
PPy-5C-COOH **53**	7.331	2.893	39.46 %	6.99 %
PA6-PPy-5C-COOH **73**	5.803	0.167	2.87 %	
PA6	5.877	0.006	0.11 %	
PPy-5C-COOH **53**	7.331	2.893	39.46 %	7.52 %
PVDF-PPy-5C-COOH **74**	5.865	0.338	5.77 %	
PVDF	5.446	0.153	2.80 %	

Table 4. Summary of TGA analysis of various fibrous materials coated with PPy derivatives

4.4.2. BET analysis

The analysis was performed on the instrument Autosorb iQ Quantachrome in a standard mode. The fibrous sample (291.8 mg) was put into 12 mm glass BET cell and degassed for 24 hours at 40 °C before measurement. Krypton was used for the analysis and the data processed using ASiQwin software. The resulting specific surface area of the analysed sample was 2.747 m^2/g.

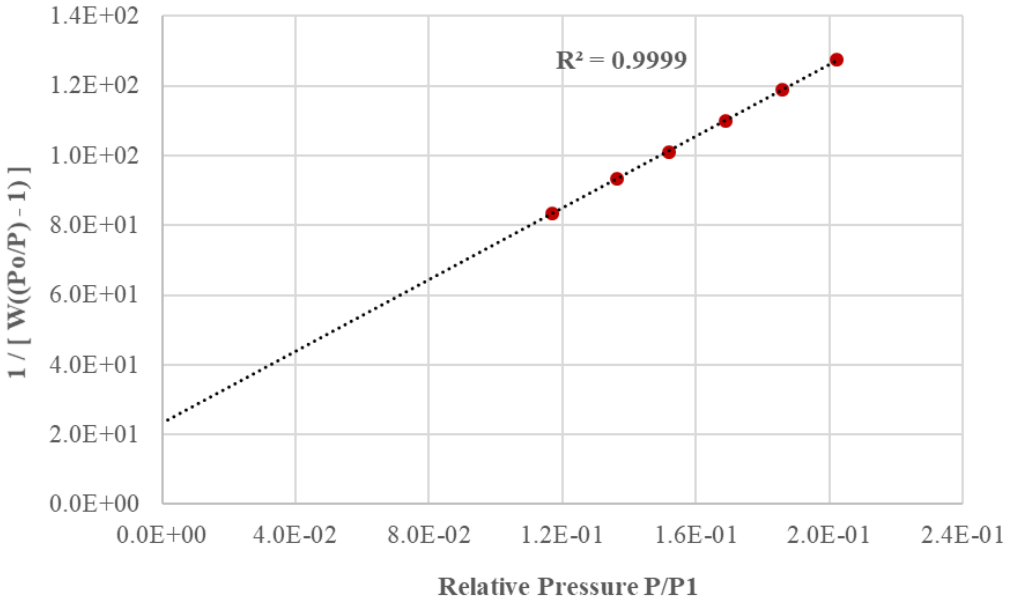

Graph 3. Specific surface area measurement (Multi-point BET plot)

4.4.3. Isothermal titration calorimetry

The host-guest interaction of β-CD **33** and Rhodamine B was studied using TA Instrument ITC version 2.0. The initial cell volume was 300 µl and the syringe volume 50 µl. Sample **33** was vacuum dried at 50 °C for 6 hours before the solution was prepared while the analytical grade of Rhodamine B was used as received. Deionised water was collected immediately before the experiment.

First, the cell was loaded with the solution of macrocycle **33** dissolved in deionised water, and the syringe was loaded with pure deionised water. The system was allowed to stabilise at 25 °C for 5 minutes, and then the stirring was turned on (250 rpm). After 25 minutes the water was added in 20 injections (2.39 µl per injection) with 240 seconds delay between additions. The first injection was excluded from the calculation, and the average heat output was later used as a blank constant. Then, the cell was filled with the solution of β-CD **33** (c = 1.08 mM) and the syringe was loaded with the solution of Rhodamine B in deionised water (c = 10.1 mM). The cell was allowed to stabilise at 25 °C for 5 minutes, before stirring was turned on at 250 rpm. After 25 minutes the solution of Rhodamine B was gradually added in 20 injections (240 seconds between additions), and the measurement was repeated three times (Graph 4). The blank was deducted from raw heat outputs of every injection and the data processed using TA instrument software (Table 5). The interaction model with one binding site was used for the calculation.

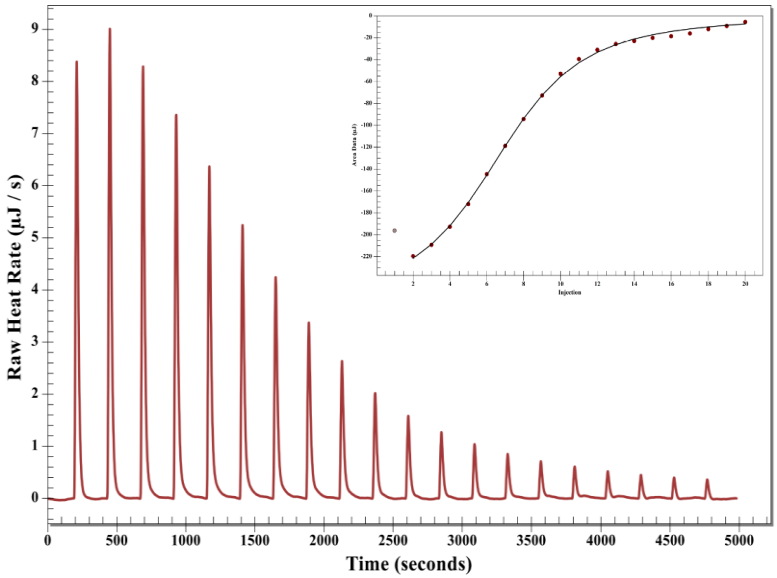

Graph 4. The course of the ITC experiment (Rhodamine B titrated into β-CD **33**)

njection	Heat [μcal]	Cell [mol]	Syringe injected [mol]	Syringe [mol]	Cell/Syringe
0		3.251E-07		5.070E-07	
1	196.3	3.01E-07	2.42E-08	4.828E-07	0.07
2	213.97	2.77E-07	4.85E-08	4.585E-07	0.15
3	209.3	2.52E-07	7.27E-08	4.343E-07	0.22
4	192.8	2.28E-07	9.69E-08	4.101E-07	0.30
5	172.1	2.04E-07	1.21E-07	3.858E-07	0.37
6	144.7	1.80E-07	1.45E-07	3.616E-07	0.45
7	119	1.55E-07	1.70E-07	3.374E-07	0.52
8	94.41	1.31E-07	1.94E-07	3.131E-07	0.60
9	72.84	1.07E-07	2.18E-07	2.889E-07	0.67
10	53.07	8.27E-08	2.42E-07	2.647E-07	0.75
11	39.63	5.85E-08	2.67E-07	2.404E-07	0.82
12	31.1	3.43E-08	2.91E-07	2.162E-07	0.89
13	25.8	1.00E-08	3.15E-07	1.920E-07	0.97
14	23.01	-1.42E-08	3.39E-07	1.677E-07	1.04
15	20.14	-3.84E-08	3.64E-07	1.435E-07	1.12
16	18.65	-6.27E-08	3.88E-07	1.192E-07	1.19
17	16.15	-8.69E-08	4.12E-07	9.501E-08	1.27
18	12.213	-1.11E-07	4.36E-07	7.078E-08	1.34
19	9.264	-1.35E-07	4.60E-07	4.654E-08	1.42
20	5.711	-1.60E-07	4.85E-07	2.231E-08	1.49

Table 5. The measurement of host-guest interaction between β-CD **33** and Rhodamine B using ITC (blanked heat output)

4.4.4. Fluorescence spectroscopy of Rhodamine B

The series of Rhodamine B solutions in methanol was prepared and the fluorescence measured in a quartz cuvette at wavelength 545 nm using spectrometer TECAN Spark. The absorbance of the blank sample (pure HPLC grade MeOH) was subtracted, and the collected data were summarised in Table 6. The results were plotted and the calibration curve created as a linear function. Then, 52.4 mg of PCL-PPy **54** or **62** (entry 8 and 10) was soaked in 4 ml of MeOH with Rhodamine B ($c = 1 \times 10^{-7}$ M) for 30 minutes and the fluorescence measured at 545 nm. Surprisingly, the value of absorbance was approximately six times higher than the starting solution. Thus, the pristine PCL was incubated in pure MeOH for 30 minutes and also measured (entry 12). The increase of fluorescence intensity was caused by the PCL matrix which was probably dissolved in MeOH at low concentration. Finally, 52.4 mg of PCL-PPy-5(10)C-CONH-β-CD **59** or **64** (entry 9 and 11) with immobilised β-CD was soaked in 4 ml of Rhodamine B solution ($c = 1 \times 10^{-7}$ M) and the fluorescence was measured as well. The entry 9 and 11 were subtracted from the absorbance of entry 8 and 10 which corresponds with the amount of Rhodamine B complexed in the β-CD cavity. Hence, the amount of immobilised of the CD on the scaffold surface can be calculated with complexation ratio 1:1 (see equations below).

Entry	Cuvette [mol/dm^3] / samples	Value	Blank	Blanked data
1	**1.0E-08**	0.0462	0.045	0.0012
2	**2.5E-08**	0.0476	0.045	0.0026
3	**5.0E-08**	0.0502	0.045	0.0052
4	**7.5E-08**	0.0531	0.045	0.0081
5	**1.0E-07**	0.0559	0.045	0.0109
6	**2.5E-07**	0.0724	0.045	0.0274
7	**5.0E-07**	0.1007	0.045	0.0557
8	PCL-PPy **54**	0.1079	0.045	0.0629
9	PCL-PPy-CD **59**	0.1037	0.045	0.0587
10	PCL-PPy **62**	0.1075	0.045	0.0625
11	PCL-PPy2-CD **64**	0.1025	0.045	0.0574
12	PCL	0.0957	0.045	0.0507

Table 6. Series of Rhodamine B solution in methanol (entry 1 – 7), measurement of Rhodamine B solution after incubation with fibrous materials (entry 8 – 12)

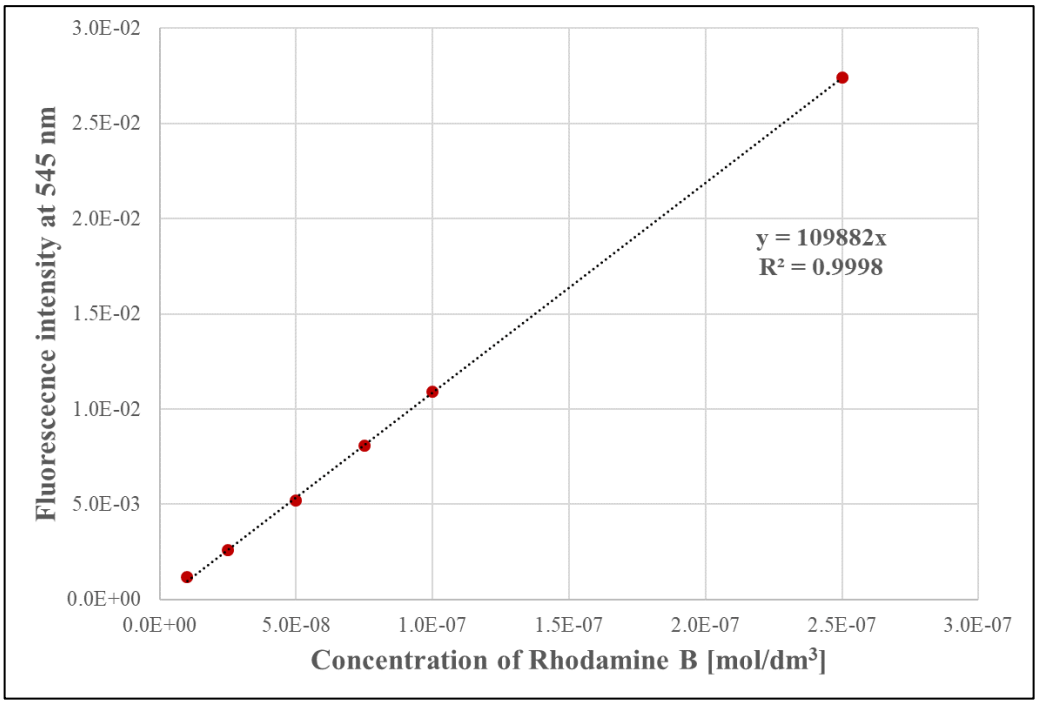

Graph 5. Calibration curve of Rhodamine B in methanol

The maximum theoretical density of β-CDs on the fibres was calculated according to the equations below using data from BET analysis (2.747 m2/g) and a dimension of β-CD with hexagonal packing arrangement. The results from the fluorescence measurement were compared with the maximal theoretical value for the completely functionalized surface.

Theoretical value:

Avogadro number	$N_A = 6.023*10^{23}$
Specific surface area	$S_{BET} = 2.747\ m^2/g$
Outer diameter of β-CD	$d_{CD} = 15.3$ A
Hexagonal packing density	$\eta = 0.9069$

area of β-CD: $$S_{CD} = \frac{\pi * d^2}{4}$$

a number of particles per gram: $$N_{surface-CD} = \frac{S_{BET}}{S_{CD}} * \eta$$

a number of moles per gram $$n_{surface-CD} = \frac{N_{surface-CD}}{N_A}$$

Measured value:

y – fluorescence

x – Rhodamine B concentration

y = 109882x

c_1 – concentration of the Rhodamine B in the solution before incubation

c_2 - concentration of the Rhodamine B in the solution after incubation

V – the volume of Rhodamine B solution for incubation

moles of Rhodamine B in the CD: $n_{sample} = (c_1 * V) - (c_2 * V)$

moles of Rhodamine B inside the CD cavity per gram: $n_{measured} = \frac{n_{sample}}{m_{sample}}$

$$ratio_{theoretical/measured} = \frac{n_{theoretical}}{n_{measured}}$$

4.4.5. X-ray photoelectron spectroscopy

X-ray Photoelectron Spectroscopy (XPS) measurements were performed in an Ultra High Vacuum (UHV) chamber with a base pressure below 1 x 10^{-7} Pa. The spectra were taken at normal emission angle using Specs XR50 x-ray source with Al and Mg anodes ($h\upsilon$ = 1486.6 eV for Al K_α and $h\upsilon$ = 1253.6 eV for Mg K_α radiation, respectively) and the VSW HA100 hemispherical analyser with multi-channel detection. The samples were measured at "as received" state without any cleaning of the surface. Thus the weak contamination of the sample surface by hydrocarbons from exposure to the air can be expected. The chemical state of the samples was investigated by the fitting of C 1s, O 1s and N 1s core level spectra in KolXPD software. Spectral lines were represented by pseudo-Voigt functions, and a Shirley-type background was subtracted from the spectra.

5. CONCLUSION

The targets of this work have been achieved by systematic work on the well-scheduled project, excellent mentoring and collaboration with many capable colleagues. In the beginning, we focused our attention on the synthesis of β-substituted pyrrole derivatives suitable for the cyclodextrin attachment. The most challenging task was to overcome an instability of some β-substituted pyrroles and find multistep reaction sequences leading to the essential intermediates. New pyrroles with iodo, cyano, azido, carbonyl, a carboxyl group or multiple terminal bond have been synthesised and spectroscopically characterised during ongoing research. Although the conjugation procedures using selective amide bond or triazole formation for cyclodextrin connection were found, the subsequent polymerisation of such bulky monomers did not proceed as expected. Therefore, suitable pyrrole monomers with a carboxy group or triple bond on carbon linker have been synthesised and later polymerised onto the fibrous PCL matrix. At first, the ideal ratio of pyrrole/oxidant/dopant in the polymerisation solution, reaction time, temperature and washing protocol were optimised on the drawn PCL fibres. Then, the procedure has been slightly changed for the deposition of functionalized PPy derivatives onto the random electrospun fibrous matrix. SEM confirmed the morphology of newly prepared materials, and the chemical structure of PPy coating was determinate using elemental analysis, IR spectroscopy, solid-state NMR, EDS or XPS. Moreover, the amount of deposited polypyrrole was quantified by TGA which has proven to be a fast and reliable method for the confirmation of successful polypyrrole deposition.

A crucial part of this thesis was the following introduction of cyclodextrins onto the core-shell PCL-PPy fibrous samples. The surface was decorated with cyclodextrins *via* the amide bond, and the number of immobilised molecules was indirectly measured by fluorescence spectroscopy. Finally, *in-vitro* experiments were used to compare the influence of surface-bound α-, β- or γ-CD on cell growth. Results suggest that PCL-PPy-CD material supports cell proliferation and growth much more than pristine PCL. However, there was no significant difference between α-, β- or γ-CD functionalized scaffolds. The effect of carbon spacer length separating the cyclodextrin from the surface on the NHDF cells growth was also compared. It can be said that less flexible linkers are preferable which is in good agreement with published literature. The original idea behind this work was to create a scaffold which supports proteins absorption and thus improves the overall cell-material interaction. An interesting finding concerning the results of *in-vitro* experiments is, that pristine PCL is superior for the protein absorption compared to functionalized samples. Nevertheless, the spatial conformation of adsorbed proteins is a far more critical parameter for the cell adhesion. Therefore, a complex study and a deeper understanding of this phenomenon would be interesting in the future.

To expand the possibilities of material functionalization, four other electrospun fibrous polymers (PDX, P4HB, PA6 and PVDF) were coated by PPy derivative under similar conditions

as described above. The amount of deposited PPy was experimentally determined and the morphology of resulting materials analysed by SEM. Besides, newly synthesised pyrrole monomers with double or triple bond were polymerised as well which further extended the possibility of surface functionalization. Huisgen dipolar cycloaddition is widely used in the field of material derivatisation even though thiol-ene/yne reactions represent a straightforward and highly selective method to utilise. This type of photo-induced reaction would bring another advantage for biomolecules immobilisation in the future. Moreover, the combination of a 3D polymeric matrix with a deposited conductive polypyrrole layer offers the opportunity to study the effect of conductivity on cell growth. Although this plan looks simple, it will be essential to find suitable polypyrrole/dopant combination with desirable conductivity, biocompatibility and superior environmental stability.

6. ABBREVIATIONS AND SYMBOLS

APCI	Atmospheric pressure ionization
br	Broad signal
BSA	Bovine serum albumin
CD	Cyclodextrin
COSY	Correlation spectroscopy
CuAAC	Copper catalysed azide-alkyne cycloaddtion
d	Doublet
DBSA	Dodecylbenzensulfonic acid
ddt	Doublet doublet of triplet
DIBAH	Diisobutylaluminium hydride
DIPEA	*N*,*N*-Diisopropylethylamine
DMSO	Dimethylsulfoxide
ECM	Extracellular matrix
EDC	*N*-(3-Dimethylaminopropyl)-*N*-ethylcarbodiimide hydrochloride
eq.	Equivalent
ESI	Electrospray ionization
EtAc	Ethyl acetate
GC-MS	Gas chromatography with mass detection
GPC	Gel permeation chromatography
HMBC	Heteronuclear multiple-bond correlation spectroscopy
HOMO	Highest occupied molecular orbital
HRMS	High resolution mass spectroscopy
HSQC	Heteronuclear single-quantum correlation spectroscopy
J	Nuclear spin-spin coupling constant (in Hz)
LDA	Lithium diisopropylamide
LC-MS	Liquid chromatography with mass detection
LUMO	Lowest unoccupied molecular orbital
m	Multiplet
MeOH	Methanol
MES	2-(*N*-morpholino)ethanesulfonic acid

MO	Methyl orange
m/z	Ratio between weight and charge (MS)
NBS	*N*-Bromosuccinimide
n-BuLi	*n*-Butyl lithium
NHDF	Normal dermal human fibroblast
NHS	*N*-hydroxysuccinimide
NIS	*N*-Iodosuccinimide
NMR	Nuclear magnetic resonance
PA6	Polyamide 6 (Nylon)
PCL	Polycaprolactone
PDX	Polydioxanone
P4HB	Polyhydroxybutyrate
PLA	Polylactic acid
ppm	Parts per million
PPy	Polypyrrole
PS	Polystyrene
PVDF	Polyvinylidenedifluoride
PyBOP	(Benzotriazol-1-yloxy)tripyrrolidinophosphonium hexafluorophosphate
q	Quartet
quint.	Quintet
Rh B	Rhodamine B
rpm	Rotations per minute
RT	Room temperature
s	Singlet
SDS-PAGE	Sodium dodecyl sulphate – polyacrylamide gel electrophoresis
S_EAr	Electrophilic aromatic substitution
SEM	Scanning electron microscopy
S_N2	Nucleophilic substitution bimolecular
t	Triplet
TBAF	Tetrabutylamonium fluoride
TBTA	Tris[(1-benzyl-1H-1,2,3-triazol-4-yl)methyl]amine
t-BuLi	*terc*-Butyl lithium

TGA	Thermogravimetric analysis
THAT	Tris(3-hydroxypropyltriazolylmethyl)amine
THF	Tetrahydrofuran
TIPS	Triisopropylsilyl
TMS	Trimethylsilyl
Ts	*para*-Toluensulfonyl
UV/VIS	Spectroscopy in ultra violet or visible part of the spectrum
WCA	Water contact angle

7. LITERATURE

(1) Hantzsch, A. Neue Bildungsweise von Pyrrolderivaten. *Berichte Dtsch. Chem. Ges.* **1890**, *23* (1), 1474–1476.

(2) Knorr, L. Synthese von Pyrrolderivaten. *Berichte Dtsch. Chem. Ges.* **1884**, *17* (2), 1635–1642.

(3) Paal, C. Ueber Die Derivate Des Acetophenonacetessigesters Und Des Acetonylacetessigesters. *Berichte Dtsch. Chem. Ges.* **1884**, *17* (2), 2756–2767.

(4) Estevez, V.; Villacampa, M.; Menendez, J. C. Recent Advances in the Synthesis of Pyrroles by Multicomponent Reactions. *Chem. Soc. Rev.* **2014**, *43* (13), 4633–4657.

(5) Bhardwaj, V.; Gumber, D.; Abbot, V.; Dhiman, S.; Sharma, P. Pyrrole: A Resourceful Small Molecule in Key Medicinal Hetero-Aromatics. *Rsc Adv.* **2015**, *5* (20), 15233–15266.

(6) O'Hagan, D. Pyrrole, Pyrrolidine, Pyridine, Piperidine and Tropane Alkaloids. *Nat. Prod. Rep.* **2000**, *17* (5), 435–446.

(7) De Rosa, M. Chlorination of Pyrrole. N-Chloropyrrole: Formation and Rearrangement to 2- and 3-Chloropyrrole. *J. Org. Chem.* **1982**, *47* (6), 1008–1010.

(8) Alvarez, A.; Guzman, A.; Ruiz, A.; Velarde, E.; Muchowski, J. Synthesis of 3-Arylpyrroles and 3-Pyrrolylacetylenes by Palladium-Catalyzed Coupling Reactions. *J. Org. Chem.* **1992**, *57* (6), 1653–1656.

(9) Zonta, C.; Fabris, F.; De Lucchi, O. The Pyrrole Approach toward the Synthesis of Fully Functionalized Cup-Shaped Molecules. *Org. Lett.* **2005**, *7* (6), 1003–1006.

(10) Bray, B.; Mathies, P.; Naef, R.; Solas, D.; Tidwell, T.; Artis, D.; Muchowski, J. N-(Triisopropylsilyl)Pyrrole - a Progenitor Par Excellence of 3-Substituted Pyrroles. *J. Org. Chem.* **1990**, *55* (26), 6317–6328.

(11) Kakushima, M.; Hamel, P.; Frenette, R.; Rokach, J. Regioselective Synthesis of Acylpyrroles. *J. Org. Chem.* **1983**, *48* (19), 3214–3219.

(12) Anderson, H.; Loader, C.; Xu, R.; Le, N.; Gogan, N.; Mcdonald, R.; Edwards, L. Pyrrole Chemistry .28. Substitution-Reactions of 1-(Phenylsulfonyl)Pyrrole and Some Derivatives. *Can. J. Chem.-Rev. Can. Chim.* **1985**, *63* (4), 896–902.

(13) Jolicoeur, B.; Chapman, E. E.; Thompson, A.; Lubell, W. D. Pyrrole Protection. *Tetrahedron* **2006**, *62* (50), 11531–11563.

(14) Fukuda, T.; Ohta, T.; Sudo, E.; Iwao, M. Directed Lithiation of N-Benzenesulfonyl-3-Bromopyrrole. Electrophile-Controlled Regioselective Functionalization via Dynamic Equilibrium between C-2 and C-5 Lithio Species. *Org. Lett.* **2010**, *12* (12), 2734–2737.

(15) Pickup, P. G. Alternating Current Impedance Study of a Polypyrrole-Based Anion-Exchange Polymer. *J. Chem. Soc. Faraday Trans.* **1990**, *86* (21), 3631–3636.

(16) Greene, R. L.; Street, G. B.; Suter, L. J. Superconductivity in Polysulfur Nitride. *Phys. Rev. Lett.* **1975**, *34* (10), 577–579.

(17) Ito, T.; Shirakawa, H.; Ikeda, S. Simultaneous Polymerization and Formation of Polyacetylene Film on Surface of Concentrated Soluble Ziegler-Type Catalyst Solution. *J. Polym. Sci. Part -Polym. Chem.* **1974**, *12* (1), 11–20.

(18) Shirakawa, H.; Louis, E. J.; MacDiarmid, A. G.; Chiang, C. K.; Heeger, A. J. Synthesis of Electrically Conducting Organic Polymers: Halogen Derivatives of Polyacetylene, (CH)x. *J. Chem. Soc. Chem. Commun.* **1977**, *0* (16), 578–580.

(19) MacDiarmid, A. G. "Synthetic Metals": A Novel Role for Organic Polymers (Nobel Lecture). *Angew. Chem.-Int. Ed.* **2001**, *40* (14), 2581–2590.

(20) Snook, G. A.; Kao, P.; Best, A. S. Conducting-Polymer-Based Supercapacitor Devices and Electrodes. *J. Power Sources* **2011**, *196* (1), 1–12.

(21) Pron, A.; Rannou, P. Processible Conjugated Polymers: From Organic Semiconductors to Organic Metals and Superconductors. *Prog. Polym. Sci.* **2002**, *27* (1), 135–190.

(22) Kumar, D.; Sharma, R. C. Advances in Conductive Polymers. *Eur. Polym. J.* **1998**, *34* (8), 1053–1060.

(23) McQuade, D. T.; Pullen, A. E.; Swager, T. M. Conjugated Polymer-Based Chemical Sensors. *Chem. Rev.* **2000**, *100* (7), 2537–2574.

(24) Guimard, N. K.; Gomez, N.; Schmidt, C. E. Conducting Polymers in Biomedical Engineering. *Prog. Polym. Sci.* **2007**, *32* (8–9), 876–921.

(25) Lee, J.; Kim, D.; Kim, C. Synthesis of Soluble Polypyrrole of the Doped State in Organic-Solvents. *Synth. Met.* **1995**, *74* (2), 103–106.

(26) Omastova, M.; Trchova, M.; Kovarova, J.; Stejskal, J. Synthesis and Structural Study of Polypyrroles Prepared in the Presence of Surfactants. *Synth. Met.* **2003**, *138* (3), 447–455.

(27) Tabaciarova, J.; Micusik, M.; Fedorko, P.; Omastova, M. Study of Polypyrrole Aging by XPS, FTIR and Conductivity Measurements. *Polym. Degrad. Stab.* **2015**, *120*, 392–401.

(28) MacDiarmid, A. G.; Heeger, A. J. Organic Metals and Semiconductors: The Chemistry of Polyacetylene, (CH)x, and Its Derivatives. *Synth. Met.* **1980**, *1* (2), 101–118.

(29) Blinova, N. V.; Stejskal, J.; Trchova, M.; Prokes, J.; Omastova, M. Polyaniline and Polypyrrole: A Comparative Study of the Preparation. *Eur. Polym. J.* **2007**, *43* (6), 2331–2341.

(30) Kulkarni, M. V.; Viswanath, A. K.; Marimuthu, R.; Seth, T. Spectroscopic, Transport, and Morphological Studies of Polyaniline Doped with Inorganic Acids. *Polym. Eng. Sci.* **2004**, *44* (9), 1676–1681.

(31) Wang, L.-X.; Li, X.-G.; Yang, Y.-L. Preparation, Properties and Applications of Polypyrroles. *React. Funct. Polym.* **2001**, *47* (2), 125–139.

(32) Tourillon, G.; Garnier, F. Effect of Dopant on the Physicochemical and Electrical Properties of Organic Conducting Polymers. *J. Phys. Chem.* **1983**, *87* (13), 2289–2292.

(33) Borole, D. D.; Kapadi, U. R.; Kumbhar, P. P.; Hundiwale, D. G. Effect of Inorganic Dopants (in Presence of Electrolyte) on the Conductivity of Polyaniline, Poly(o-Toluidine) and Their Copolymer Thin Films. *Mater. Lett.* **2002**, *57* (4), 844–852.

(34) Borole, D. D.; Kapadi, U. R.; Kumbhar, P. P.; Hundiwale, D. G. Studies on Influence of Inorganic Dopants in Presence of Electrolyte on the Conductivity of Polyaniline, Poly(o-Anisidine), and Their Copolymer Thin Films. *Polym.-Plast. Technol. Eng.* **2003**, *42* (3), 415–430.

(35) Nicolas-Debarnot, D.; Poncin-Epaillard, F. Polyaniline as a New Sensitive Layer for Gas Sensors. *Anal. Chim. Acta* **2003**, *475* (1), 1–15.

(36) Kuwabata, S.; Okamoto, K.-I.; Ikeda, O.; Yoneyama, H. Effect of Organic Dopants on Electrical Conductivity of Polypyrrole Films. *Synth. Met.* **1987**, *18* (1), 101–104.

(37) Peres, R. C. D.; Pernaut, J. M.; Paoli, M.-A. D. Polypyrrole/Dodecylsulfate: Effects of Different Synthesis Conditions. *J. Polym. Sci. Part Polym. Chem.* **1991**, *29* (2), 225–231.

(38) Yue, J.; Epstein, A. J. Synthesis of Self-Doped Conducting Polyaniline. *J. Am. Chem. Soc.* **1990**, *112* (7), 2800–2801.

(39) Kar, P.; Pradhan, N. C.; Adhikari, B. Induced Doping by Sodium Ion in Poly(m-Aminophenol) through the Functional Groups. *Synth. Met.* **2010**, *160* (13), 1524–1529.

(40) Diaz, A.; Kanazawa, K.; Gardini, G. Electrochemical Polymerization of Pyrrole. *J. Chem. Soc.-Chem. Commun.* **1979**, No. 14, 635–636.

(41) Armes, S. Optimum Reaction Conditions for the Polymerization of Pyrrole by Iron(Iii) Chloride in Aqueous-Solution. *Synth. Met.* **1987**, *20* (3), 365–371.

(42) Diaz, A.; Castillo, J.; Logan, J.; Lee, W. Electrochemistry of Conducting Polypyrrole Films. *J. Electroanal. Chem.* **1981**, *129* (1–2), 115–132.

(43) Mao, J.; Li, C.; Park, H. J.; Rouabhia, M.; Zhang, Z. Conductive Polymer Waving in Liquid Nitrogen. *ACS Nano* **2017**, *11* (10), 10409–10416.

(44) Hoffman, D. M.; Gibson, H. W.; Epstein, A. J.; Tanner, D. B. Conversion of Cis-Polyacetylene to Trans-Polyacetylene during Doping. *Phys. Rev. B* **1983**, *27* (2), 1454–1457.

(45) Hogervorst, A. C. R. Dopant Migration in Conducting Polymers. *Synth. Met.* **1994**, *62* (1), 27–34.

(46) Heinze, J. Electrochemistry of Conducting Polymers. *Synth. Met.* **1991**, *43* (1), 2805–2823.

(47) Wang, L. X.; Li, X. G.; Yang, Y. L. Preparation, Properties and Applications of Polypyrroles. *React. Funct. Polym.* **2001**, *47* (2), 125–139.

(48) Mihály, L.; Pekker, S.; Jánossy, A. N.m.r. Investigation of the Structure of Pure and Iodine-Doped Polyacetylene. *Synth. Met.* **1980**, *1* (4), 349–355.

(49) Tan, Y.; Ghandi, K. Kinetics and Mechanism of Pyrrole Chemical Polymerization. *Synth. Met.* **2013**, *175*, 183–191.

(50) Geetha, S.; Rao, C. R. K.; Vijayan, M.; Trivedi, D. C. Biosensing and Drug Delivery by Polypyrrole. *Anal. Chim. Acta* **2006**, *568* (1–2), 119–125.

(51) Wajs, E.; Fernandez, N.; Fragoso, A. Supramolecular Biosensors Based on Electropolymerised Pyrrole-Cyclodextrin Modified Surfaces for Antibody Detection. *Analyst* **2016**, *141* (11), 3274–3279.

(52) Guiseppi-Elie, A. Electroconductive Hydrogels: Synthesis, Characterization and Biomedical Applications. *Biomaterials* **2010**, *31* (10), 2701–2716.

(53) Balint, R.; Cassidy, N. J.; Cartmell, S. H. Conductive Polymers: Towards a Smart Biomaterial for Tissue Engineering. *Acta Biomater.* **2014**, *10* (6), 2341–2353.

(54) Song, R.-B.; Wu, Y.; Lin, Z.-Q.; Xie, J.; Tan, C. H.; Loo, J. S. C.; Cao, B.; Zhang, J.-R.; Zhu, J.-J.; Zhang, Q. Living and Conducting: Coating Individual Bacterial Cells with In Situ Formed Polypyrrole. *Angew. Chem.-Int. Ed.* **2017**, *56* (35), 10516–10520.

(55) Thompson, B. C.; Moulton, S. E.; Richardson, R. T.; Wallace, G. G. Effect of the Dopant Anion in Polypyrrole on Nerve Growth and Release of a Neurotrophic Protein. *Biomaterials* **2011**, *32* (15), 3822–3831.

(56) Vallejo-Giraldo, C.; Kelly, A.; Biggs, M. J. P. Biofunctionalisation of Electrically Conducting Polymers. *Drug Discov. Today* **2014**, *19* (1), 88–94.

(57) Green, R. A.; Lovell, N. H.; Wallace, G. G.; Poole-Warren, L. A. Conducting Polymers for Neural Interfaces: Challenges in Developing an Effective Long-Term Implant. *Biomaterials* **2008**, *29* (24–25), 3393–3399.

(58) Cai, L.; Zhang, L.; Dong, J.; Wang, S. Photocured Biodegradable Polymer Substrates of Varying Stiffness and Microgroove Dimensions for Promoting Nerve Cell Guidance and Differentiation. *Langmuir* **2012**, *28* (34), 12557–12568.

(59) Bugnicourt, G.; Brocard, J.; Nicolas, A.; Villard, C. Nanoscale Surface Topography Reshapes Neuronal Growth in Culture. *Langmuir ACS J. Surf. Colloids* **2014**, *30* (15), 4441–4449.

(60) Schmidt, C. E.; Shastri, V. R.; Vacanti, J. P.; Langer, R. Stimulation of Neurite Outgrowth Using an Electrically Conducting Polymer. *Proc. Natl. Acad. Sci. U. S. A.* **1997**, *94* (17), 8948–8953.

(61) Ghasemi-Mobarakeh, L.; Prabhakaran, M. P.; Morshed, M.; Nasr-Esfahani, M. H.; Baharvand, H.; Kiani, S.; Al-Deyab, S.; Ramakrishna, S. Application of Conductive Polymers, Scaffolds and Electrical Stimulation for Nerve Tissue Engineering. *J. Tissue Eng. Regen. Med.* **2011**, *5* (4), 17–35.

(62) Kotwal, A.; Schmidt, C. E. Electrical Stimulation Alters Protein Adsorption and Nerve Cell Interactions with Electrically Conducting Biomaterials. *Biomaterials* **2001**, *22* (10), 1055–1064.

(63) Xie, J.; MacEwan, M. R.; Willerth, S. M.; Li, X.; Moran, D. W.; Sakiyama-Elbert, S. E.; Xia, Y. Conductive Core-Sheath Nanofibers and Their Potential Application in Neural Tissue Engineering. *Adv. Funct. Mater.* **2009**, *19* (14), 2312–2318.

(64) Szentivanyi, A.; Chakradeo, T.; Zernetsch, H.; Glasmacher, B. Electrospun Cellular Microenvironments: Understanding Controlled Release and Scaffold Structure. *Adv. Drug Deliv. Rev.* **2011**, *63* (4–5), 209–220.

(65) Mager, M. D.; LaPointe, V.; Stevens, M. M. Exploring and Exploiting Chemistry at the Cell Surface. *Nat. Chem.* **2011**, *3* (8), 582–589.

(66) Ratner, B. D. The Biocompatibility Manifesto: Biocompatibility for the Twenty-First Century. *J Cardiovasc. Transl. Res.* **2011**, *4* (5), 523–527.

(67) Li, Y.; Xiao, Y.; Liu, C. The Horizon of Materiobiology: A Perspective on Material-Guided Cell Behaviors and Tissue Engineering. *Chem. Rev.* **2017**. *117* (5), 4376-4421.

(68) Wang, J. H. C.; Thampatty, B. P. An Introductory Review of Cell Mechanobiology. *Biomech. Model. Mechanobiol.* **2006**, *5* (1), 1–16.

(69) Wei, Q.; Becherer, T.; Angioletti-Uberti, S.; Dzubiella, J.; Wischke, C.; Neffe, A. T.; Lendlein, A.; Ballauff, M.; Haag, R. Protein Interactions with Polymer Coatings and Biomaterials. *Angew. Chem.-Int. Ed.* **2014**, *53* (31), 8004–8031.

(70) Holle, A. W.; Young, J. L.; Van Vliet, K. J.; Kamm, R. D.; Discher, D.; Janmey, P.; Spatz, J. P.; Saif, T. Cell-Extracellular Matrix Mechanobiology: Forceful Tools and Emerging Needs for Basic and Translational Research. *Nano Lett.* **2018**, *18* (1), 1–8.

(71) Frantz, C.; Stewart, K. M.; Weaver, V. M. The Extracellular Matrix at a Glance. *J Cell Sci* **2010**, *123* (24), 4195–4200.

(72) Calderwood, D. A.; Ginsberg, M. H. Talin Forges the Links between Integrins and Actin. *Nat. Cell Biol.* **2003**, *5* (8), 694–697.

(73) Ariga, K.; Minami, K.; Ebara, M.; Nakanishi, J. What Are the Emerging Concepts and Challenges in NANO? Nanoarchitectonics, Hand-Operating Nanotechnology and Mechanobiology. *Polym. J.* **2016**, *48* (4), 371–389.

(74) Bacakova, L.; Filova, E.; Parizek, M.; Ruml, T.; Svorcik, V. Modulation of Cell Adhesion, Proliferation and Differentiation on Materials Designed for Body Implants. *Biotechnol. Adv.* **2011**, *29* (6), 739–767.

(75) Zhuang, Y. X.; Hansen, O. Correlation of Effective Dispersive and Polar Surface Energies in Heterogeneous Self-Assembled Monolayer Coatings. *Langmuir* **2009**, *25* (10), 5437–5441.

(76) Heitz, J.; Švorčík, V.; Bačáková, L.; Ročková, K.; Ratajová, E.; Gumpenberger, T.; Bäuerle, D.; Dvořánková, B.; Kahr, H.; Graz, I.; et al. Cell Adhesion on Polytetrafluoroethylene Modified by UV-Irradiation in an Ammonia Atmosphere. *J. Biomed. Mater. Res. A* **2003**, *67A* (1), 130–137.

(77) Detrait, E.; Lhoest, J.-B.; Knoops, B.; Bertrand, P.; van den Bosch de Aguilar, P. Orientation of Cell Adhesion and Growth on Patterned Heterogeneous Polystyrene Surface. *J. Neurosci. Methods* **1998**, *84* (1), 193–204.

(78) Kasálková, N.; Kolářová, K.; Bačáková, L.; Pařízek, M.; Macková, A.; Švorčík, V. Cell Adhesion and Proliferation on Modified Polyethylene. *Mater. Sci. Forum* **2008**, *567-568*, 269-272.

(79) Parizek, M.; Kasalkova, N.; Bacakova, L.; Slepicka, P.; Lisa, V.; Blazkova, M.; Svorcik, V. Improved Adhesion, Growth and Maturation of Vascular Smooth Muscle Cells on Polyethylene Grafted with Bioactive Molecules and Carbon Particles. *Int. J. Mol. Sci.* **2009**, *10* (10), 4352–4374.

(80) Lesný, P.; Přádný, M.; Jendelová, P.; Michálek, J.; Vacík, J.; Syková, E. Macroporous Hydrogels Based on 2-Hydroxyethyl Methacrylate. Part 4: Growth of Rat Bone Marrow Stromal Cells in Three-Dimensional Hydrogels with Positive and Negative Surface Charges and in Polyelectrolyte Complexes. *J. Mater. Sci. Mater. Med.* **2006**, *17* (9), 829–833.

(81) Liu, L.; Chen, S.; Giachelli, C. M.; Ratner, B. D.; Jiang, S. Controlling Osteopontin Orientation on Surfaces to Modulate Endothelial Cell Adhesion. *J. Biomed. Mater. Res. A* **2005**, *74A* (1), 23–31.

(82) Masui, M.; Takata, H.; Kominami, T. Cell Adhesion and the Negative Cell Surface Charges in Embryonic Cells of the Starfish Asterina Pectinifera. *Electrophoresis* **2002**, *23* (13), 2087–2095.

(83) Stoltz, J. F.; Muller, S.; Wang, X.; Dumas, D.; Boisseau, M.; Legrand, S.; Labrador, V. Hemorheology and Vascular Endothelial Cells. *Clin. Hemorheol. Microcirc.* **1999**, *20* (2), 127–139.

(84) Lee, H. J.; Hong, J.-K.; Goo, H. C.; Lee, W. K.; Park, K. D.; Kim, S. H.; Yoo, Y. M.; Kim, Y. H. Improved Blood Compatibility and Decreased VSMC Proliferation of Surface-Modified Metal Grafted with Sulfonated PEG or Heparin. *J. Biomater. Sci. Polym. Ed.* **2002**, *13* (8), 939–952.

(85) Park, H. D.; Lee, W. K.; Ooya, T.; Park, K. D.; Kim, Y. H.; Yui, N. Anticoagulant Activity of Sulfonated Polyrotaxanes as Blood-Compatible Materials. *J. Biomed. Mater. Res.* **2002**, *60* (1), 186–190.

(86) Sun, S.; Liu, Y.; Lipsky, S.; Cho, M. Physical Manipulation of Calcium Oscillations Facilitates Osteodifferentiation of Human Mesenchymal Stem Cells. *FASEB J.* **2007**, *21* (7), 1472–1480.

(87) Khatib, L.; Golan, D. E.; Cho, M. Physiologic Electrical Stimulation Provokes Intracellular Calcium Increase Mediated by Phospholipase C Activation in Human Osteoblasts. *FASEB J.* **2004**, *18* (15), 1903–1905.

(88) Stevens, M. M.; George, J. H. Exploring and Engineering the Cell Surface Interface. *Science* **2005**, *310* (5751), 1135–1138.

(89) Sammons, R. L.; Lumbikanonda, N.; Gross, M.; Cantzler, P. Comparison of Osteoblast Spreading on Microstructured Dental Implant Surfaces and Cell Behaviour in an Explant Model of Osseointegration. *Clin. Oral Implants Res.* **2005**, *16* (6), 657–666.

(90) Kim, H. J.; Kim, S. H.; Kim, M. S.; Lee, E. J.; Oh, H. G.; Oh, W. M.; Park, S. W.; Kim, W. J.; Lee, G. J.; Choi, N. G.; et al. Varying Ti-6Al-4V Surface Roughness Induces

Different Early Morphologic and Molecular Responses in MG63 Osteoblast-like Cells. *J. Biomed. Mater. Res. A* **2005**, *74* (3), 366–373.

(91) Curtis, A. S. G.; Wilkinson, C. D. Reactions of Cells to Topography. *J. Biomater. Sci.-Polym. Ed.* **1998**, *9* (12), 1313–1329.

(92) Price, R. L.; Ellison, K.; Haberstroh, K. M.; Webster, T. J. Nanometer Surface Roughness Increases Select Osteoblast Adhesion on Carbon Nanofiber Compacts. *J. Biomed. Mater. Res. A* **2004**, *70* (1), 129–138.

(93) Berry, C. C.; Campbell, G.; Spadiccino, A.; Robertson, M.; Curtis, A. S. G. The Influence of Microscale Topography on Fibroblast Attachment and Motility. *Biomaterials* **2004**, *25* (26), 5781–5788.

(94) Webster, T. J.; Ergun, C.; Doremus, R. H.; Siegel, R. W.; Bizios, R. Specific Proteins Mediate Enhanced Osteoblast Adhesion on Nanophase Ceramics. *J. Biomed. Mater. Res.* **2000**, *51* (3), 475–483.

(95) Dee, K. C.; Andersen, T. T.; Bizios, R. Design and Function of Novel Osteoblast-Adhesive Peptides for Chemical Modification of Biomaterials. *J. Biomed. Mater. Res.* **1998**, *40* (3), 371–377.

(96) Webster, T. J.; Schadler, L. S.; Siegel, R. W.; Bizios, R. Mechanisms of Enhanced Osteoblast Adhesion on Nanophase Alumina Involve Vitronectin. *Tissue Eng.* **2001**, *7* (3), 291–301.

(97) Raimondo, T.; Puckett, S.; Webster, T. J. Greater Osteoblast and Endothelial Cell Adhesion on Nanostructured Polyethylene and Titanium. *Int. J. Nanomedicine* **2010**, *5*, 647–652.

(98) Saino, E.; Focarete, M. L.; Gualandi, C.; Emanuele, E.; Cornaglia, A. I.; Imbriani, M.; Visai, L. Effect of Electrospun Fiber Diameter and Alignment on Macrophage Activation and Secretion of Proinflammatory Cytokines and Chemokines. *Biomacromolecules* **2011**, *12* (5), 1900–1911.

(99) Cortese, B.; Gigli, G.; Riehle, M. Mechanical Gradient Cues for Guided Cell Motility and Control of Cell Behavior on Uniform Substrates. *Adv. Funct. Mater.* **2009**, *19* (18), 2961–2968.

(100) Engler, A.; Bacakova, L.; Newman, C.; Hategan, A.; Griffin, M.; Discher, D. Substrate Compliance versus Ligand Density in Cell on Gel Responses. *Biophys. J.* **2004**, *86* (1 Pt 1), 617–628.

(101) Bacakova, L.; Filova, E.; Kubies, D.; Machova, L.; Proks, V.; Malinova, V.; Lisa, V.; Rypacek, F. Adhesion and Growth of Vascular Smooth Muscle Cells in Cultures on Bioactive RGD Peptide-Carrying Polylactides. *J. Mater. Sci. Mater. Med.* **2007**, *18* (7), 1317–1323.

(102) Engler, A. J.; Sen, S.; Sweeney, H. L.; Discher, D. E. Matrix Elasticity Directs Stem Cell Lineage Specification. *Cell* **2006**, *126* (4), 677–689.

(103) Rehfeldt, F.; Engler, A. J.; Eckhardt, A.; Ahmed, F.; Discher, D. E. Cell Responses to the Mechanochemical Microenvironment--Implications for Regenerative Medicine and Drug Delivery. *Adv. Drug Deliv. Rev.* **2007**, *59* (13), 1329–1339.

(104) Ruoslahti, E. RGD and Other Recognition Sequences for Integrins. *Annu. Rev. Cell Dev. Biol.* **1996**, *12*, 697–715.

(105) Mann, B. K.; West, J. L. Cell Adhesion Peptides Alter Smooth Muscle Cell Adhesion, Proliferation, Migration, and Matrix Protein Synthesis on Modified Surfaces and in Polymer Scaffolds. *J. Biomed. Mater. Res.* **2002**, *60* (1), 86–93.

(106) Neff, J. A.; Tresco, P. A.; Caldwell, K. D. Surface Modification for Controlled Studies of Cell–Ligand Interactions. *Biomaterials* **1999**, *20* (23), 2377–2393.

(107) Cavalcanti-Adam, E. A.; Volberg, T.; Micoulet, A.; Kessler, H.; Geiger, B.; Spatz, J. P. Cell Spreading and Focal Adhesion Dynamics Are Regulated by Spacing of Integrin Ligands. *Biophys. J.* **2007**, *92* (8), 2964–2974.

(108) Lim, S. H.; Liu, X. Y.; Song, H.; Yarema, K. J.; Mao, H.-Q. The Effect of Nanofiber-Guided Cell Alignment on the Preferential Differentiation of Neural Stem Cells. *Biomaterials* **2010**, *31* (34), 9031–9039.

(109) Meng, J.; Han, Z.; Kong, H.; Qi, X.; Wang, C.; Xie, S.; Xu, H. Electrospun Aligned Nanofibrous Composite of MWCNT/Polyurethane to Enhance Vascular Endothelium Cells Proliferation and Function. *J. Biomed. Mater. Res. A* **2010**, *95* (1), 312–320.

(110) Balaban, N. Q.; Schwarz, U. S.; Riveline, D.; Goichberg, P.; Tzur, G.; Sabanay, I.; Mahalu, D.; Safran, S.; Bershadsky, A.; Addadi, L.; et al. Force and Focal Adhesion Assembly: A Close Relationship Studied Using Elastic Micropatterned Substrates. *Nat. Cell Biol.* **2001**, *3* (5), 466–472.

(111) Bershadsky, A. D.; Balaban, N. Q.; Geiger, B. Adhesion-Dependent Cell Mechanosensitivity. *Annu. Rev. Cell Dev. Biol.* **2003**, *19*, 677–695.

(112) Stefan, K.; Schuhmann, W.; Parlar, H.; Korte, F. Synthesis of New 3-Substituted Pyrroles. *Chem. Ber.* **1989**, *122* (1), 169–174.

(113) Kolb, H. C.; Finn, M. G.; Sharpless, K. B. Click Chemistry: Diverse Chemical Function from a Few Good Reactions. *Angew. Chem.-Int. Ed.* **2001**, *40* (11), 2004–2021.

(114) Kolb, H. C.; Sharpless, K. B. The Growing Impact of Click Chemistry on Drug Discovery. *Drug Discov. Today* **2003**, *8* (24), 1128–1137.

(115) Huisgen, R. 1.3-Dipolare Cycloadditionen - Ruckschau Und Ausblick. *Angew. Chem.-Int. Ed.* **1963**, *75* (13), 604–637.

(116) Biffis, A.; Centomo, P.; Del Zotto, A.; Zecca, M. Pd Metal Catalysts for Cross-Couplings and Related Reactions in the 21st Century: A Critical Review. *Chem. Rev.* **2018**, *118* (4), 2249–2295.

(117) Heravi, M. M.; Hajiabbasi, P. Recent Advances in Kumada-Tamao-Corriu Cross-Coupling Reaction Catalyzed by Different Ligands. *Monatshefte Chem.* **2012**, *143* (12), 1575–1592.

(118) Negishi, E.; Kotora, M.; Xu, C. D. Direct Synthesis of Terminal Alkynes via Pd-Catalyzed Cross Coupling of Aryl and Alkenyl Halides with Ethynylmetals Containing Zn, Mg, and Sn. Critical Comparison of Counteractions. *J. Org. Chem.* **1997**, *62* (25), 8957–8960.

(119) Yang, L. M.; Huang, L. F.; Luh, T. Y. Kumada-Corriu Reactions of Alkyl Halides with Alkynyl Nucleophiles. *Org. Lett.* **2004**, *6* (9), 1461–1463.

(120) Rutledge, T. Sodium Acetylide .2. Reactions of Sodium Acetylide in Organic Diluents - Preparation of Monoalkyl Acetylenes. *J. Org. Chem.* **1959**, *24* (6), 840–842.

(121) Smith, W.; Beumel, O. Preparation of Alkynes and Dialkynes by Reaction of Monohalo-Alkanes and Dihaloalkanes with Lithium Acetylenide-Ethylenediamine Complex. *Synth.-Stuttg.* **1974**, No. 6, 441–442.

(122) Corey, E.; Fuchs, P. Synthetic Method for Formyl Ethynyl Conversion (Rcho-Rc=ch or Rc=cr'). *Tetrahedron Lett.* **1972**, No. 36, 3769-3772.

(123) Brown, H.; Garg, C. Selective Reductions. .4. Partial Reduction of Nitriles with Lithium Triethoxyaluminohydride-Convenient Aldehyde Synthesis. *J. Am. Chem. Soc.* **1964**, *86* (6), 1085-1089.

(124) Miller, A.; Biss, J.; Schwartzman, L. Reductions with Dialkylaluminum Hydrides. *J. Org. Chem.* **1959**, *24* (5), 627–630.

(125) Kornblum, N.; Jones, W.; Anderson, G. A New and Selective Method of Oxidation - the Conversion of Alkyl Halides and Alkyl Tosylates to Aldehydes. *J. Am. Chem. Soc.* **1959**, *81* (15), 4113–4114.

(126) Dave, P.; Byun, H.; Engel, R. An Improved Direct Oxidation of Alkyl-Halides to Aldehydes. *Synth. Commun.* **1986**, *16* (11), 1343–1346.

(127) Bratulescu, G. Synthesis of Aromatic Aldehydes by a Fast Method Involving Kornblum's Reaction. *Synth. Commun.* **2008**, *38* (16), 2748–2752.

(128) Friedman, L.; Shechter, H. Preparation of Nitriles from Halides and Sodium Cyanide - an Advantageous Nucleophilic Displacement in Dimethyl Sulfoxide. *J. Org. Chem.* **1960**, *25* (6), 877–879.

(129) Tang, W.; Ng, S.-C. Facile Synthesis of Mono-6-Amino-6-Deoxy-α-, β-, γ-Cyclodextrin Hydrochlorides for Molecular Recognition, Chiral Separation and Drug Delivery. *Nat. Protoc.* **2008**, *3* (4), 691–697.

(130) Mojr, V.; Herzig, V.; Budesinsky, M.; Cibulka, R.; Kraus, T. Flavin-Cyclodextrin Conjugates as Catalysts of Enantioselective Sulfoxidations with Hydrogen Peroxide in Aqueous Media. *Chem. Commun.* **2010**, *46* (40), 7599–7601.

(131) Chmurski, K.; Stepniak, P.; Jurczak, J. Improved Synthesis of C2 and C6 Monoderivatives of Alpha- and Beta-Cyclodextrin via the Click Chemistry Approach. *Synth.-Stuttg.* **2015**, *47* (13), 1838–1843.

(132) Yanilmaz, M.; Sarac, A. S. A Review: Effect of Conductive Polymers on the Conductivities of Electrospun Mats. *Text. Res. J.* **2014**, *84* (12), 1325–1342.

(133) Wang, X. D.; Gu, X. S.; Yuan, C. W.; Chen, S. J.; Zhang, P. Y.; Zhang, T. Y.; Yao, J.; Chen, F.; Chen, G. Evaluation of Biocompatibility of Polypyrrole in Vitro and in Vivo. *J. Biomed. Mater. Res. A* **2004**, *68A* (3), 411–422.

(134) Yang, K.; Xu, H.; Cheng, L.; Sun, C.; Wang, J.; Liu, Z. In Vitro and In Vivo Near-Infrared Photothermal Therapy of Cancer Using Polypyrrole Organic Nanoparticles. *Adv. Mater.* **2012**, *24* (41), 5586–5592.

(135) Ateh, D. D.; Navsaria, H. A.; Vadgama, P. Polypyrrole-Based Conducting Polymers and Interactions with Biological Tissues. *J. R. Soc. Interface* **2006**, *3* (11), 741–752.

(136) Sletten, E. M.; Bertozzi, C. R. Bioorthogonal Chemistry: Fishing for Selectivity in a Sea of Functionality. *Angew. Chem.-Int. Ed.* **2009**, *48* (38), 6974–6998.

(137) Spicer, C. D.; Pashuck, E. T.; Stevens, M. M. Achieving Controlled Biomolecule-Biomaterial Conjugation. *Chem. Rev.* **2018**, *118* (16), 7702–7743.

(138) Zhou, H.-X.; Pang, X. Electrostatic Interactions in Protein Structure, Folding, Binding, and Condensation. *Chem. Rev.* **2018**, *118* (4), 1691–1741.

(139) Bock, V. D.; Hiemstra, H.; van Maarseveen, J. H. Cu-I-Catalyzed Alkyne-Azide "Click" Cycloadditions from a Mechanistic and Synthetic Perspective. *Eur. J. Org. Chem.* **2006**, No. 1, 51–68.

(140) Binder, W. H.; Sachsenhofer, R. "Click" Chemistry in Polymer and Materials Science. *Macromol. Rapid Commun.* **2007**, *28* (1), 15–54.

(141) Chan, T. R.; Hilgraf, R.; Sharpless, K. B.; Fokin, V. V. Polytriazoles as Copper(I)-Stabilizing Ligands in Catalysis. *Org. Lett.* **2004**, *6* (17), 2853–2855.

(142) Goldmann, A. S.; Glassner, M.; Inglis, A. J.; Barner-Kowollik, C. Post-Functionalization of Polymers via Orthogonal Ligation Chemistry. *Macromol. Rapid Commun.* **2013**, *34* (10), 810–849.

(143) Hensarling, R. M.; Doughty, V. A.; Chan, J. W.; Patton, D. L. "Clicking" Polymer Brushes with Thiol-Yne Chemistry: Indoors and Out. *J. Am. Chem. Soc.* **2009**, *131* (41), 14673–14675.

(144) Hoogenboom, R. Thiol-Yne Chemistry: A Powerful Tool for Creating Highly Functional Materials. *Angew. Chem.-Int. Ed.* **2010**, *49* (20), 3415–3417.

(145) Hoyle, C. E.; Bowman, C. N. Thiol-Ene Click Chemistry. *Angew. Chem.-Int. Ed.* **2010**, *49* (9), 1540–1573.

(146) Lowe, A. B.; Hoyle, C. E.; Bowman, C. N. Thiol-Yne Click Chemistry: A Powerful and Versatile Methodology for Materials Synthesis. *J. Mater. Chem.* **2010**, *20* (23), 4745–4750.

(147) Martinelli, J.; Thangavel, K.; Tei, L.; Botta, M. Dendrimeric Beta-Cyclodextrin/Gd-III Chelate Supramolecular Host-Guest Adducts as High-Relaxivity MRI Probes. *Chem.-Eur. J.* **2014**, *20* (35), 10944–10952.

(148) Hu, X.; Tan, H.; Wang, X.; Chen, P. Surface Functionalization of Hydrogel by Thiol-Yne Click Chemistry for Drug Delivery. *Colloids Surf. -Physicochem. Eng. Asp.* **2016**, *489*, 297–304.

(149) Ghirardello, M.; Oberg, K.; Staderini, S.; Renaudet, O.; Berthet, N.; Dumy, P.; Hed, Y.; Marra, A.; Malkoch, M.; Dondoni, A. Thiol-Ene and Thiol-Yne-Based Synthesis of Glycodendrimers as Nanomolar Inhibitors of Wheat Germ Agglutinin. *J. Polym. Sci. Part -Polym. Chem.* **2014**, *52* (17), 2422–2433.

(150) Espeel, P.; Du Prez, F. E. "Click"-Inspired Chemistry in Macromolecular Science: Matching Recent Progress and User Expectations. *Macromolecules* **2015**, *48* (1), 2–14.

7.1. List of author's publications

1) Lukasek, J.; Boehm, S.; Dvorakova, H.; Eigner, V.; Lhotak, P. Regioselective Halogenation of Thiacalix[4]arenes in the Cone and 1,3-Alternate Conformations. *Org. Lett.* **2014**, *16* (19), 5100–5103.

2) Lukasek, J.; Strnadova, K.; Krabicova, I.; Rezanka, M.; Stibor, I. New Aligned Microfibers for Tissue Engineering. *Nanocon 2015: 7th International Conference on Nanomaterials - Research & Application* **2015**, 399–403.

3) Strnadová, K.; Lukášek, J.; Krabicová, I.; Stanislav, L.; Řezanka, M.; Jenčová, V.; Beranová, Š.; Stibor, I.; Lukáš, D. Functionalization and biocompatibility evaluation of drawn fibers for neural tissue implants. *Fiber Society 2016 Spring Conference: Textile Innovations - Opportunities and Challenges* **2016**, 126–127.

4) Lukášek, J.; Řezanková, M.; Stibor, I.; Řezanka, M. Synthesis of cyclodextrin–pyrrole conjugates possessing tuneable carbon linkers. *J Incl Phenom Macrocycl Chem* **2018**, *92* (3), 339–346.

5) Strnadová, K.; Stanislav, L.; Krabicová, I.; Sabol, F.; Lukášek, J.; Řezanka, M.; Lukáš, D.; Jenčová, V. Drawn aligned polymer microfibres for tissue engineering. *Journal of Industrial Textiles* **2019**, in press.

6) Lukášek, J.; Hauzerová, Š.; Havlíčková, K.; Strnadová, K.; Mašek, K.; Stuchlík, M.; Stibor, I.; Jenčová, V.; Řezanka, M. Cyclodextrin-Polypyrrole Coatings of Scaffolds for Tissue Engineering. *Polymers* **2019**, *11* (3), 459.